Galaxies **2014**, *2*, 89-159; doi:10.3390/galaxies2010089

OPEN ACCESS

galaxies

ISSN 2075-4434

www.mdpi.com/journal/galaxies

Article

Thermodynamics of Rotating Black Holes and Black Rings: Phase Transitions and Thermodynamic Volume

Natacha Altamirano [1,2], David Kubizňák [1], Robert B. Mann [1,3,*] and Zeinab Sherkatghanad [3,4]

[1] Perimeter Institute, 31 Caroline St. N., Waterloo, ON N2L 2Y5, Canada;
E-Mails: naltamirano@famaf.unc.edu.ar (N.A.); dkubiznak@perimeterinstitute.ca (D.K.);

[2] Facultad de Matemática, Astronomía y Física, FaMAF, Universidad Nacional de Córdoba, Instituto de Física Enrique Gaviola, IFEG, CONICET, Ciudad Universitaria, Córdoba 5000, Argentina

[3] Department of Physics and Astronomy, University of Waterloo, Waterloo, ON N2L 3G1, Canada;
E-Mail: zsherkat@uwaterloo.ca

[4] Department of Physics, Isfahan University of Technology, Isfahan 84156-83111, Iran

* Author to whom correspondence should be addressed; E-Mail: rbmann@sciborg.uwaterloo.ca;
Tel.: +1-519-882-1211.

Received: 9 January 2014; in revised form: 6 February 2014 / Accepted: 7 February 2014 / Published: 3 March 2014

Abstract: In this review we summarize, expand, and set in context recent developments on the thermodynamics of black holes in extended phase space, where the cosmological constant is interpreted as thermodynamic pressure and treated as a thermodynamic variable in its own right. We specifically consider the thermodynamics of higher-dimensional rotating asymptotically flat and AdS black holes and black rings in a canonical (fixed angular momentum) ensemble. We plot the associated thermodynamic potential—the Gibbs free energy—and study its behavior to uncover possible thermodynamic phase transitions in these black hole spacetimes. We show that the multiply-rotating Kerr-AdS black holes exhibit a rich set of interesting thermodynamic phenomena analogous to the "every day thermodynamics" of simple substances, such as reentrant phase transitions of multicomponent liquids, multiple first-order solid/liquid/gas phase transitions, and liquid/gas phase transitions of the van der Waals type. Furthermore, the reentrant phase transitions also occur for multiply-spinning asymptotically flat Myers–Perry black holes. These phenomena do not require a variable cosmological constant, though they are more naturally understood in the context of the extended phase space. The thermodynamic volume, a quantity conjugate to the thermodynamic pressure, is studied for AdS black rings and demonstrated to satisfy the reverse isoperimetric inequality; this provides a first example of calculation confirming the

validity of isoperimetric inequality conjecture for a black hole with non-spherical horizon topology. The equation of state $P = P(V,T)$ is studied for various black holes both numerically and analytically—in the ultraspinning and slow rotation regimes.

Keywords: black holes; thermodynamics; gauge-gravity duality

Classification: PACS 04.50.Gh, 04.70.-s, 05.70.Ce

---

1. Introduction

The subject of black hole thermodynamics continues to be one of import in gravitational physics. Despite long-established notions that black holes have a temperature proportional to their surface gravity, an entropy proportional to their horizon area, and obey a version of the first law of thermodynamics, the subject is still not fully understood. Investigations in asymptotically anti-de Sitter (AdS) spacetimes have been carried out in considerable detail for three decades since it was pointed out that radiation/large AdS black hole phase transitions can take place [1]. Thermodynamic equilibrium can be defined, and many additional corroborative results have been obtained that provide strong evidence that such objects indeed behave as thermodynamic systems.

The proposal that the mass of an AdS black hole should be interpreted as the *enthalpy* of the spacetime represents an interesting new development in this subject. It emerged from geometric derivations of the Smarr formula for AdS black holes [2] that suggested the cosmological constant should be considered as a thermodynamic variable [3] analogous to pressure in the first law [4]. This has led to a number of investigations of black hole thermodynamics in this extended phase space [5–39]. Extensions of this idea to asymptotically de Sitter space times have also been recently explored, with the resultant thermodynamic notions for black holes remaining intact [40] (see also [41–49]).

The purpose of this paper is to provide a detailed overview and investigation of the thermodynamics of rotating asymptotically flat and AdS black holes and black rings in a canonical (fixed angular momentum) ensemble. Despite the intensive study such objects have been subject to [50], we find a variety of novel features emerge. In particular, we shall show that the thermodynamics of multiply-rotating Kerr-AdS black holes are, under certain circumstances, analogous to the "every day thermodynamics" of simple substances, such as reentrant phase transitions of multicomponent liquids, multiple first-order solid/liquid/gas phase transitions, and liquid/gas phase transitions of the van der Waals type. We also find that some of these phenomena, such as reentrant phase transitions, also occur for multiply-spinning asymptotically flat Myers–Perry black holes [51]. We compute the thermodynamic volume (conjugate to the pressure), and demonstrate that in all examples we consider it satisfies the reverse isoperimetric inequality. In particular, we find that this inequality remains true even for the thin asymptotically AdS black rings—providing a first confirmation of the reverse isoperimetric inequality conjecture for a black hole with non-spherical horizon topology.

1.1. Canonical Ensemble and Phase Transitions

Concentrating entirely on asymptotically flat and AdS black holes, we consider the proposal that *thermodynamic pressure* is given by:

$$P = -\frac{1}{8\pi}\Lambda = \frac{(d-1)(d-2)}{16\pi l^2} \tag{1}$$

where d stands for the number of spacetime dimensions, Λ is the cosmological constant, and l denotes the AdS radius. The asymptotically flat case has $P = 0$.

We shall study the thermodynamics in a *canonical ensemble*, that is for fixed black hole angular momenta J_i, and/or, in the case of charged black holes for fixed charge Q. The stability of supersymmetric AdS vacua [52] ensures that these kinds of thermodynamic ensembles can in principle be prepared by coupling an asymptotically AdS space-time to a bath that allows transfer of energy but not angular momentum or charge by coupling only to operators with $J_i = 0$, $Q = 0$. Hence within this context one can prepare a canonical ensemble with any fixed J_i and Q.

The equilibrium thermodynamics is governed by the *Gibbs free energy*, $G = G(T, P, J_i, Q)$, whose *global minimum* yields the state of a system for a fixed (T, P, J_i, Q). Note that there are states of matter, for example supercooled water, which do not correspond to the global minimum of G but rather are "metastable". Since mass of the black hole M is interpreted as the enthalpy, we have the following thermodynamic relation:

$$G = M - TS = G(P, T, J_1, \ldots, J_N, Q) \tag{2}$$

Here T and S stand for the horizon temperature and black hole entropy.

Understanding the behavior of G is essential for uncovering possible *thermodynamic phase transitions*. We shall see that it is often impossible to write the relation $G = G(T, P, J_i, Q)$ explicitly. For this reason we fix the pressure and angular momenta (and charge)—usually expressed parametrically through the horizon radius r_+—to particular values and plot G numerically. In this way we obtain $G - T$ diagrams which incorporate the information about possible phase transitions. An interesting alternative proposal which attracted attention in past few years is to consider an "effective thermodynamic geometry" and study its curvature singularities [53–58]. These then provide an information about presence of critical points and hence possible phase transitions in the given spacetime. However, in this paper we do not follow this strategy and concentrate entirely on analyzing the Gibbs free energy.

The *local thermodynamic stability* of a canonical ensemble is characterized by positivity of the specific heat at constant pressure:

$$C_P \equiv C_{P,J_1,\ldots,J_N,Q} = T\left(\frac{\partial S}{\partial T}\right)_{P,J_1,\ldots,J_N,Q} \tag{3}$$

We take negativity of C_P as a sign of local thermodynamic instability. Note that in this relation we automatically assume fixed J_i (and/or Q in the case of charged black holes). That is, our specific heat at constant P is in fact a specific heat at constant (P, J_i, Q) and coincides with C_J and/or C_Q considered in previous studies, e.g., [59,60]. When plotting the Gibbs free energy we shall plot branches with $C_P > 0$ in *red solid lines* and branches with $C_P < 0$ in *dashed blue lines*.

Once the behavior of the Gibbs free energy is known, we construct the associated *phase diagrams*. These are usually drawn in the $P - T$ plane and display the *coexistence lines* of various black hole

phases, inter-related by the first-order phase transitions, as well as reveal possible *critical points* where the coexistence lines terminate/merge together.

A renowned example of a transition in black hole spacetimes is the radiation/black hole first-order phase transition of Hawking and Page observed for Schwarzschild-AdS black holes immersed in a bath of radiation [1]. Such a phenomenon (discussed further in the next section) has a dual interpretation for a boundary quantum field theory via the AdS/CFT correspondence and is related to a confinement/deconfinement phase transition in the dual quark gluon plasma [61]. For charged or rotating black holes one likewise observes a small/large black hole first order phase transition reminiscent of the liquid/gas transition of the *van der Waals* fluid [4,6,8,15–17,21,22,27,28,33,39,62–71].

Interesting new phenomena appear in higher dimensions. Recently it has been shown [25] that in all dimensions $d \geq 6$ singly spinning Kerr-AdS black holes demonstrate the peculiar behavior of large/small/large black hole transitions reminiscent of *reentrant phase transitions* (RPT) observed for multicomponent fluid systems, gels, ferroelectrics, liquid crystals, and binary gases, e.g., [72]. A system undergoes an RPT if a monotonic variation of any thermodynamic quantity results in two (or more) phase transitions such that the final state is macroscopically similar to the initial state. For singly spinning Kerr-AdS black holes it was found [25] that for a fixed pressure within a certain range (and for a given angular momentum) a monotonic lowering of the temperature yields a large/small/large black hole transition. The situation is accompanied by a discontinuity in the global minimum of the Gibbs free energy, referred to as a *zeroth-order phase transition*, a phenomenon seen in superfluidity and superconductivity [73]. The RPT was also found for the four-dimensional Born–Infeld-AdS black hole spacetimes, deep in the non-linear regime of the Born–Infeld theory [16]. Remarkably, here we show (see Section 4) that a similar phenomenon is observed for the asymptotically flat doubly-spinning Myers–Perry black holes of vacuum Einstein gravity. Hence, neither exotic matter nor a cosmological constant (and hence the AdS/CFT correspondence) are required for this phenomena to occur in black hole spacetimes.

More intriguingly, other qualitatively different interesting phenomena known from the "every day thermodynamics" emerge when multiply rotating Kerr-AdS black holes are considered [26]. Depending on the ratios of the angular momenta, we find an analogue of a solid/liquid phase transition, multiple first-order *small/intermediate/large* black hole phase transitions with one *tricritical* (triple) and two critical points reminiscent of the solid/liquid/gas phase transition, and the 'standard' liquid/gas behavior of a van der Waals fluid. We review and provide more detail concerning these phenomena in the following sections.

1.2. Thermodynamic Volume

A conjugate quantity to the thermodynamic pressure is the *thermodynamic volume* V. For AdS black hole spacetimes this can formally be obtained from the *first law* of black hole thermodynamics by allowing the pressure, given by Equation (1), (and hence the cosmological constant) to vary:

$$\delta M = T\delta S + \sum_i \Omega_i \delta J_i + \Phi \delta Q + V \delta P \tag{4}$$

Here, Ω_i stand for the horizon angular velocities and Φ for the horizon electrostatic potential. The extended first law Equation (4) is consistent with the following *Smarr–Gibbs–Duhem relation*:

$$\frac{d-3}{d-2}M = TS + \sum_i \Omega_i J_i + \frac{d-3}{d-2}\Phi Q - \frac{2}{d-2}VP \tag{5}$$

an integrated formula relating the black hole mass to other thermodynamic quantities.

Euler's theorem enables one to derive the Smarr–Gibbs–Duhem relation [2]. This theorem states that if a function $f(x_1, \ldots, x_n)$ obeys the scaling relation $f(\alpha^{p_1}x_1, \ldots, \alpha^{p_n}x_n) = \alpha^r f(x_1, \ldots, x_n)$, then the function and its partial derivatives satisfy:

$$rf(x_1, \ldots, x_n) = p_1\left(\frac{\partial f}{\partial x_1}\right) + p_2\left(\frac{\partial f}{\partial x_2}\right) + \cdots + p_n\left(\frac{\partial f}{\partial x_n}\right) \tag{6}$$

If we consider the mass M of the black hole as a function of the area A, the charge Q, the various angular momenta J_i, and the pressure P, and taking in account that under a change of length scale $M \propto L^{d-3}$, $A \propto L^{d-2}$, $Q \propto L^{d-3}$, $J_i \propto L^{d-2}$ and $P \propto L^{-2}$ we can apply Euler's theorem Equation (6) and obtain:

$$(d-3)\,M = (d-2)\left(\frac{\partial M}{\partial A}\right)A + (d-2)\sum_i\left(\frac{\partial M}{\partial J_i}\right)J_i + (d-3)\left(\frac{\partial M}{\partial Q}\right)Q - \frac{2}{d-2}\left(\frac{\partial M}{\partial P}\right)P \tag{7}$$

Using the first law Equation (4) the Smarr–Gibbs–Duhem relation takes the form Equation (5).

Either of these relations can be used for calculating the thermodynamic volume V of AdS black holes. As we shall see in each case of interest, the final expression for V has a smooth limit for $P \to 0$, which defines a thermodynamic volume for asymptotically flat black holes. Alternatively, one can calculate V using the method of Killing co-potentials [2,10]. This consists of finding a co-potential 2-form whose divergence gives the Killing vector that is a horizon generator of the black hole spacetime under consideration. Once known, such a co-potential is integrated to give the thermodynamic volume. However finding the co-potential is not easy. For spherical rotating black hole spacetimes this was possible due to the presence of a special hidden symmetry of a Killing–Yano tensor [74]. This symmetry does not exist for black rings or black saturns.

The thermodynamic volume has dimensions of (length)$^{d-1}$ and describes a spatial volume characterizing the black hole spacetime. For alternative definitions of various volumes associated with black hole spacetimes, see [42,75–77]. In particular, for the Schwarzschild black hole in $d = 4$ one obtains the intriguing relation:

$$V = \frac{4}{3}\pi r_+^3 \tag{8}$$

which is the volume of a ball of radius r_+ in the Euclidean space, with r_+ being the horizon radius in Schwarzschild coordinates. For a wide variety of asymptotically flat and AdS black hole spacetimes with spherical horizon topology the thermodynamic volume has been calculated in [10]. Although much more complicated in the presence of angular momenta and various additional charges, the thermodynamic volume in all cases studied so far was found to obey the so called *reverse isoperimetric inequality*, an inequality between the horizon area (black hole entropy) and the thermodynamic volume.

In Euclidean space $\mathbb{E}^{d-1}$, the isoperimetric inequality for the volume $\mathcal{V}$ of a connected domain whose area is $\mathcal{A}$ states that the ratio:

$$\mathcal{R} = \left(\frac{(d-1)\mathcal{V}}{\omega_{d-2}}\right)^{\frac{1}{d-1}}\left(\frac{\omega_{d-2}}{\mathcal{A}}\right)^{\frac{1}{d-2}} \tag{9}$$

where:

$$\omega_d = \frac{2\pi^{\frac{d+1}{2}}}{\Gamma\left(\frac{d+1}{2}\right)} \tag{10}$$

is the volume of the unit d-sphere, obeys $\mathcal{R} \leq 1$, with equality if and only if the domain is a standard round ball. It was *conjectured* in [10] that a *reverse isoperimetric inequality*:

$$\mathcal{R} \geq 1 \tag{11}$$

holds for any asymptotically AdS black hole, where $\mathcal{A}$ is the black hole horizon area and $\mathcal{V}$ is the thermodynamic volume V, the bound being saturated for Schwarzschild-AdS black holes. In other words, for a fixed thermodynamic volume the entropy of the black hole is maximized for the Schwarzschild-AdS spacetime. Up to now this conjecture has been verified for a variety of (charged rotating) black holes with the horizon of spherical topology. In Section 6 we show that it remains true for (thin) black rings with toroidal horizon topology.

1.3. Equation of State

Once the thermodynamic volume is known and the cosmological constant identified with the thermodynamic pressure, one can, for a given black hole, write down the corresponding "fluid" *equation of state* relating the pressure, temperature, volume and other external parameters characterizing the black hole, $P = P(V, T, J_i, Q)$. Similar to references [15,16], instead of V we employ a new quantity v, corresponding to the "*specific volume*" of the fluid, defined by:

$$v = \frac{4}{d-2}\left(\frac{(d-1)V}{\omega_{d-2}}\right)^{\frac{1}{d-1}} \tag{12}$$

where in physical units one has to replace $v \to v l_P^{d-2}$ with l_P being the Planck length. Hence we consider the following *equation of state*:

$$P = P(v, T, J_i, Q) \tag{13}$$

We pause to note an interesting coincidence pointed to us by Jennie Traschen in private communications. Similar to the specific volume of the fluid which as per usual is taken to be the total volume of the fluid divided by the number of particles, for non-rotating AdS black holes one may define their specific volume to be:

$$\tilde{v} = V/N \tag{14}$$

with V being the thermodynamic volume and N being identified with the number of degrees of freedom associated with the black hole, which is proportional to its horizon area in Planck units, *i.e.*, $N = \frac{1}{4}\frac{d-2}{d-1}\frac{A}{l_P^2}$. Although the two definitions agree for non-rotating black holes, they differ significantly when the rotation is taken into account. In particular, for the ultraspinning black holes (discussed in Section 3) v defined by Equation (12) remains finite whereas $\tilde{v}$ diverges to infinity since N goes to zero in this limit.

The equation of state allows one to employ standard thermodynamic machinery and for instance calculate the critical exponents associated with the critical point. For example, the "$P - v$" criticality of charged AdS black holes in four dimensions was studied in [15]. The system exhibits a first-order phase transition à la van der Waals, with the coexistence line terminating at a critical point where the

phase transition becomes second-order [32] and is characterized by the following (mean field theory) critical exponents:

$$\alpha = 0\,, \quad \beta = \frac{1}{2}\,, \quad \gamma = 1\,, \quad \delta = 3 \tag{15}$$

The same remains true for charged AdS black holes in higher dimensions [16,17,27]. In what follows we extend the analysis to singly spinning Kerr-AdS black holes in all dimensions. Since in the rotating case the equation of state Equation (13) cannot be constructed analytically for any value of the rotation parameter, we investigate it numerically and develop a systematic analytic expansion in the ultraspinning and slow rotation regimes. The *slow rotation expansion* allows us to approximately calculate the critical exponents and verify that they remain as predicted in Equation (15) by mean field theory. The *ultraspinning expansion* approximates the properties of black membranes and relates to the effective blackfold description [78] and the Gregory–Laflamme instability [79].

The plan of our paper is as follows. In the next section we recapitulate the relevant thermodynamic results for four-dimensional black holes. Section 3 deals with the thermodynamics and various phase transitions of higher-dimensional Kerr-AdS black holes, whereas Section 4 studies their asymptotically flat cousins. Section 5 is devoted to analytically known 5-dimensional vacuum black holes with non-spherical horizon topology. In Section 6 AdS black rings in all dimensions are studied in the thin (ultraspinning) approximation. The aforementioned thermodynamic phase transitions are put in context with various classical instabilities in Section 7. Section 8 is devoted to the final discussion.

2. Black Holes in 4d

To set the stage for higher-dimensional results in this section we review some interesting features about the thermodynamics of four-dimensional black holes. We concentrate our attention on plotting the Gibbs free energy and discussing the associated phase diagrams. For asymptotically flat black holes we have $P = 0$, whereas from Equation (1), $P = 3/(8\pi l^2)$ for asymptotically AdS black holes.

2.1. Asymptotically Flat Black Holes

2.1.1. Schwarzschild Solution

To start with let us consider a spherically symmetric (four-dimensional) metric element:

$$ds^2 = -f(r)dt^2 + \frac{dr^2}{f(r)} + r^2 d\Omega^2_{(k)} \tag{16}$$

where $d\Omega^2_{(k)} = d\theta^2 + \frac{1}{k}\sin^2\!\big(\sqrt{k}\theta\big)d\varphi^2$ is a standard metric on a compact 2-surface, with $k = \{1, 0, -1\}$ denoting spherical, planar, and hyperbolic geometries. Setting $k = 1$, the horizon radius is the largest r_+ solving:

$$f(r_+) = 0 \tag{17}$$

In our examples, limited to vacuum spacetimes with possibly a negative cosmological constant and Maxwell field, one gets the following expressions for the black hole temperature, horizon entropy, and thermodynamic volume:

$$T = \frac{f'(r_+)}{4\pi}\,, \quad S = \frac{A}{4} = \pi r_+^2\,, \quad V = \frac{4}{3}\pi r_+^3 \tag{18}$$

Once the mass M is determined the Gibbs free energy is given by Equation (2), $G = M - TS$.

In particular, for the *Schwarzschild black hole* one has:

$$f = 1 - \frac{2M}{r} \tag{19}$$

and the corresponding thermodynamic quantities are :

$$M = \frac{r_+}{2}\,, \quad T = \frac{1}{4\pi r_+}\,, \quad G = \frac{r_+}{4} = \frac{1}{16\pi T} \tag{20}$$

and it is clear the Smarr relation Equation (5), $M = 2TS$, is satisfied. It is not difficult to show that $C_P = -2\pi r_+^2 < 0$, which corresponds to the well known fact that the Schwarzschild black hole is locally thermodynamically unstable. This is related to the Gregory–Laflamme instability of the corresponding Schwarzschild black string [79]. The thermodynamic instability of a black hole can be related to the corresponding classical instability, see, e.g., [80–84]. The Gibbs free energy, displayed in Figure 1, has no interesting features and indicates no phase transitions.

Figure 1. Gibbs free energy: Schwarzschild black hole. The dashed blue line corresponds to a negative specific heat; for an asymptotically flat Schwarzschild black hole this quantity is negative for any temperature.

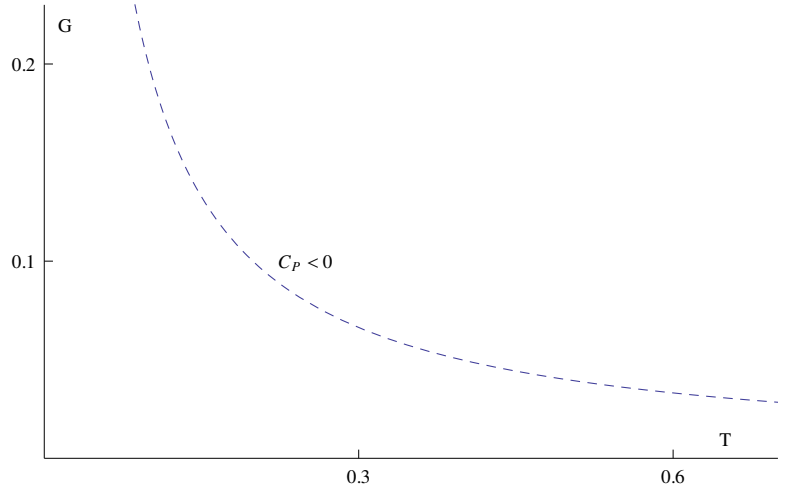

2.1.2. Charged Black Hole: Reissner–Nordström Solution

When the charge Q is added to the Schwarzschild black hole, we obtain the Reissner–Nordström (RN) solution, for which the metric is Equation (16) with:

$$f(r) = 1 - \frac{2M}{r} + \frac{Q^2}{r^2} \tag{21}$$

The thermodynamic quantities are:

$$\begin{aligned} T &= \frac{r_+^2 - Q^2}{4\pi r_+^3}\,, \quad M = \frac{r_+^2 + Q^2}{2r_+}\,, \quad \Phi = \frac{Q}{r_+} \\ G &= \frac{r_+^2 + 3Q^2}{4r_+}\,, \quad C_P = 2\pi r_+^2 \frac{r_+^2 - Q^2}{3Q^2 - r_+^2} \end{aligned} \tag{22}$$

and the Smarr relation Equation (5) is again satisfied. The specific heat capacity is positive for small strongly charged black holes:

$$\sqrt{3}|Q| > r_+ > |Q| \tag{23}$$

or, equivalently, $\sqrt{3}M/2 < |Q| < M$. This range corresponds to a thermodynamically stable branch of near extremal black holes which globally minimize the Gibbs free energy, see Figure 2. Consequently and counter-intuitively in a fixed charge canonical ensemble strongly charged small RN black holes are thermodynamically preferred to weakly charged (almost Schwarzschild-like) large black holes. (Despite the fact that the entropy is larger on the upper branch in Figure 2, since it increases quadratically with r_+, the Gibbs free energy in the lower branch is the global minimum at fixed Q due to the larger enthalpy contribution in the upper branch.) A directly related result is that in the range Equation (23) there are no negative modes in the Euclidean action, whereas the negative mode appears for $r_+ \geq \sqrt{3}|Q|$, indicating the onset of Schwarzschild-like behavior [59] .

Figure 2. Gibbs free energy: RN black hole. The Gibbs free energy of $Q = 1$ RN black hole is displayed. The horizon radius r_+ increases from left to right and then up; $T = 0$ corresponds to the extremal black hole with $r_+ = M = Q = 1$. For a fixed temperature there are two branches of RN black holes. The lower thermodynamically preferred branch corresponds to small strongly charged nearly extremal black holes with positive C_P. The upper branch of weakly charged RN (almost Schwarzschild-like) black holes has higher Gibbs free energy and negative specific heat and hence is thermodynamically unstable. Its Euclidean action also possesses a negative zero mode. The situation for the Kerr-AdS black hole is qualitatively similar, with fixed J replacing fixed Q.

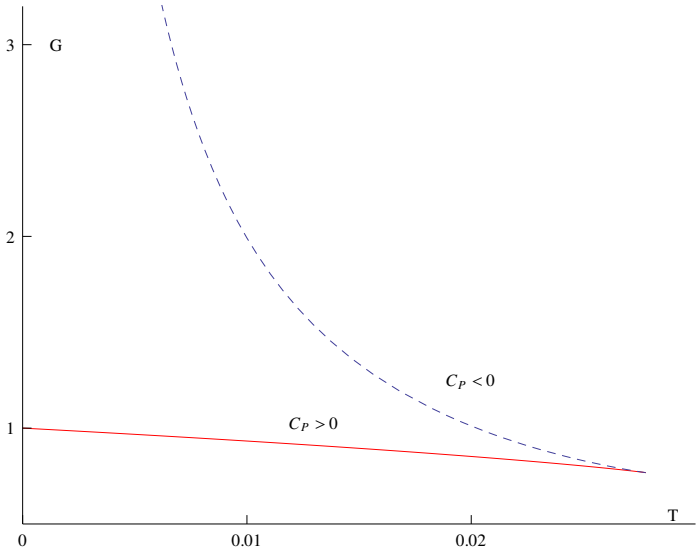

2.1.3. Rotating Black Hole: Kerr Solution

The rotating black hole metric described by the Kerr solution is written:

$$\begin{aligned} ds^2 &= -dt^2 + \frac{2Mr}{\Sigma}\left(dt - a\sin^2\theta d\phi\right)^2 + \frac{\Sigma}{\Delta}dr^2 \\ &+ \Sigma d\theta^2 + \left(r^2 + a^2\right)\sin^2\theta d\phi^2 \end{aligned} \tag{24}$$

where:

$$\Sigma = r^2 + a^2\cos^2\theta\,, \quad \Delta = r^2 + a^2 - 2Mr \tag{25}$$

The thermodynamic quantities are:

$$\begin{aligned} M &= \frac{r_+^2 + a^2}{2r_+}\,, \quad T = \frac{1}{2\pi}\left[\frac{r_+}{a^2 + r_+^2} - \frac{1}{2r_+}\right], \quad S = \pi(a^2 + r_+^2) = \frac{A}{4} \\ J &= \frac{a}{2r_+}(a^2 + r_+^2)\,, \quad \Omega = \frac{a}{r_+^2 + a^2}\,, \quad V = \frac{r_+ A}{3}\left(1 + \frac{a^2}{2r_+^2}\right) \\ G &= \frac{3a^2 + r_+^2}{4r_+}\,, \quad C_P = \frac{2\pi(r_+^2 - a^2)(r_+^2 + a^2)^2}{3a^4 + 6r_+^2 a^2 - r_+^4} \end{aligned} \tag{26}$$

and satisfy Equation (5).

The behavior of the Gibbs free energy is qualitatively very similar to that of the charged black hole [15], given by Figure 2, with fixed J replacing fixed Q. In fact the thermodynamic behavior remains qualitatively same even in the charged rotating Kerr–Newman case. As for the RN black hole we observe two branches of the Gibbs free energy. The lower one occurs for:

$$\sqrt{3 + 2\sqrt{3}}|a| > r_+ > |a| \tag{27}$$

or, equivalently, $M > |a| > M\sqrt{2\sqrt{3} - 3}$. It is thermodynamically preferred and corresponds to small fast rotating nearly extremal black holes with positive C_P. The upper branch of slowly rotating (almost Schwarzschild-like) black holes has higher Gibbs free energy and negative specific heat and is thermodynamically unstable. Its Euclidean action also possesses a negative zero mode [60].

We conclude that in the canonical ensemble of fixed J, the nearly extremal fast spinning black holes are thermodynamically preferred to the slowly rotating ones.

2.2. AdS Black Holes

2.2.1. Schwarzschild-AdS

The simplest (spherical) asymptotically AdS black hole is described by the Schwarzschild-AdS spacetime. The metric takes the form Equation (16) with:

$$f = 1 - \frac{2M}{r} + \frac{r^2}{l^2} \tag{28}$$

The thermodynamic quantities are:

$$\begin{aligned} T &= \frac{1}{4\pi r_+ l^2}(l^2 + 3r_+^2)\,, \quad S = \pi r_+^2\,, \quad V = \frac{4}{3}\pi r_+^3 \\ M &= \frac{r_+}{2}\left(1 + \frac{r_+^2}{l^2}\right), \quad G = \frac{r_+}{4}\left(1 - \frac{r_+^2}{l^2}\right), \quad C_P = 2\pi r_+^2 \frac{3r_+^2 + l^2}{3r_+^2 - l^2} \end{aligned} \tag{29}$$

and satisfy Equation (5), $M = 2TS - 2VP$, due to the presence of the PV term.

We observe a qualitatively different thermodynamic behavior when compared to the asymptotically flat Schwarzschild case. Specifically C_P is no longer always negative: it becomes positive for large (when compared to the AdS radius) black holes:

$$r_+ > r_{\text{min}} = \frac{l}{\sqrt{3}} \tag{30}$$

while it is negative for $r_+ < r_{\text{min}}$ and ill defined at $r_+ = r_{\text{min}}$.

The behavior of the Gibbs free energy G is displayed in Figure 3. We observe a minimum temperature $T_{\text{min}} = 2\sqrt{3}/(4\pi l)$, corresponding to r_{min}, below which no black holes can exist. Above this temperature we have two branches of black holes. The upper one describes small (Schwarzschild-like) black holes with negative specific heat; these are thermodynamically unstable and cannot be in a thermal equilibrium with a thermal bath of radiation. The large ($r_+ > r_{\text{min}}$) black holes at lower branch have positive specific heat and hence are locally thermodynamically stable. However, just above T_{min} the Gibbs free energy of such black holes is positive and the thermal AdS space with approximately zero Gibbs free energy represents a globally preferred thermodynamic state. We refer to a thermal AdS space as a (global) AdS space coupled to a bath of thermal radiation. Since the number of particle quanta representing the radiation is relatively small, the corresponding Gibbs free energy approximately equals zero. This continues until temperature $T_{\text{HP}} \approx 1/(\pi l)$ for which the black hole Gibbs free energy becomes negative, with the corresponding black hole radius given by:

$$r_{\text{HP}} = l \tag{31}$$

Black holes with $r_+ > r_{\text{HP}}$ have negative Gibbs free energy and represent the globally preferred state. This means that at $T = T_{\text{HP}}$ there is a first order *Hawking–Page* [1] phase transition between thermal radiation and large black holes. This phase transition can be interpreted as a confinement/deconfinement phase transition in the dual quark gluon plasma [61].

Considering an extended phase space, the coexistence line of thermal radiation/large black hole phases, determined from $G = 0$, reads:

$$P|_{\text{coexistence}} = \frac{3\pi}{8} T^2 \tag{32}$$

The corresponding $P - T$ phase diagram is displayed in Figure 4.

Figure 3. Gibbs free energy: Schwarzchild-AdS black hole. When compared to the asymptotically flat Schwarzschild case (Figure 1) for $P > 0$ the Gibbs free energy acquires a new thermodynamically stable branch of large black holes. For $T > T_{\text{HP}}$ this branch has negative Gibbs free energy and the corresponding black holes represent the globally thermodynamically preferred state.

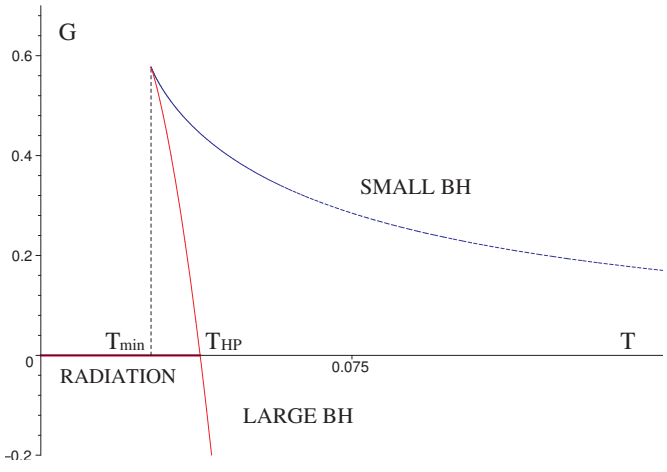

Figure 4. Hawking–Page transition is a first-order phase transition between thermal radiation in AdS and large stable Schwarzschild-AdS black hole. It occurs when G of the Schwarzschild-AdS black hole approximately vanishes. Considering various pressures P gives the radiation/large black hole coexistence line Equation (32) displayed in this figure. Similar to a "solid/liquid" phase transition, this line continues all the way to infinite pressure and temperature.

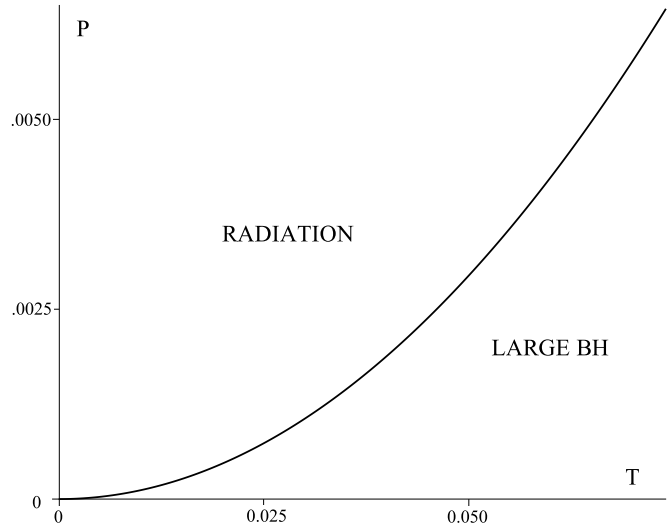

By rewriting the temperature Equation (29) while using Equation (1), we get a corresponding 'fluid equation of state' for the Schwarzschild-AdS black hole, given by:

$$P = \frac{T}{v} - \frac{1}{2\pi v^2}, \quad v = 2\Big(\frac{3V}{4\pi}\Big)^{1/3} = 2r_+ \tag{33}$$

The behavior of this equation is displayed in the $P - V$ diagram in Figure 5. For each isotherm there is a maximum which occurs for $v = 1/(\pi T)$. For a given temperature this precisely corresponds to $r_+ = r_{\text{min}}$; the dashed blue curves with positive slope (and possibly negative pressures) to the left of the maximum correspond to small black holes with negative C_P which are thermodynamically unstable, whereas solid red curves correspond to large black holes with positive C_P that are locally thermodynamically stable.

Let us compare the fluid equation of state of the Schwarzschild-AdS black hole Equation (33) with the famous *van der Waals (VdW) equation*, e.g., [85], which is a popular two parameter closed form modification of the ideal gas law that approximates the behavior of real fluids. The VdW equation takes into account the nonzero size of fluid molecules (described by a constant $b > 0$) and the attraction between them (described by a constant $a > 0$) and is often used to capture basic qualitative features of the liquid–gas phase transition. The equation reads (setting the Boltzmann constant $k_B = 1$):

$$P = \frac{T}{v - b} - \frac{a}{v^2} \tag{34}$$

where $v = V/N$ is the specific volume of the fluid, P its pressure, T its temperature, and the fluid parameters a and b are characteristics of a given fluid. The characteristic VdW $P-v$ diagram is displayed in Figure 6. The equation admits a critical point, described by $\{T_c, v_c, P_c\}$, with universal critical ratio:

$$\rho_c = \frac{P_c v_c}{T_c} = \frac{3}{8} \tag{35}$$

and the mean field theory critical exponents Equation (15).

Figure 5. Equation of state: Schwarzschild-AdS black hole. The equation of state Equation (33) is displayed for various temperatures. For a given temperature the maximum occurs at $v = 2r_0$. The dashed blue curves correspond to small unstable black holes. The red curves depict the stable large black hole branch; we observe 'ideal gas' behavior for large temperatures.

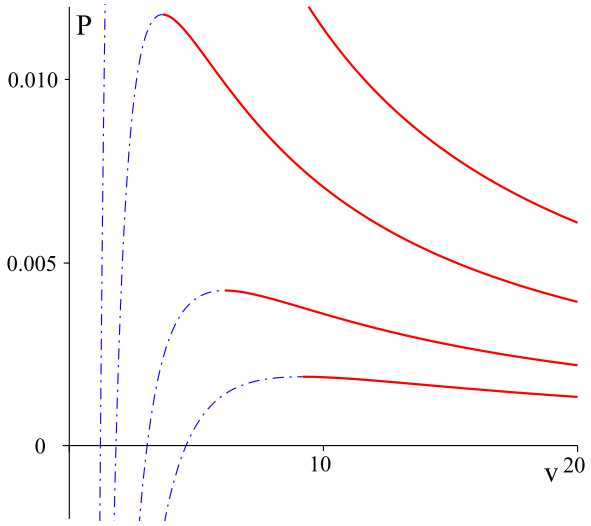

Figure 6. $P-v$ diagram of van der Waals fluid. The temperature of isotherms decreases from top to bottom. The two upper dashed lines correspond to the "ideal gas" phase for $T > T_c$, the critical isotherm $T = T_c$ is denoted by the thick solid line, lower solid lines correspond to temperatures smaller than the critical temperature; for $T < T_c$ parts of the isotherms are actually unphysical, and must be replaced by a constant pressure line according to the Maxwell's equal area prescription [15]. Constants a and b were set equal to one.

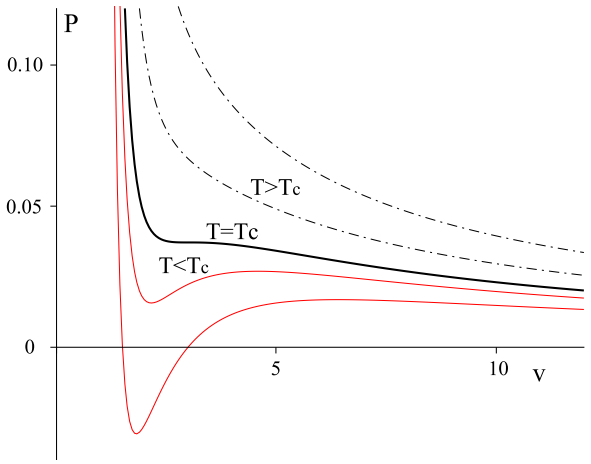

We pause to consider topological Schwarzschild-AdS black holes. Making use of the metric Equation (16) for arbitrary k, the formulae (29) take the following more general form:

$$\begin{aligned} M &= \frac{r_+ A_k}{8}\left(k + \frac{r_+^2}{\ell^2}\right), \quad S = \frac{\pi A_k}{4} r_+^2 \\ T &= \frac{k\ell^2 + 3r_+^2}{4\pi \ell^3 r_+}, \quad V = \frac{\pi A_k}{3} r_+^3 \end{aligned} \tag{36}$$

where A_k is the area of the constant-curvature space divided by π; for a sphere, $A_{k=1} = 4$, for a torus, $A_{k=0} = AB$, where A and B and the sides of the torus, and there is no nice simple formula for $A_{k=-1}$. In all cases the Smarr formula (5) and first law Equation (4) hold. It is then straightforward to show that the fluid corresponding to the Schwarzschild-AdS black hole is characterized by:

$$a = \frac{k}{2\pi}, \quad b = 0 \tag{37}$$

That is, its equation of state differs from the ideal gas law by the presence of a nontrivial parameter $a = k/(2\pi)$. This is directly related to the topology of the horizon. For *planar* Schwarzschild-AdS black holes, $k = 0$ and we recover the ideal gas law characterized by $a = 0 = b$:

$$Pv = T \tag{38}$$

whereas for the $k = -1$ hyperbolic case we get a peculiar 'repulsion' feature $a = -\frac{1}{2\pi} < 0$, with $b = 0$, the volume of molecules still vanishing.

We note one more interesting fact for the planar ($k = 0$) AdS black holes. In this case the following specific Smarr-like relation has been employed e.g., [86,87]:

$$3M = 2TS \tag{39}$$

[or $(d-1)M = (d-2)TS$ in d-dimensions] without any reference to the PV term. The value of our Smarr relation (5) is that it follows from the general geometric argument and applies to a wide class of (even possibly unknown) solutions that satisfy the assumptions of the theorem, whereas Equation (39) is a 'phenomenological' observation valid for a particular sub-class of solutions. We also note that this relation is not related to the corresponding first law, $dM = TdS$, by a dimensional scaling argument.

2.2.2. Charged AdS Black Hole

The charged AdS black hole metric is described by Equation (16) with:

$$f = 1 - \frac{2M}{r} + \frac{Q^2}{r^2} + \frac{r^2}{l^2} \tag{40}$$

The thermodynamic quantities are:

$$\begin{aligned} T &= \frac{1}{4\pi r_+^3 l^2}\left(l^2(r_+^2 - Q^2) + 3r_+^4\right), \quad S = \pi r_+^2 \\ V &= \frac{4}{3}\pi r_+^3, \quad \Phi = \frac{Q}{r_+}, \quad G = \frac{l^2 r_+^2 - r_+^4 + 3Q^2 l^2}{4 l^2 r_+} \\ C_P &= 2\pi r_+^2 \frac{3r_+^4 + l^2 r_+^2 - Q^2 l^2}{3r_+^4 - l^2 r_+^2 + 3Q^2 l^2} \end{aligned} \tag{41}$$

The specific heat is negative for:

$$\frac{l\sqrt{1-\sqrt{1-36Q^2/l^2}}}{\sqrt{6}} < r_+ < \frac{l\sqrt{1+\sqrt{1-36Q^2/l^2}}}{\sqrt{6}} \tag{42}$$

and positive otherwise.

It was first noticed in [62,63] that in a canonical (fixed charge) ensemble, charged AdS black holes allow for a first order *small-black-hole/large-black-hole* phase (SBH/LBH) transition which is in many ways reminiscent of the liquid/gas transition of a van der Waals fluid. This analogy becomes more complete in extended phase space [15]. Namely, the equation of state:

$$P = \frac{T}{v} - \frac{1}{2\pi v^2} + \frac{2Q^2}{\pi v^4}\,, \quad v = 2r_+ \tag{43}$$

mimics qualitatively the behavior of the van der Waals equation, shown in Figure 6, with its black hole counterpart Equation (43) illustrated in Figure 7. Below P_c, the Gibbs free energy displays a characteristic swallowtail behavior, depicted in Figure 8, indicating a first-order SBH/LBH phase transition. The corresponding coexistence line is displayed in Figure 9. It terminates at a critical point, characterized by:

$$T_c = \frac{\sqrt{6}}{18\pi Q}\,, \quad v_c = 2\sqrt{6}Q\,, \quad P_c = \frac{1}{96\pi Q^2} \tag{44}$$

where the phase transition becomes of the second order [32,88], and is characterized by the mean field theory critical exponents Equation (15). Remarkably the relation $\rho_c = P_c v_c/T_c = 3/8$ is identical to the van der Waals case. The overall situation reminds one of the liquid/gas phase transition. A similar situation occurs for charged AdS black holes in higher dimensions [16].

Figure 7. Equation of state: charged AdS black hole. The temperature of isotherms decreases from top to bottom. The two upper dashed lines correspond to the "ideal gas" one-phase behavior for $T > T_c$, the critical isotherm $T = T_c$ is denoted by the thick solid line, lower solid lines correspond to temperatures smaller than the critical temperature. We have set $Q = 1$. $P - v$ diagram for the Kerr-AdS black hole with $J = 1$ is qualitatively similar.

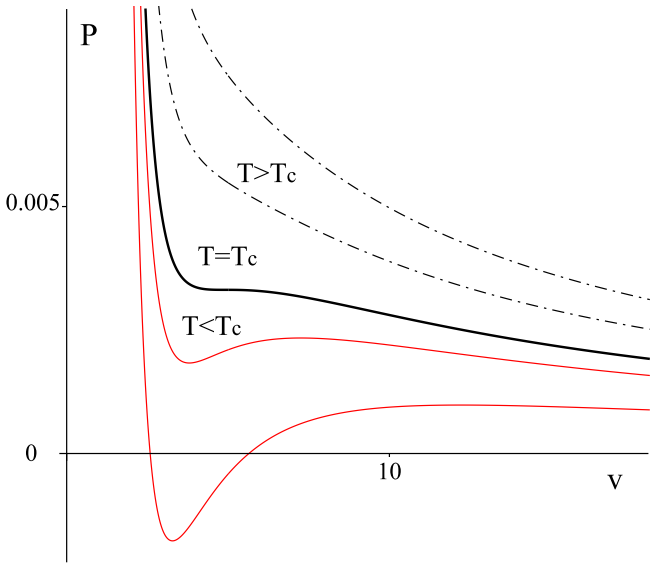

Figure 8. Gibbs free energy: charged AdS black hole. Characteristic swallowtail behavior is observed for $P < P_c$, corresponding to a small/large black hole phase transition. An unstable branch of the Gibbs free energy is displayed in dashed blue line. We have set $Q = 1$. The behavior of G for Kerr-AdS black hole with $J = 1$ is qualitatively similar.

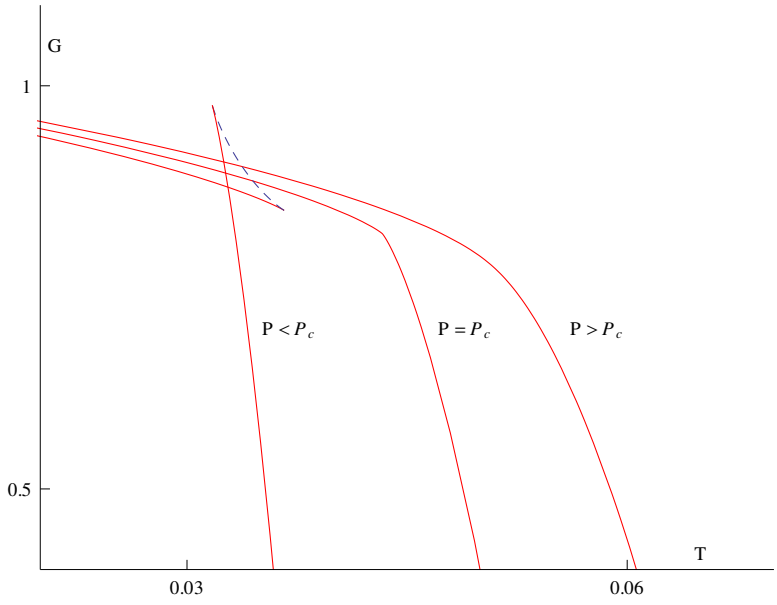

Figure 9. Phase diagram: charged AdS black hole. The coexistence line of the SBH/LBH phase transition of the charged AdS black hole system in (P, T)-plane is displayed. The critical point is highlighted by a small circle at the end of the coexistence line. The phase diagram for a Kerr-AdS black hole with $J = 1$ is qualitatively similar.

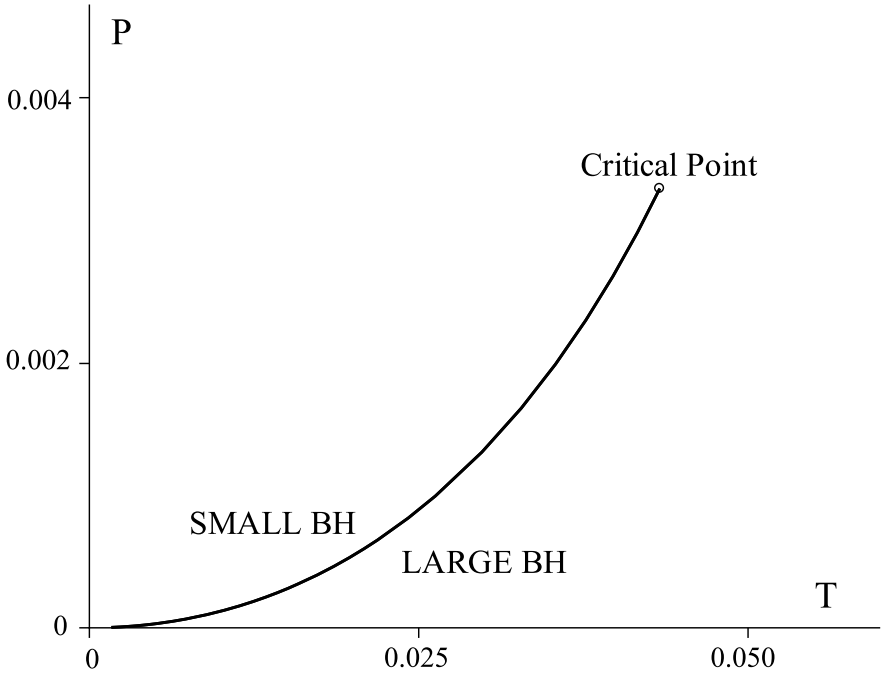

We remark that the Hawking–Page phase transition as well as the SBH/LBH phase transition à la van der Waals can be also observed for asymptotically flat or de Sitter charged black holes provided these are placed in a finite cavity [89].

We close this subsection by noting that strongly charged small AdS black holes are subject to superradiant instabilities. For a charged scalar field coupled to Einstein–Maxwell theory a similar situation occurs: at small temperatures charged scalar hair forms and the resulting "hairy black holes" are thermodynamically preferred [90–97]. This means that in the presence of a charged scalar field, the left-most branch of small black holes in the Gibbs free diagram Figure 8, although locally thermodynamically stable, does not globally minimize the Gibbs free energy. Rather, there is another branch of hairy black holes with lower Gibbs free energy. The hair/no-hair black hole phase transition is of the second order and underlies the theory of holographic superconductors.

2.2.3. Kerr-AdS

The thermodynamics of four-dimensional rotating AdS black holes is qualitatively similar to the charged AdS case. In fact qualitatively similar behavior occurs for charged rotating AdS black holes, see [4]. The metric is:

$$ds^2 = -\frac{\Delta}{\rho^2}(dt - \frac{a}{\Xi}\sin^2\theta d\varphi)^2 + \frac{\rho^2}{\Delta}dr^2 + \frac{\rho^2}{\Sigma}d\theta^2 + \frac{\Sigma\sin^2\theta}{\rho^2}[adt - \frac{(r^2+a^2)}{\Xi}d\varphi]^2 \tag{45}$$

where:

$$\begin{aligned} \Delta &= (r^2+a^2)(1+\frac{r^2}{l^2}) - 2mr\,, \quad \Sigma = 1 - \frac{a^2}{l^2}\cos^2\theta \\ \Xi &= 1 - \frac{a^2}{l^2} \quad \rho^2 = r^2 + a^2\cos^2\theta \end{aligned}$$

The thermodynamic quantities read:

$$\begin{aligned} M &= \frac{m}{\Xi^2}\,, \quad J = \frac{ma}{\Xi^2}\,, \quad \Omega = \frac{a}{l^2}\frac{r_+^2+l^2}{r_+^2+a^2} \\ T &= \frac{1}{2\pi r_+}\Big[\frac{(a^2+3r_+^2)(r_+^2/l^2+1)}{2(a^2+r_+^2)} - 1\Big] \\ S &= \pi\frac{(a^2+r_+^2)}{\Xi} = \frac{A}{4}\,, \quad V = \frac{r_+A}{3}\Big(1 + \frac{1+r_+^2/l^2}{2r_+^2}\frac{a^2}{\Xi}\Big) \\ G &= \frac{(r_+^2+3a^2)l^4 - (r_+^2-a^2)^2l^2 + (a^2+3r_+^2)a^2r_+^2}{l^4\Xi^2 r_+} \end{aligned} \tag{46}$$

and satisfy the Smarr relation Equation (5); rather lengthy formula for C_P can be found in [60].

The Gibbs free energy, equation of state, and the $P-T$ phase diagram are qualitatively similar to Figures 7–9—with fixed J replacing fixed Q. For any fixed J, there is a critical point, characterized by (P_c, V_c, T_c), that can be determined numerically. For $P < P_c$, the Gibbs free energy displays swallowtail behavior and there is a corresponding SBH/LBH first order phase transition with a phase diagram similar to Figure 9. It will be shown in the next section that in the limit of slow rotation, $a \ll l$, the equation of state can be approximated by:

$$\begin{aligned} P &= \frac{T}{v} - \frac{1}{2\pi v^2} + \frac{48J^2}{\pi v^6} - \frac{384J^4(7+8\pi Tv)}{(1+\pi Tv)^2\pi v^{10}} + \frac{36864(13\pi Tv+11)J^6}{\pi v^{14}(1+\pi Tv)^3} + O\big[(a/l)^8\big] \\ v &= 2\Big(\frac{3V}{4\pi}\Big)^{1/3} \end{aligned} \tag{47}$$

The first three terms were first obtained in [16]. Using this equation of state, one can approximately find the critical point and study its characteristics. In particular, one finds that the critical exponents remain as predicted by the mean field theory, given by Equation (15).

We pause to remark that, similar to the charged AdS case, the rotating AdS black holes close to extremality are unstable with respect to superradiant instabilities; the resultant objects (hairy black hole, soliton, or boson star) are expected to globally minimize the Gibbs free energy [98–101].

3. Higher-Dimensional Kerr-AdS Black Hole Spacetimes

3.1. General Metrics

General Kerr-AdS black hole spacetimes [102,103] are d-dimensional metrics that solve the Einstein equations with cosmological constant:

$$R_{ab} = \frac{2\Lambda}{(d-2)} g_{ab} \tag{48}$$

and generalize the d-dimensional asymptotically-flat rotating black hole spacetimes of Myers and Perry [51]. In Boyer–Lindquist coordinates the metric takes the form:

$$\begin{aligned} ds^2 &= -W\Big(1+\frac{r^2}{l^2}\Big)d\tau^2 + \frac{2m}{U}\Big(Wd\tau - \sum_{i=1}^{N}\frac{a_i\mu_i^2 d\varphi_i}{\Xi_i}\Big)^2 + \sum_{i=1}^{N}\frac{r^2+a_i^2}{\Xi_i}\mu_i^2 d\varphi_i^2 + \frac{Udr^2}{F-2m} \\ &\quad + \sum_{i=1}^{N+\varepsilon}\frac{r^2+a_i^2}{\Xi_i}d\mu_i^2 - \frac{l^{-2}}{W(1+r^2/l^2)}\Big(\sum_{i=1}^{N+\varepsilon}\frac{r^2+a_i^2}{\Xi_i}\mu_i d\mu_i\Big)^2 \end{aligned} \tag{49}$$

where:

$$\begin{aligned} W &= \sum_{i=1}^{N+\varepsilon}\frac{\mu_i^2}{\Xi_i}, \quad U = r^{\varepsilon}\sum_{i=1}^{N+\varepsilon}\frac{\mu_i^2}{r^2+a_i^2}\prod_{j}^{N}(r^2+a_j^2) \\ F &= r^{\varepsilon-2}\Big(1+\frac{r^2}{l^2}\Big)\prod_{i=1}^{N}(r^2+a_i^2), \quad \Xi_i = 1-\frac{a_i^2}{l^2} \end{aligned} \tag{50}$$

To treat even ($\varepsilon = 1$) odd ($\varepsilon = 0$) spacetime dimensionality d simultaneously, we have parametrized:

$$d = 2N + 1 + \varepsilon \tag{51}$$

and in even dimensions set for convenience $a_{N+1} = 0$. The coordinates μ_i are not independent, but obey the constraint:

$$\sum_{i=1}^{N+\varepsilon}\mu_i^2 = 1 \tag{52}$$

In general the spacetime admits N independent angular momenta J_i, described by N rotation parameters a_i, and generalizes the previously known d-dimensional singly-spinning and 5-dimensional doubly spinning cases [104]. In $d = 4$ it reduces to the four-dimensional Kerr-AdS metric studied in the previous section. With this metric it shares a remarkable property—it possesses a hidden symmetry associated with the Killing–Yano tensor [74] that is responsible for integrability of geodesic motion and various test field equations in these spacetimes, see, e.g., review [105].

The thermodynamic quantities associated with Kerr-AdS black holes were first calculated in [106]. The mass M, the angular momenta J_i, and the angular velocities of the horizon Ω_i read:

$$M = \frac{m\omega_{d-2}}{4\pi(\prod_j \Xi_j)}\Big(\sum_{i=1}^{N}\frac{1}{\Xi_i} - \frac{1-\varepsilon}{2}\Big)\,, \quad J_i = \frac{a_i m\omega_{d-2}}{4\pi\Xi_i(\prod_j \Xi_j)}\,, \quad \Omega_i = \frac{a_i(1+\frac{r_+^2}{l^2})}{r_+^2+a_i^2} \tag{53}$$

while the temperature T, the horizon area A, and the entropy S are given by:

$$\begin{aligned} T &= \frac{1}{2\pi}\Big[r_+\Big(\frac{r_+^2}{l^2}+1\Big)\sum_{i=1}^{N}\frac{1}{a_i^2+r_+^2} - \frac{1}{r_+}\Big(\frac{1}{2}-\frac{r_+^2}{2l^2}\Big)^{\varepsilon}\Big] \\ A &= \frac{\omega_{d-2}}{r_+^{1-\varepsilon}}\prod_{i=1}^{N}\frac{a_i^2+r_+^2}{\Xi_i}\,, \quad S = \frac{A}{4} \end{aligned} \tag{54}$$

The horizon radius r_+ is determined as the largest root of $F - 2m = 0$ and ω_d is given by Equation (10).

The thermodynamic volume reads [9,10]:

$$V = \frac{r_+ A}{d-1}\left[1 + \frac{1+r_+^2/l^2}{(d-2)r_+^2}\sum_i \frac{a_i^2}{\Xi_i}\right] = \frac{r_+ A}{d-1} + \frac{8\pi}{(d-1)(d-2)}\sum_i a_i J_i \tag{55}$$

and indeed is required to ensure that the Smarr formula (5) holds. It is known to obey the *reverse isoperimetric inequality* Equation (11) provided that in Equation (9) we identify $\mathcal{A} = A$ and $\mathcal{V} = V$ as given by Equations (54) and (55). In fact the inequality is saturated for non-rotating black holes, whereas it becomes most extreme ($\mathcal{R} \to \infty$) in the ultraspinning limit, see discussion around Equation (96).

Note that the "naive" *geometric volume* [10,75–77] (given by the spatial integral of $\sqrt{-g}$ integrated up to the horizon radius):

$$V' = \frac{r_+ A}{d-1} \tag{56}$$

and the thermodynamic volume V in Equation (55) differ by an $\sum_i a_i J_i$ term and behave differently in the limits of slow and fast rotation. Whereas the thermodynamic volume Equation (55) is dominated by its first geometric term for slow rotations:

$$V_{\text{slow}} \approx V'_{\text{slow}} \approx \frac{\omega_{d-2} r_+^{d-1}}{d-1} \tag{57}$$

in the ultraspinning regime the second (angular momentum) term dominates. To see this let us, for simplicity, consider for a moment a singly spinning Myers–Perry black hole ($a_1 = a$, other $a_i = 0$, and $l \to \infty$). In this case the formula (55) reduces to the following expression:

$$V = V' + \frac{4\pi}{d-1}\frac{J^2}{M} \tag{58}$$

which is also valid for the $d = 4$ Kerr-AdS case. In $d \geq 6$ there is no limit on how large the rotation parameter a can be [107] and one can, in principle, take the *ultraspinning limit* $a \to \infty$. For fixed M this implies $r_+ \to 0$, and the second term in the previous formula dominates. Hence, for the ultraspinning black holes, the thermodynamic volume differs significantly from the geometric one, being approximately given by:

$$V \approx \frac{4\pi}{d-1}\frac{J^2}{M} \approx \frac{\omega_{d-2} a^4 r_+^{d-5}}{(d-1)(d-2)} \tag{59}$$

which is to be compared with formula (57). The conclusions for multiply-spinning and/or AdS black holes are analogous.

The Gibbs free energy is given by Equation (2) and is related to the Euclidean action I [106]:

$$I = \frac{\omega_{d-2}}{8\pi T\left(\prod_j \Xi_j\right)}\left(m - \frac{r_+^{\varepsilon}}{l^2}\prod_{i=1}^{N}(r_+^2 + a_i^2)\right) \tag{60}$$

by

$$G = M - TS = TI + \sum_i \Omega_i J_i \tag{61}$$

see also Section 7 where I is used to estimate the onset of ultraspinning instabilities. In what follows we shall discuss in detail some special cases of these general metrics and the associated interesting thermodynamic features.

3.2. Classical Swallowtail

The behavior of the Gibbs free energy G, Equation (61), depends crucially on the number of spacetime dimensions d and the number and ratios of the nontrivial angular momenta.

The dimension $d = 5$ is an exception. The Gibbs free energy is in principle a function of two possible angular momenta J_1 and J_2. However, as long as at least one of them is nontrivial, there exists a critical pressure P_c below which we observe the qualitatively same characteristic swallowtail behavior indicating the small/large black hole phase transition, as shown in Figure 10. The situation is in fact very similar to what happens for Kerr-AdS in $d = 4$. The corresponding $P - V$ and $P - T$ diagrams (not shown) are reminiscent of what was observed for charged or rotating black holes in $d = 4$ and are analogous to the van der Waals $P - V$ and $P - T$ diagrams.

The classical swallowtail behavior is also observed for *equal-spinning* ($J_1 = J_2 = ... = J_N = J$) Kerr-AdS black holes in all $d \geq 5$ dimensions.

Figure 10. Gibbs free energy: Kerr-AdS in $d = 5$. The Gibbs free energy of equal spinning Kerr-AdS black hole is displayed for $J_1 = J_2 = 1$. The situation is very similar to what happens for charged or rotating black holes in four dimensions. A qualitatively similar swallowtail behavior, indicating a SBH/LBH phase transition, is observed for any ratio of the two angular momenta, as long as, at least one of them is non-trivial. Equal spinning Kerr-AdS black holes in all $d \geq 5$ demonstrate the qualitatively same feature.

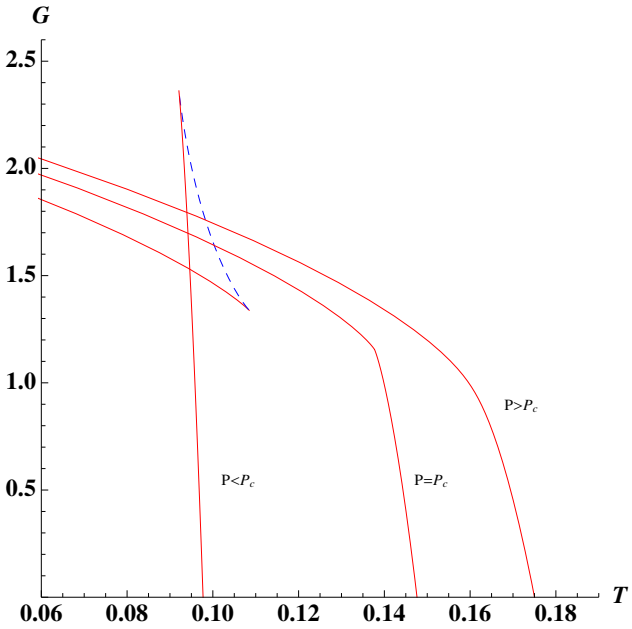

3.3. Reentrant Phase Transition

It was observed in [25] that in all $d \geq 6$ dimensions the *singly spinning* Kerr-AdS black holes admit a reentrant large/small/large black hole phase transition. This is quite exciting as similar reentrant phase transitions are commonly observed for multicomponent fluid systems, gels, ferroelectrics, liquid crystals, and binary gases, e.g., [72], and the observed feature could provide a toy gravitational model for such 'everyday' thermodynamic phenomena.

In general, a system undergoes a reentrant phase transition if a monotonic variation of one thermodynamic quantity results in two (or more) phase transitions such that the final state is macroscopically similar to the initial state. For singly spinning Kerr-AdS black holes in a certain range of pressures (and a given angular momentum) it was found [25] that a monotonic lowering of the black hole temperature yields a large/small/large black hole transition. The situation is accompanied by a zeroth-order phase transition, a discontinuity in the global minimum of the Gibbs free energy, a phenomenon seen in superfluidity and superconductivity [73], and recently in four-dimensional Born–Infeld black holes [16]. Interestingly, such reentrant phase transitions were recently found to be absent in higher-dimensional Born–Infeld-AdS black holes, giving the four-dimensional result a special significance [33].

In this subsection we provide more detail about this interesting transition. We start with a review of singly spinning Kerr-AdS black holes.

For singly spinning ($a_1 = a$ and other $a_i = 0$) Kerr-AdS black holes the metric Equation (49) significantly simplifies and reduces to:

$$\begin{aligned} ds^2 &= -\frac{\Delta}{\rho^2}(dt - \frac{a}{\Xi}\sin^2\theta d\varphi)^2 + \frac{\rho^2}{\Delta}dr^2 + \frac{\rho^2}{\Sigma}d\theta^2 \\ &+ \frac{\Sigma\sin^2\theta}{\rho^2}[adt - \frac{r^2+a^2}{\Xi}d\varphi]^2 + r^2\cos^2\theta d\Omega_{d-4}^2 \end{aligned} \tag{62}$$

where:

$$\begin{aligned} \Delta &= (r^2+a^2)(1+\frac{r^2}{l^2}) - 2mr^{5-d}\,, \quad \Sigma = 1 - \frac{a^2}{l^2}\cos^2\theta \\ \Xi &= 1 - \frac{a^2}{l^2}\,, \quad \rho^2 = r^2 + a^2\cos^2\theta \end{aligned} \tag{63}$$

and $d\Omega_d^2$ denotes the metric element on a d-dimensional sphere. The associated thermodynamic quantities become:

$$\begin{aligned} M &= \frac{\omega_{d-2}}{4\pi}\frac{m}{\Xi^2}\Big(1 + \frac{(d-4)\Xi}{2}\Big)\,, \quad J = \frac{\omega_{d-2}}{4\pi}\frac{ma}{\Xi^2} \\ \Omega &= \frac{a}{l^2}\frac{r_+^2+l^2}{r_+^2+a^2}\,, \quad S = \frac{\omega_{d-2}}{4}\frac{(a^2+r_+^2)r_+^{d-4}}{\Xi} = \frac{A}{4} \\ T &= \frac{1}{2\pi}\Big[r_+\Big(\frac{r_+^2}{l^2}+1\Big)\Big(\frac{1}{a^2+r_+^2} + \frac{d-3}{2r_+^2}\Big) - \frac{1}{r_+}\Big] \\ G &= \frac{\omega_{d-2}r_+^{d-5}}{16\pi\Xi^2}\Big(3a^2 + r_+^2 - \frac{(r_+^2-a^2)^2}{l^2} + \frac{3a^2r_+^4 + a^4r_+^2}{l^4}\Big) \\ V &= \frac{r_+A}{d-1}\Big[1 + \frac{a^2}{\Xi}\frac{1+r_+^2/l^2}{(d-2)r_+^2}\Big] \end{aligned} \tag{64}$$

where r_+ is the largest positive real root of $\Delta = 0$.

To analyze the behaviour of $G = G(P, T, J)$ for fixed J and P we proceed as follows. We first express $a = a(J, r_+, P)$ from the (quartic) J Equation (64). Inserting the (well-behaved) solution into the expressions for G and T, consequently expressed as functions of P and r_+, we can then plot G *vs.* T parametrically. Similarly, we obtain an expression for the specific heat $C_P(r_+, P, J)$ and plot this function for fixed P and J (not displayed) to see for which regions of r_+ it becomes negative, thereby finding which branches of G are thermodynamically unstable.

The resulting Gibbs free energy in $d = 6$ is illustrated in Figure 11; the behaviour in higher dimensions is qualitatively similar. As with the Schwarzschild-AdS case discussed in Section 2, for a given pressure P there is a minimum temperature T_{min} for which the black holes can exist. Above this temperature we observe two (or more) branches of black holes. The branch corresponding to the largest black holes has positive C_P and is locally thermodynamically stable. Its Gibbs free energy becomes negative above a certain temperature, analogous to T_{HP}. The new feature present in six and higher dimensions is that between T_{min} and T_{HP} the branch of largest black holes may not correspond to a global minimum of the Gibbs free energy.

Figure 11. Gibbs free energy: singly spinning Kerr-AdS in $d = 6$. The behavior of G for $d \geq 6$ is completely different from that of $d < 6$, cf., Figures 8 and 10. The Gibbs free energy for a singly spinning black hole is displayed for increasing pressure (from left to right). As with Schwarzschild-AdS black holes, for $P \geq P_c$, the (lower) large black hole branch is thermodynamically stable whereas the upper branch is unstable. For $P = P_c$ we observe critical behavior. In a range of pressures $P \in (P_t, P_z)$, we observe a discontinuity in the global minimum of G or zeroth-order phase transition, signifying the presence of a reentrant phase transition. This feature is qualitatively similar and present for all $d \geq 6$ singly spinning Kerr-AdS black holes. For $P < P_t$ only one branch of stable large black holes exists. Note that the specific heat is positive in zones where the Gibbs free energy reaches a global minimum.

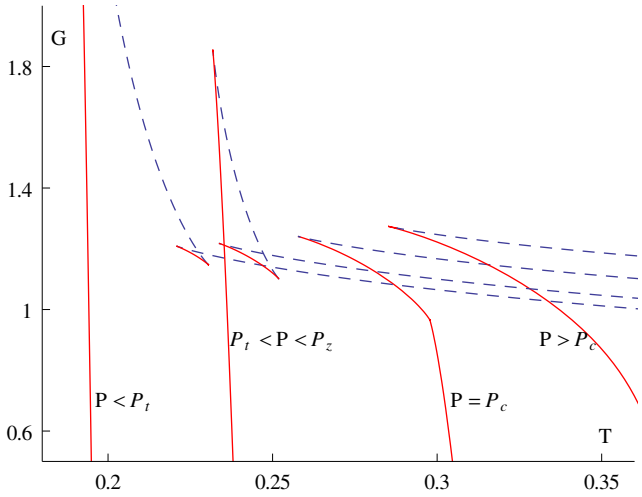

The complicated behaviour of G between T_{min} and T_{HP} stems from the presence of a critical point occurring in the large black hole branch at (T_c, P_c).

The complicated behavior of G between T_{min} and T_{HP} stems from the presence of a critical point occurring in the large black hole branch at (T_c, P_c). For $P > P_c$, G resembles the curve characteristic for the Schwarzschild-AdS black hole seen in Section 2, Figure 3. However, below P_c the situation is more subtle, as displayed in Figure 12. The reentrant phase transition occurs for a range of pressures $P \in (P_t, P_z)$. The pressure P_z, see Figure 12b, is a pressure for which $T_{\text{min}}(P_z) = T_z$ occurs for two locally thermodynamically stable branches of black holes. Slightly below this pressure we observe a reentrant phase transition, Figure 12c. It is connected with the discontinuity of the global minimum of the Gibbs free energy at $T = T_0$, where we observe a zeroth order phase transition between small and large black holes. The reentrant phase transition terminates at $P = P_t$ below which the global minimum of the Gibbs free energy is again continuous and occurs for a branch of large black holes. We also note a presence of the first order SBH/LBH phase transition at $T = T_1$ in the range of pressures $P \in (P_t, P_c)$. As displayed in Figure 12d, at $P = P_t$ temperatures T_0 and T_1 coincide to give $T_0 = T_1 = T_t$. At T_t both the zeroth order and the first order phase transitions terminate and we observe a "virtual triple point", characterized by (P_t, T_t), where three black hole phases (small, large and intermediate) coexist together. We use the term "virtual triple point" to stress a distinction from the standard triple point where three first-order phase transition coexistence lines join together. In a virtual triple point a zeroth-order phase

transition coexistence line joins the first order phase transition coexistence lines where "three types" of black holes meet.

Figure 12. Reentrant phase transition: singly spinning Kerr-AdS black holes in $d = 6$. The figure (a close up of Figure 11) illustrates the behaviour of the Gibbs free energy for various pressures, $P = \{0.073, Pz = 0.0579, 0.0564, P_t = 0.0553\}$ (from top to bottom), when the reentrant phase transition is present. We have set $J = 1$, for which $P_c = 0.0958$. Solid-red/dashed-blue lines correspond to C_P positive/negative respectively. (a) Describes a LBH/SBH first order phase transition at temperature T_1 as indicated by a dashed vertical line. (b) Displays the behaviour of G for $P = P_z$ for which the 'upper peak' occurs at the same temperature $T = T_z$ as the lower peak—indicating the 'entrance' of the reentrant phase transition. The LBH/SBH first order phase transition is still present and occurs at $T = T_1 > T_z$. (c) Displays a typical behaviour of G when the reentrant phase transition is present, $P \in (P_t, P_z)$. Black arrows indicate increasing r_+. (d) Shows the behaviour for $P = P_t$ when the lower peak merges with the vertical red line. For this pressure temperature of the zeroth-order phase transition T_0 coincides with the temperature of the first-order phase transition T_1, we call it $T_t = T_0 = T_1$.

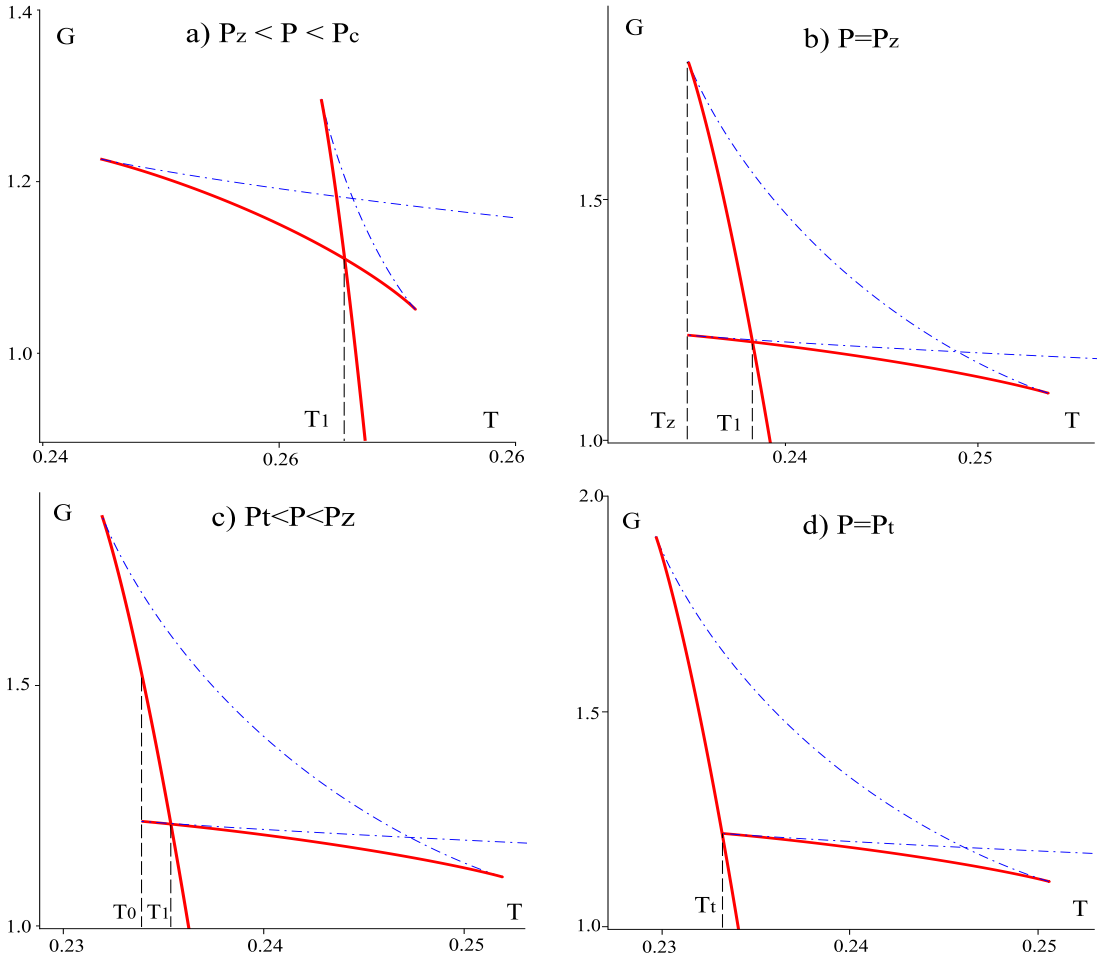

Figure 12c illustrates in detail the typical behavior of G when the reentrant phase transition is present, $P \in (P_t, P_z)$. Black arrows indicate increasing r_+. If we start decreasing the temperature from, say

$T = 0.24$, the system follows the lower vertical solid red curve of large stable black holes until it joins the upper horizontal solid red curve of small stable black holes—this corresponds to a first order LBH/SBH phase transition at $T = T_1$. As T continues to decrease the system follows this upper curve until $T = T_0$, where G has a discontinuity at its global minimum. Further decreasing T, the system jumps to the uppermost vertical red line of large stable black hole—this corresponds to the zeroth order phase transition between small and large black holes. In other words, as T continuously decreases, we observe LBH/SBH/LBH reentrant phase transition. We note that the blue dashed curve with the smallest r_+ admits black holes subject to the ultraspinning instabilities (Section 7), whereas all other branches are stable with respect to this instability.

This interesting situation is clearly illustrated in the $P-T$ diagram in Figure 13. There is the expected SBH/LBH line of coexistence corresponding to the liquid/gas Van der Walls case, ending in a critical point at (T_c, P_c). On the other end this line terminates at (T_t, P_t), where there is a virtual triple point where the large, small, and large again black holes coexist. For $T \in (T_t, T_z)$ a new LBH/SBH line of coexistence emerges (see inset of Figure 13) that terminates in another "critical point" at (T_z, P_z). We note that the range for the reentrant phase transition is quite narrow and must be determined numerically. For example for $J = 1$ and $d = 6$ we obtain $(T_t, T_z, T_c) \approx (0.2332, 0.2349, 0.3004)$ and $(P_t, P_z, P_c) \approx (0.0553, 0.0579, 0.0958)$.

Figure 13. Reentrant phase transition in $P - T$ plane. The coexistence line of the first order phase transition between small and large black holes is depicted by a thick black solid line for $J = 1$ and $d = 6$. It initiates from the critical point (P_c, T_c) and terminates at virtual triple point at (P_t, T_t). The red solid line (inset; shown in detail in figure 14) indicates the "coexistence line" of small and intermediate black holes, separated by a finite gap in G, indicating the reentrant phase transition. It commences from (T_z, P_z) and terminates at (P_t, T_t). The "No BH region", given by T_{min}, is to the left of the dashed oblique curve, containing the (T_z, P_z) point. A similar figure is valid for any $d \geq 6$.

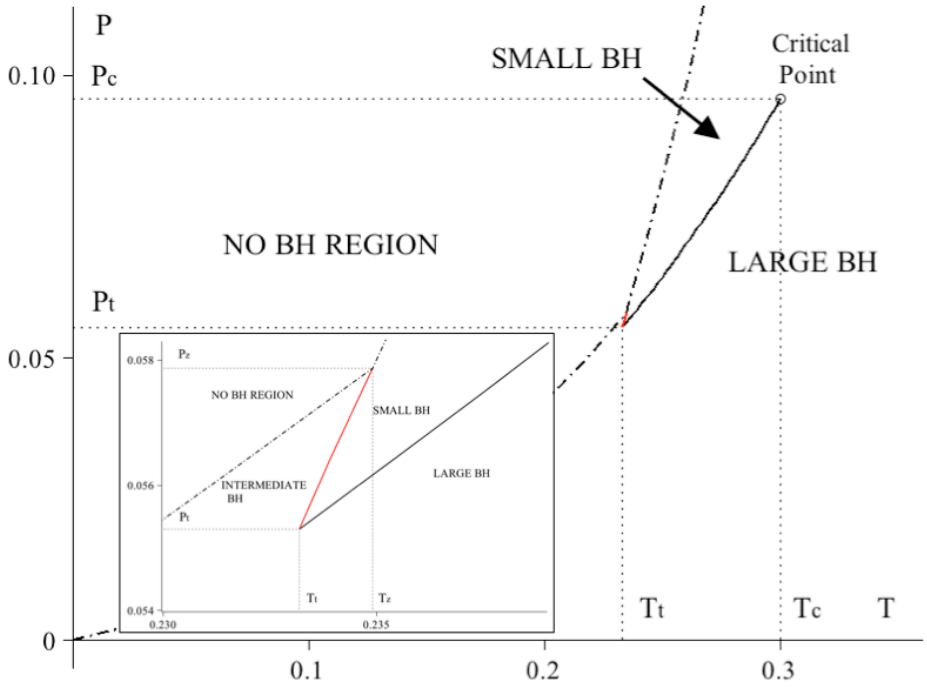

Several remarks are in order:

(a) It is well known that in $d \geq 6$ dimensions there is no "kinematic" limit on how fast the singly spinning Kerr-AdS black holes can rotate. However, fast spinning black holes are subject to various dynamical instabilities, such as ultraspinning instability, superradiant instability, or bar mode instability; these will be discussed in greater detail in Section 7. It turns out that black holes which participate in the reentrant phase transition are stable with respect to the ultraspinning instability: in Figure 12 c only the blue dashed curve with the smallest r_+ admits black holes subject to this instability. Unfortunately, this is no longer true for the superradiant and bar mode instability, which "compete" with the reentrant phase transition.

(b) One may wonder why the reentrant phase transition, which is characteristic for multicomponent systems where various phenomena compete among each other to result in reentrance, should occur at all in a "homogeneous" system of one black hole. What are the competing phenomena in our case? A possible explanation is related to the ultraspinning regime. If so, this would also explain why we see reentrance in $d \geq 6$ dimensions but not in $d = 4$ or 5 where such a regime does not exist. It is well known that as we spin the spherical black hole faster and faster, its horizon flattens and the resulting object is in many respects similar to a black brane, see the next subsection. However, the thermodynamic behaviour of black branes is completely different from that of spherical black holes. It happens that small black holes that participate in the reentrant phase transition are "almost ultraspinning" and hence possess almost black brane behavior. For this reason it may be the competition between the black brane thermodynamic behavior and the black hole thermodynamic behavior which causes the 'multicomponency' and results in the reentrant phase transition.

(c) We note that all the interesting behaviour leading to the reentrant phase transition occurs for a positive Gibbs free energy, *i.e.*, below temperature T_{HP}. For this reason, one may expect that the thermal AdS (see Section 2) is actually preferred thermodynamic state in this region and the various black holes participating in the reentrant phase transition are actually metastable. If so, the reentrant phase transition may actually be destroyed and one would simply observe a Hawking–Page transition between thermal radiation and large black holes at $T = T_{\text{HP}}$. We stress that similar arguments also apply to the four-dimensional charged AdS black hole discussed in Section 2 and the corresponding "van der Waals" phase transition.

(d) The observed reentrant phase transition is well suited for the AdS/CFT interpretation. Although first observed [25] in the context of extended phase space thermodynamics, the existence of the reentrant phase transition does not require a variable cosmological constant. For any fixed value of Λ within the allowed range of pressure, the reentrant phase transition will take place. This opens up a possibility for an AdS/CFT interpretation—in particular in the dual CFT there will be a corresponding reentrant phase transition within the allowed range of N. In fact, we can fix the pressure and construct a phase diagram plotting J vs. T (Figure 15) showing that reentrant phase behaviour occurs. Hence in the dual CFT at this fixed pressure there will be a corresponding reentrant transition as the relative values of the quantities dual to the angular momenta are adjusted.

(e) The existence of reentrant phase transitions in the context of black hole thermodynamics seems quite general. Similar phenomena have been observed in Born–Infeld black hole spacetimes [16]. We shall also see in Section 4, that reentrant phase transitions are observed for the asymptotically flat doubly-spinning Myers–Perry black holes of vacuum Einstein gravity. Hence, neither exotic matter nor a cosmological constant (and hence AdS/CFT correspondence) are required for this phenomenon to occur in black hole spacetimes.

Figure 14. Reentrant phase transition in $P - T$ plane – Inset of Figure 13.

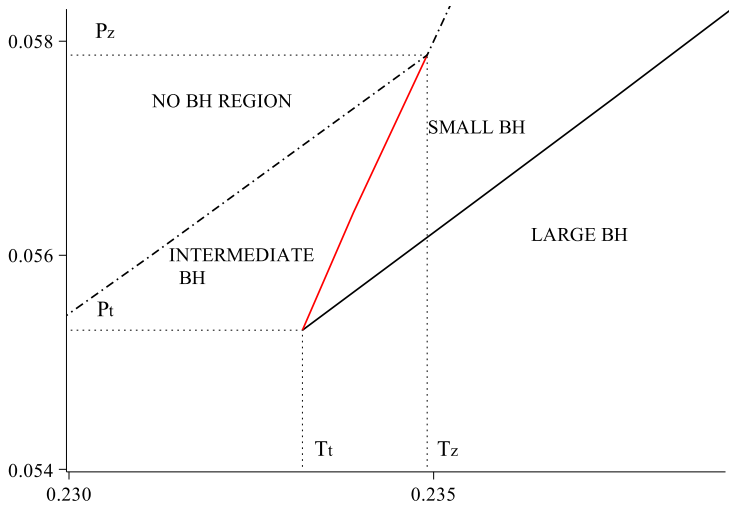

Figure 15. Reentrant phase transition in $J - T$ plane. The coexistence line of the first order phase transition between small and large black holes is depicted by a thick black solid line. The red curve denotes a zeroth-order phase transition between small and intermediate (large) black holes. The dashed line outlines the 'no black hole region'. The diagram is displayed for fixed $l \approx 2.656$ and $d = 6$.

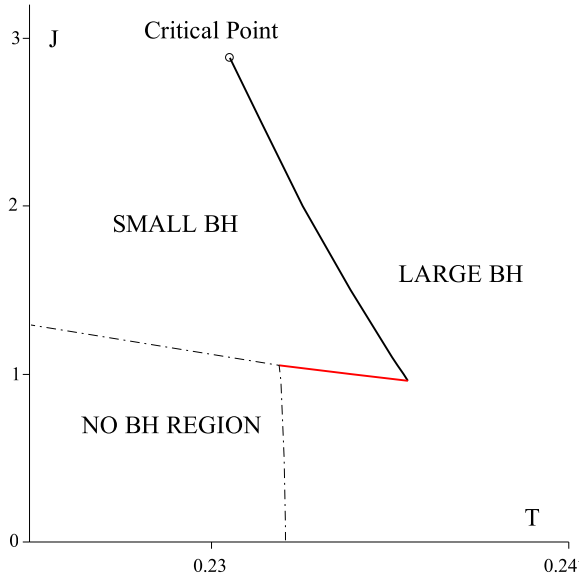

3.4. Equation of State

Let us now look at the equation of state. For simplicity we shall first study the case of singly spinning Kerr-AdS black holes, given by Equations (62)–(64); the case of equal spinning Kerr-AdS black holes is discussed towards the end.

The aim is to express the pressure P as a function of the specific volume v, the black hole temperature T, and the angular momentum J:

$$P = P(v, T, J) \tag{65}$$

which is the equation of state (13). Finding this relation for general J is algebraically involved. For this reason we plot the exact solution numerically: we solve the quartic J Equation (64) for $a = a(r_+, J, P)$, obtain the resulting expressions $T = T(r_+, J, P)$ and $v = v(r_+, J, P)$, and then solve them for fixed J and T. The result in $d = 5$ is qualitatively similar to what was observed in four dimensions, whereas in $d \geq 6$ the situation is more interesting, as shown in Figure 16.

Figure 16. Exact $P-v$ diagram: Kerr-AdS black holes. In $d = 5$ (inset) we observe standard van der Waals like behavior, similar to $d = 4$ in Figure 7. In $d \geq 6$ the $P - v$ diagram is more complex than that of the standard van der Waals, reflecting the interesting behaviour of the Gibbs free energy and a possible reentrant phase transition. Namely, whereas for large v the isotherms approximate the van der Waals behavior, for small v, similar to Schwarzschild-AdS in Figure 5, the isotherms turn and lead back to a region with negative pressures.

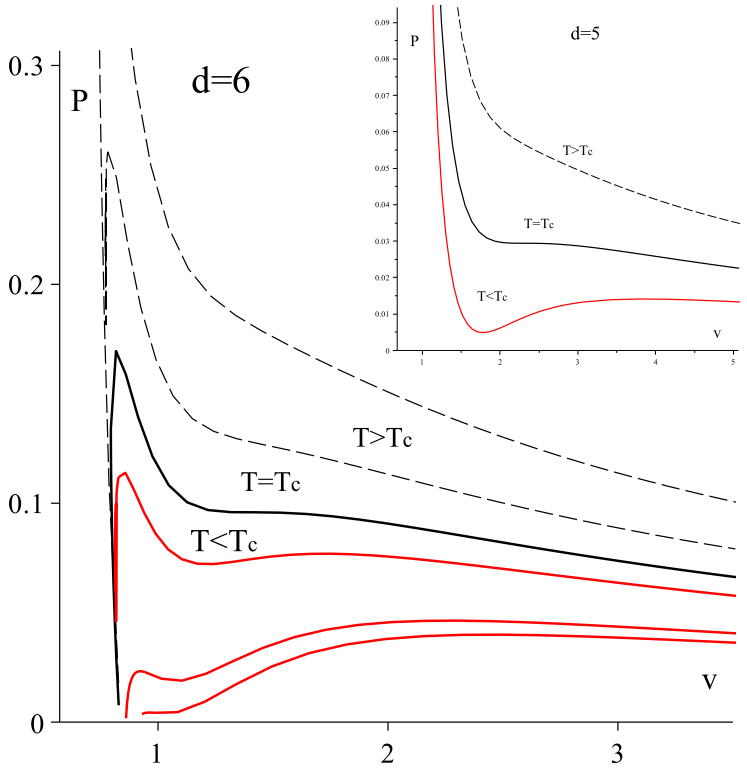

In two cases of physical interest—the slowly rotating case and the ultraspinning regime—the equation of state Equation (65) can be approximated analytically. In the former case, as with $d = 4$ [16], we consider an $\epsilon = a/l$ expansion. This slow rotation expansion allows us to approximate the

equation of state demonstrating the van der Waals behavior and to study the corresponding critical point. In the ultraspinning regime, $\Xi = 1 - a^2/l^2 \to 0$, black hole geometry approaches that of a black membrane [107], and is characterized by completely different thermodynamic behavior. We also construct the Kerr-AdS equation of state at the very ultraspinning limit and show in Section 6 that it coincides with the equation of state for ultraspinning black rings.

3.4.1. Slow Rotation Expansion

Here we demonstrate that in the regime of slow rotation, where the equation of state can be well approximated, a van der Waals type of phase transition takes place. Within the validity of the slow rotation expansion we can analytically study the properties of the critical point as well as the critical exponents.

The slow rotation expansion is an expansion in the parameter:

$$\epsilon = \frac{a}{l} \to 0 \tag{66}$$

where we keep the pressure P and the mass M of the black hole fixed.

To obtain the expansion for the equation of state and the Gibbs free energy we proceed as follows. First we solve the equation:

$$\frac{4\pi M \Xi^2}{\omega_{d-2}\left(1+\frac{d-4}{2}\Xi\right)} = m = \frac{1}{2} r_+^{d-5}(r_+^2 + a^2)\left(1 + \frac{r_+^2}{l^2}\right) \tag{67}$$

for r_+ in terms of M and l, while we express $a = \epsilon l$. The l.h.s. of this equation comes from M Equation (64) and the r.h.s. from $\Delta = 0$. We expand:

$$r_+ = \sum_{I=0}^{k} r_I \epsilon^I \tag{68}$$

to some given order k and solve Equation (67) order by order. The first term yields the relation:

$$M = \frac{\omega_{d-2}(d-2) r_0^{d-3}}{16\pi}\left(1 + \frac{r_0^2}{l^2}\right) \tag{69}$$

which determines r_0 in terms of M; higher-order r_I are obtained from subsequent terms and are complicated expressions depending on M and l, or alternatively on r_0 and l.

Inserting the expansion (68) and the solution (69) into the expressions for J, T and V, in Equation (64), we find:

$$\begin{aligned} J &= \frac{\omega_{d-2} r_0^{d-3}(l^2 + r_0^2)}{8\pi l}\epsilon + \sum_{I=2} J_I \epsilon^I \\ T &= \frac{r_0^2(d-1) + l^2(d-3)}{4\pi r_0 l^2} + \sum_{I=1} T_I \epsilon^I \\ v &= \frac{r_0}{\kappa} + \sum_{I=1} v_I \epsilon^I \end{aligned} \tag{70}$$

while P is given in terms of l through Equation (1). Here $\{J_I, T_I, v_I\}$ are some concrete functions of l and r_0. Note that as $\epsilon \to 0$, $J \to 0$, whereas all other quantities remain finite.

In order to get $P = P(v, T, J)$ we proceed perturbatively in ϵ, successively eliminating r_0 and ϵ from the resultant expressions. To zeroth order we find:

$$P = \frac{T}{v} - \frac{d-3}{\pi(d-2)v^2} + O(\epsilon^2) \tag{71}$$

To obtain the first correction we note that $J \propto \epsilon$ and hence the first correction is proportional to J^2, while we fix the dependence on T and v using dimensional analysis:

$$P = \frac{T}{v} - \frac{d-3}{\pi(d-2)v^2} + \frac{\pi(d-1)16^d}{4\omega_{d-2}^2(d-2)^{2(d-1)}}\frac{J^2}{v^{2(d-1)}} + O(\epsilon^4) \tag{72}$$

When $d = 4$ this expression reduces to the one presented in [16], albeit obtained in a different fashion. In principle by expanding to a sufficiently high order k, one can algorithmically find the equation of state to an arbitrary order in ϵ. However in the vicinity of the critical point the exact $P - v$ relation is "well approximated" by the first three terms in Equation (72); Figure 17 illustrates the situation for $d = 6$. This allows us to study the properties of the critical point using the truncation Equation (72). We shall comment on the possible deviation beyond this approximation in the end of this subsection. The Gibbs free energy can likewise be obtained in the slow rotating expansion.

Figure 17. The two approximations. Exact critical and subcritical isotherms, depicted by black crosses, are compared to the slow spinning expansion (72) denoted by red curves and the ultraspinning expansion (91) denoted by a blue curve; value of $r+$ decreases right to left. Obviously, the slow rotation approximation is valid for $r_+ \to \infty$ whereas the ultraspinning one for $r_+ \to 0$. In the regime of very small P (not displayed), v grows arbitrarily large for any temperature T, according to Equation (89). Note that the ultraspinning black holes correspond to the upper branch in the Gibbs free energy in Figure 11, which is unstable. We have set $d = 6$ and $J = 1$.

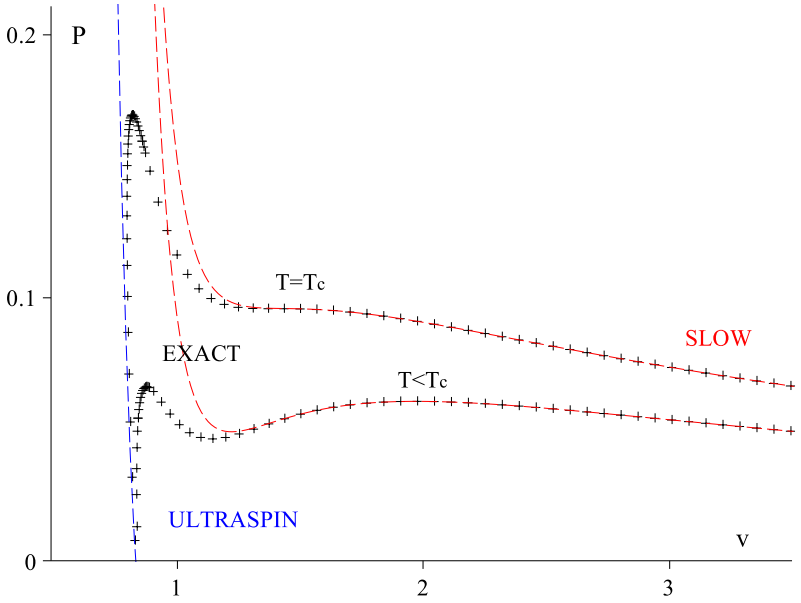

3.4.2. Critical Point

The critical point $\{P_c, v_c, T_c\}$ of the truncated equation of state Equation (72) is obtained from solving:

$$\frac{\partial P}{\partial v} = 0\,, \quad \frac{\partial^2 P}{\partial v^2} = 0 \tag{73}$$

which yields:

$$\begin{aligned} v_c &= \frac{4}{d-2}\Big[\frac{2^6\pi^2(2d-3)(d-1)^2J^2}{(d-2)(d-3)\omega_{d-2}^2}\Big]^{\frac{1}{2(d-2)}} \\ T_c &= \frac{4(d-3)}{\pi(2d-3)}\frac{1}{v_c}\,, \quad P_c = \frac{d-3}{\pi(d-1)}\frac{1}{v_c^2} \end{aligned} \tag{74}$$

We note the critical ratio [cf. Equation (35)]:

$$\rho_c = \frac{P_c v_c}{T_c} = \frac{2d-3}{4(d-1)} \tag{75}$$

which reduces to $\rho_c = 5/12$ for $d = 4$ [16].

Introducing new variables:

$$p = \frac{P}{P_c}\,, \quad \nu = \frac{v}{v_c}\,, \quad \tau = \frac{T}{T_c} \tag{76}$$

the parameter J can be "scaled away" and we obtain the *law of corresponding states* of the form:

$$p = \frac{1}{\rho_c}\frac{\tau}{\nu} + h(\nu) \tag{77}$$

with ρ_c given by Equation (75) and:

$$h(\nu) = -\frac{d-1}{\nu^2(d-2)} + \frac{1}{(d-2)(2d-3)\nu^{2(d-1)}} \tag{78}$$

It was shown in [16] that when the law of corresponding states takes the form Equation (77) and $1 - \frac{1}{6}\rho_c h^{(3)}(1) > 0$, which in our case is satisfied, we recover the mean field theory critical exponents:

$$\beta = \frac{1}{2}\,, \quad \gamma = 1\,, \quad \delta = 3 \tag{79}$$

Moreover, since:

$$S(T, v) = \frac{\omega_{d-2}\big[v(d-2)\big]^{d-2}}{4^{d-1}} + O(\epsilon^4) \tag{80}$$

which implies that to cubic order in ϵ we have $C_v = T\left(\frac{\partial S}{\partial T}\right)_v = 0$, and so the critical exponent α is:

$$\alpha = 0 \tag{81}$$

which also coincides with the mean field theory prediction Equation (15).

3.4.3. Remark on Exact Critical Exponents in $d = 4$

So far we have studied the properties of the critical point using the truncated equation of state Equation (72). Although this provides a good approximation to the exact equation of state, the exact critical point will be shifted from the preceding values and one may wonder whether the critical exponents will be modified. We argue that this is unlikely to happen. For simplicity, we limit ourselves to $d = 4$.

For this purpose we approximate the exact equation of state by the slow rotating expansion to a higher order than Equation (72), writing:

$$P_{(d=4)} = \frac{T}{v} - \frac{1}{2\pi v^2} + \frac{48J^2}{\pi v^6} - \frac{384J^4(7+8\pi Tv)}{(1+\pi Tv)^2\pi v^{10}} + \frac{36864(13\pi Tv+11)J^6}{\pi v^{14}(1+\pi Tv)^3} + O(\epsilon^8) \quad (82)$$

Near a critical point, it can be shown numerically that this approximation to high precision reproduces the exact equation of state. Since Equation (82) does not give rise to the law of the corresponding states of the form Equation (77) the critical exponents may, in principle, be different. Similarly we have:

$$S_{(d=4)} = \frac{\pi v^2}{4} - \frac{192\pi J^4}{v^6(1+\pi Tv)^2} + \frac{36864\pi J^6}{v^{10}(1+\pi Tv)^3} + O(\epsilon^8) \quad (83)$$

to this same level of approximation. Using these two equations, we have found numerically the critical point, with ρ_c slightly different from $5/12$, and (within the numerical accuracy) confirmed it to be characterized by the same critical exponents $\alpha = 0, \beta = \frac{1}{2}, \gamma = 1, \delta = 3$.

3.4.4. Ultraspinning Expansion

In $d \geq 6$ singly spinning spherical black holes admit an interesting feature, the so called *ultraspinning regime*, which is present already for asymptotically flat Myers–Perry black holes [107]. This limit consists of rotating the black hole faster and faster, while keeping its mass and the cosmological constant fixed. Consequently, the black hole horizon flattens, becomes pancake-like, and the black hole enters the regime of black membrane-like behavior. For asymptotically flat Myers–Perry black holes, the ultraspinning limit is achieved when the rotation parameter $a \to \infty$. In the presence of a negative cosmological constant one instead considers $a \to l$ (for an alternative see [108]), or, equivalently:

$$\epsilon = \Xi^{\frac{1}{d-5}} = \left(1 - \frac{a^2}{l^2}\right)^{\frac{1}{d-5}} \to 0 \quad (84)$$

In this subsection we derive the form of the equation of state and the Gibbs free energy employing the ultraspinning expansion. As a by-product we obtain the thermodynamic volume of the ultraspinning membrane-like black hole and demonstrate that it remains finite.

Similar to the slow rotating case discussed in the previous section, in the ultraspinning expansion we expand in small parameter ϵ, Equation (84), while we keep the pressure P and the mass M of the black hole fixed.

We again solve the equation:

$$\frac{4\pi M\Xi^2}{\omega_{d-2}\left(1+\frac{d-4}{2}\Xi\right)} = m = \frac{1}{2}r_+^{d-5}(r_+^2+a^2)\left(1+\frac{r_+^2}{l^2}\right) \quad (85)$$

to find the expansion:

$$r_+ = r_2\epsilon^2 + \sum_{I=3}^{k} r_I \epsilon^I \,, \quad r_2 = \left(\frac{8\pi M}{l^2\omega_{d-2}}\right)^{\frac{1}{d-5}} \tag{86}$$

up to some order k ; the r_I are calculable functions of M and l. Plugging this solution into the expressions for J, T and V in Equation (64), we find the following expansions:

$$\begin{aligned} J &= Ml + \sum_{I=1} J_I \epsilon^I \\ T &= \frac{d-5}{4\pi r_2 \epsilon^2} + \sum_{I=-1} T_I \epsilon^I \\ v &= \frac{4}{d-2}\left[\frac{8\pi M l^2}{\omega_{d-2}(d-2)}\right]^{\frac{1}{d-1}} + \sum_{I=1} v_I \epsilon^I \end{aligned} \tag{87}$$

while P is given by Equation (1). Here $\{J_I, T_I, v_I\}$ are calculable functions of l and M. We note that in the $\epsilon \to 0$ limit, the radius of the horizon $r_+ \to 0$ and the temperature diverges, whereas both the (specific) volume as well the angular momentum remain finite. We also find:

$$A = \omega_{d-2} l^2 \epsilon^{d-3} r_2^{d-4} + o(\epsilon^{d-3}) \tag{88}$$

and hence the number of degrees of freedom associated with the horizon, $N \propto A/l_P^2$ vanishes.

To find the equation of state $P = P(v, T, J)$, as well as other quantities, to any order in ϵ, we proceed algorithmically, as in the case of the slow rotating expansion. In particular, to the zeroth order we find:

$$\begin{aligned} P &= \frac{4\pi}{(d-1)(d-2)}\frac{J^2}{V^2} + \dots \\ &= \frac{\pi(d-1)16^d}{4\omega_{d-2}^2(d-2)^{2d-1}}\frac{J^2}{v^{2(d-1)}} + \dots \end{aligned} \tag{89}$$

We note the interesting coincidence that this expression coincides with the 3rd term in slow rotation expansion (72). Higher-order terms depend crucially on the number of dimensions. For example, the next term in the expansion (86) reads:

$$\begin{aligned} d < 9 : &\qquad r_{d-3} = r_2 \frac{6-d}{2(d-5)} \\ d = 9 : &\qquad r_6 = -r_2\left(\frac{3}{8} + \frac{r_2^2}{2l^2}\right) \\ d > 9 : &\qquad r_6 = -\frac{2r_2^3}{l^2(d-5)} \end{aligned} \tag{90}$$

and we observe dimension-dependent "branching".

For this reason, we give up on finding a general expression and provide rather the expanded equations of state and the Gibbs free energies in selected dimensions ($d = 6, 7, 8, 9$ and 10). The first three non-trivial terms in the expansion of equation of state read:

$$\begin{aligned}
P_6 &= \frac{\pi J^2}{5V^2} - \frac{\sqrt{5\omega_4}}{16\sqrt{\pi^3 VT}} + \frac{9\sqrt{5\omega_4}J^2}{3200\sqrt{\pi^3 V^5 T^5}} \\
P_7 &= \frac{2\pi J^2}{15V^2} - \frac{\sqrt{30\omega_5}}{32\sqrt{\pi^4 VT^2}} + \frac{\sqrt{30\omega_5}J^2}{300\sqrt{\pi^4 V^5 T^6}} \\
P_8 &= \frac{2\pi J^2}{21V^2} - \frac{9\sqrt{14\omega_6}}{128\sqrt{\pi^5 VT^3}} + \frac{135\sqrt{14\omega_5}J^2}{12544\sqrt{\pi^5 V^5 T^7}} \\
P_9 &= \frac{\pi J^2}{14V^2} - \frac{\sqrt{7\omega_7}}{4\sqrt{2\pi^6 VT^4}} + \frac{9\sqrt{\omega_7}J^2}{28\sqrt{14\pi^6 V^5 T^8}} \\
P_{10} &= \frac{\pi J^2}{18V^2} - \frac{75\sqrt{5\omega_8}}{128\sqrt{2\pi^7 VT^5}} + \frac{4375\sqrt{5\omega_8}J^2}{36864\sqrt{2\pi^7 V^5 T^9}}
\end{aligned} \tag{91}$$

Similarly, for the Gibbs free energy we find:

$$\begin{aligned}
G_6 &= \frac{2\sqrt{5\pi P}J}{5} + \frac{5^{\frac{1}{4}}\sqrt{\omega_4 J}}{8\pi\sqrt{T}(\pi P)^{\frac{1}{4}}} - \frac{5\omega_4}{1024\pi^3 TP} \\
G_7 &= \frac{2\sqrt{30\pi P}J}{15} + \frac{2^{3/4}15^{1/4}\sqrt{\omega_5 J}}{16\pi^{7/4}P^{1/4}T} - \frac{15\omega_5}{2048\pi^4 PT^2} \\
G_8 &= \frac{2\sqrt{42\pi P}J}{21} + \frac{6^{3/4}7^{1/4}3\sqrt{\omega_6 J}}{64\pi^{9/4}P^{1/4}T^{3/2}} - \frac{567\omega_6}{32768\pi^5 PT^3} \\
G_9 &= \frac{\sqrt{2\pi P}J}{\sqrt{7}} + \frac{14^{1/4}\sqrt{J\omega_7}}{4\pi^{11/4}P^{1/4}T^2} + \frac{3\sqrt{\omega_7 J}14^{1/4}P^{3/4}}{14\pi^{15/4}T^4} - \frac{7\omega_7}{128\pi^6 PT^4} \\
G_{10} &= \frac{1}{3}\sqrt{2\pi P}J + \frac{25\sqrt{15}2^{1/4}\sqrt{J\omega_8}}{128\pi^{13/4}P^{1/4}T^{5/2}} + \frac{4375\sqrt{15}2^{1/4}P^{3/4}\sqrt{J\omega_9}}{18432\pi^{17/4}T^{9/2}}
\end{aligned} \tag{92}$$

We display the two expansions, the slow rotating one and the ultraspinning one together with the exact quantities in Figure 17.

3.4.5. Ultraspinning Limit: Black Membranes

The full ultraspinning limit, in which ϵ given by Equation (84) actually equals zero, is obtained by keeping only the dominant terms in the ultraspinning expansion Equations (87) and (88). For Kerr-AdS black holes this was studied in [109] (see also [108] for an alternative approach). As noted above, in this limit the black hole horizon radius shrinks to zero, the black hole temperature becomes infinite, the angular momentum and the (specific) thermodynamic volume remain finite, and the horizon area (and hence also the entropy) shrinks to zero; the angular velocity of the horizon goes as $\Omega_H l \to 1$.

These ultraspinning black holes share many properties with black membranes, including the Gregory–Laflamme instability [107]. In fact, when the limit is accompanied with the following change of coordinates:

$$\tau = \frac{t}{\epsilon^2}, \quad \rho = \frac{r}{\epsilon^2}, \quad \sigma = \epsilon^{\frac{7-d}{2}} l \sin\theta \tag{93}$$

together with defining $\mu = \frac{8\pi M}{\omega_{d-2} l^2}$, the ultraspinning black hole metric becomes (up to a constant conformal prefactor) that of a black membrane [109]:

$$\begin{aligned}
ds_M^2 &= -f d\tau^2 + \frac{d\rho^2}{f} + d\sigma^2 + \sigma^2 d\varphi^2 + \rho^2 d\Omega_{d-4}^2 \\
f &= 1 - \frac{\mu}{\rho^{d-5}}
\end{aligned} \tag{94}$$

We emphasize again that the thermodynamic volume remains finite and reads:

$$V = \frac{8\pi M l^2}{(d-1)(d-2)} \tag{95}$$

At the same time the area of the black hole vanishes according to Equation (88). This implies that in the full ultraspinning limit the isoperimetric ratio Equation (9) diverges to infinity:

$$\mathcal{R} \to \infty \tag{96}$$

Since $TS = O(\epsilon^{d-5})$, the Gibbs free energy is:

$$G = M = \sqrt{\frac{16\pi P}{(d-1)(d-2)}} J \tag{97}$$

while the equation of state takes interesting form:

$$P = \frac{4\pi}{(d-1)(d-2)} \frac{J^2}{V^2} \tag{98}$$

We shall see in Section 6 that exactly the same equation of state is valid for the ultraspinning black rings.

3.4.6. Equal Spinning AdS Black Holes

Let us briefly mention how the equation of state gets modified for the equal spinning Kerr-AdS black holes. Equal spinning Kerr-AdS black holes are characterized by $N = (d - \varepsilon - 1)/2$ equal angular momenta:

$$J_1 = J_2 = \cdots = J_N = J \tag{99}$$

In this case the symmetry of the spacetime is significantly enhanced and the general metric Equation (49) and its thermodynamic characteristics Equations (53)–(55) simplify considerably. For example, the thermodynamic volume now reads:

$$V = \frac{r_+ A}{d-1}\Big[1 + \frac{Na^2}{\Xi}\frac{1 + r_+^2/l^2}{(d-2)r_+^2}\Big] \tag{100}$$

As mentioned above, the Gibbs free energy exhibits a classical swallowtail, see Figure 10, with a critical point at (T_c, P_c) and the corresponding equation of state mimics the van der Waals behavior.

Repeating the procedure for the slow rotation expansion, $\frac{a}{l} \to 0$, as we did for the singly spinning case, we recover:

$$P = \frac{T}{v} - \frac{d-3}{\pi(d-2)v^2} + \frac{\pi(d-1)^{2-\varepsilon}16^d}{8\omega_{d-2}^2(d-2)^{2(d-1)-\varepsilon}} \frac{J^2}{v^{2(d-1)}} + O\big[(a/l)^4\big] \tag{101}$$

The equation of state (101) admits a critical point at:

$$\begin{aligned} v_c &= \frac{4}{d-2}\Big[\frac{2^6\pi^2}{\omega_{d-2}^2}\frac{2d-3}{d-3}\frac{(d-1)^{3-\varepsilon}}{(d-2)^{1-\varepsilon}}J^2\Big]^{\frac{1}{2(d-2)}} \\ T_c &= \frac{4(d-3)}{\pi(2d-3)}\frac{1}{v_c}, \quad P_c = \frac{d-3}{\pi(d-1)}\frac{1}{v_c^2} \end{aligned} \tag{102}$$

The critical ratio reads $\rho_c = \frac{P_c v_c}{T_c} = \frac{2d-3}{4(d-1)}$, and is the same as for singly spinning case, Equation (75). Also the critical exponents of Equation (101) remain as predicted by the mean field theory, Equation (15).

3.5. An Analogue of Triple Point and Solid/Liquid/Gas Phase Transition

We now turn to a study of the thermodynamic behaviour of multi-spinning $d = 6$ Kerr-anti de Sitter black holes with two fixed (non-trivial) angular momenta J_1 and J_2. Following [26], depending on the ratio:

$$q = J_2/J_1 \tag{103}$$

we find qualitatively different interesting phenomena known from the "every day thermodynamics" of simple substances. In addition to the large/small/large reentrant phase transition seen for $q = 0$ in previous subsections, we find for $0 < q < 0.00905$ an analogue of a 'solid/liquid' phase transition. Furthermore, the system exhibits a large/intermediate/small black hole phase transition with one triple and two critical points for $q \in (0.00905, 0.0985)$. This behavior is reminiscent of the solid/liquid/gas phase transition although the coexistence line of small and intermediate black holes does not continue for an arbitrary value of pressure (similar to the solid/liquid coexistence line) but rather terminates at one of the critical points. Finally, for $q > 0.0985$ we observe the 'standard liquid/gas behavior' of a van der Waals fluid.

Specifying to $d = 6$, we consider the Gibbs free energy $G = G(P, T, J_1, J_2)$, obtained from the expression (61) by eliminating parameters (l, r_+, a_1, a_2) in favor of (P, T, J_1, J_2) using Equations (1), (53) and (54). An analytic solution is not possible since higher-order polynomials are encountered and so we proceed numerically: for a given P, r_+, J_1 and J_2, we solve J_i equations in Equation (53) for a_1 and a_2 and thence calculate the values of T and G using Equations (54) and (61), yielding a $G - T$ diagram. Once the behavior of G is known, we compute the corresponding phase diagram, coexistence lines, and critical points in the $P - T$ plane. We display our results in Figures 18–20. Since the qualitative behavior of the system depends only on $q = J_2/J_1$ we set everywhere $J_1 = 1$.

3.5.1. Solid/Liquid Analogue

For $0 < q < q_1 \approx 0.00905$ the behaviour of G, displayed for $q = 0.005$ in Figure 18, completely changes to the $q = 0$ behaviour discussed in the previous subsection, cf. Figures 11 and 12. Namely the unstable branch of tiny hot black holes on the right of the $G - T$ diagram in Figure 11 disappears and a new branch of (locally) stable tiny cold black holes appears to the left. The $q = 0$ "no black hole region" is eliminated and the situation is very similar to what happens when a small charge is added to a Schwarzschild black hole, cf. Section 2. The zeroth-order phase transition is "replaced" by a "solid/liquid"-like phase transition of small to large black holes. Although in this range of angular momenta G admits two critical points (one at $P = P_c$ and another at $P = P_v < P_c$), only the one at $P = P_c$ occurs for stable black holes that minimize G globally. Consequently we observe one phase transition between small and large black holes. The corresponding coexistence line (not displayed) terminates at a critical point characterized by (T_c, P_c) and is qualitatively similar to Figure 9. As q decreases, the critical point occurs for larger and larger pressures P_c and temperatures T_c and in the limit $q \to 0$ we find 'an infinite' coexistence line, similar to what happens for a solid/liquid phase transition. This is indicated in Figure 21.

Figure 18. Gibbs free energy for $q = 0.005$ Kerr-AdS black hole in $d = 6$ is displayed for decreasing pressures (from top to bottom). The horizon radius r_+ increases from left to right. The uppermost isobar corresponds to $P = P_c = 4.051$; for higher pressures only one branch of (stable) black holes with positive C_P exists. The second uppermost isobar displays the swallowtail behaviour and implies the existence of a first order phase transition. For $P = P_v \approx 0.0958$ another critical point emerges but occurs for a branch that does not minimize G globally. Consequently, out of the two swallowtails for $P < P_v$ only one occurs in the branch globally minimizing G and describes a "physical" first order phase transition.

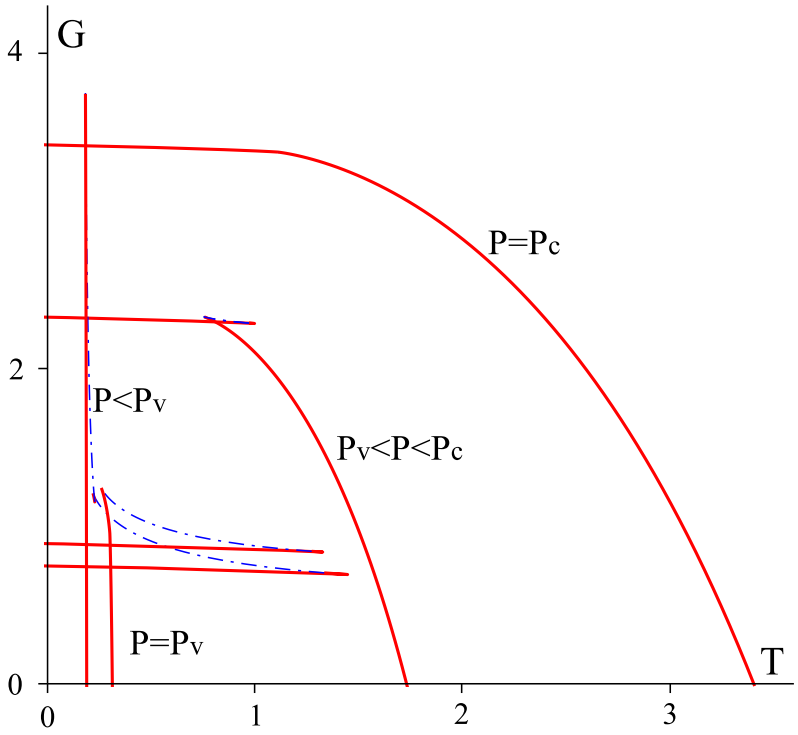

3.5.2. Triple Point and Solid/Liquid/Gas Analogue

For fixed $q_1 < q < q_2 \approx 0.0985$ a new phenomenon occurs: for a certain range of pressures we observe two swallowtails in the stable branch of black holes, see Figure 19, corresponding to a small/intermediate/large black hole phase transition. As pressure decreases, the two swallowtails move closer together until, at $P = P_{tr}$, the corresponding first order phase transitions coincide—giving a triple point. Below P_{tr}, only one of the first order phase transitions continues to occur in a stable branch. The whole situation is reminiscent of the solid/liquid/gas phase transition.

Let us describe in more detail what happens for fixed $q = 0.05$ as pressure decreases, illustrated in Figures 19 and 20. For very large pressures there are no swallowtails and only one branch of locally stable black holes with positive C_P exists. Decreasing the pressure, at $P = P_{c_1} \approx 0.260$ a critical point occurs; slightly below P_{c_1} we observe a first order phase transition between large and small black holes. This continues to happen until at $P = P_{c_2} \approx 0.0957$ we observe another critical point. Slightly below P_{c_2} the system exhibits two swallowtails in the stable branch of black holes and thence two first order phase transitions between various size black holes are present: from small to intermediate and from

intermediate to large. As P decreases even further, the two swallowtails move closer to each other, until at $P = P_{tr} \approx 0.0642$ the corresponding first order phase transitions coincide—we observe a triple point. Below P_{tr} only one of the first order phase transitions continues to occur in the stable branch of black holes. The corresponding $P - T$ phase diagram displaying all the features is depicted in Figure 20; in many respects it is reminiscent of a solid/liquid/gas phase diagram.

Figure 19. Gibbs free energy for $q = 0.05$ Kerr-AdS black hole in $d = 6$ is displayed for various pressures (from top to bottom) $P = 0.260, 0.170, 0.087, 0.0642, 0.015$. The horizon radius r_+ increases from left to right. The uppermost isobar corresponds to $P = P_{c_1} = 0.260$; for higher pressures only one branch of stable black hole with positive C_P exists. The second uppermost isobar displays the swallowtail behavior, implying a first order phase transition. The third isobar corresponds to P between $P_{c_2} = 0.0957$ and P_{c_1} for which we have "two swallowtails". For such pressures there are two first order phase transitions. The fourth isobar displays the tricritical pressure $P_{tr} = 0.0642$ where the two swallowtails "merge" and the triple point occurs. Finally the lower-most isobar corresponds to $P < P_{tr}$.

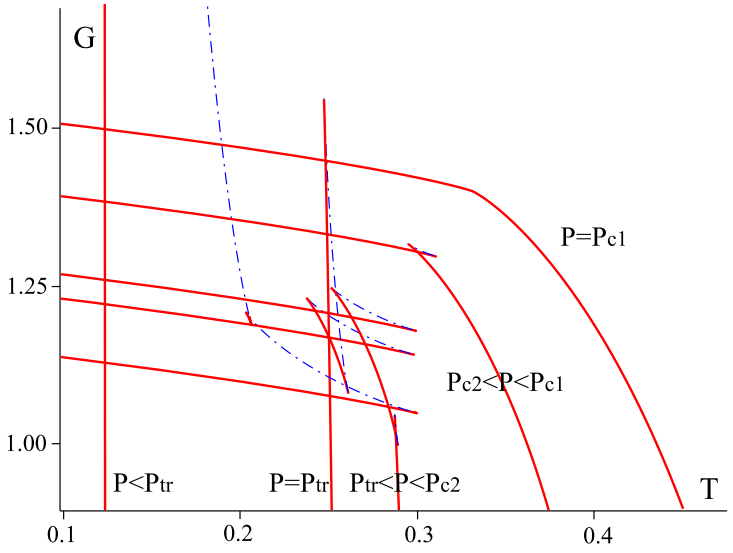

So far we considered a fixed parameter $q = 0.05$. Let us now look at what happens as we allow q to vary, see Figure 21. We already know that for $q < q_1$ we observe one first order phase transition terminating at a critical point characterized by (T_{c_1}, P_{c_1}), as described in the previous subsection. Qualitatively new feature occurs at $q = q_1$: a triple point and a second critical point emerge from the coexistence line at $P_{tr} = P_{c_2} \approx 0.09577$ and $T_{tr} = T_{c_2} \approx 0.30039$. As q increases, the triple point moves away from the second critical point; the values of T_{tr} and P_{tr} decrease, while the values of T_{c_2} and P_{c_2} almost do not change. A small/intermediate/large black hole phase transition may occur and the situation resembles that of the solid/liquid/gas phase transition. At the same time as q increases, the first critical point moves towards the triple point (P_{c_1} rapidly decreases). At $q = q_{eq} \approx 0.08121$ both critical points occur at the same pressure $P_{c_1} = P_{c2} \approx 0.0953$, whereas $T_{c_1} \approx 0.2486 < T_{c_2} \approx 0.2997$. Increasing q even further, the first critical point moves closer and closer to the triple point and finally for $q = q_2 \approx 0.0985$ the two merge at $P_{tr} = P_{c_1} \approx 0.049$. Above q_2 only the second critical point remains.

Figure 20. $P - T$ diagram for $q = 0.05$. The diagram is analogous to the solid/liquid/gas phase diagram. Note however that there are two critical points. That is, small/intermediate black hole coexistence line does not extend to infinity but rather terminates, similar to the "liquid/gas" coexistence line, in a critical point.

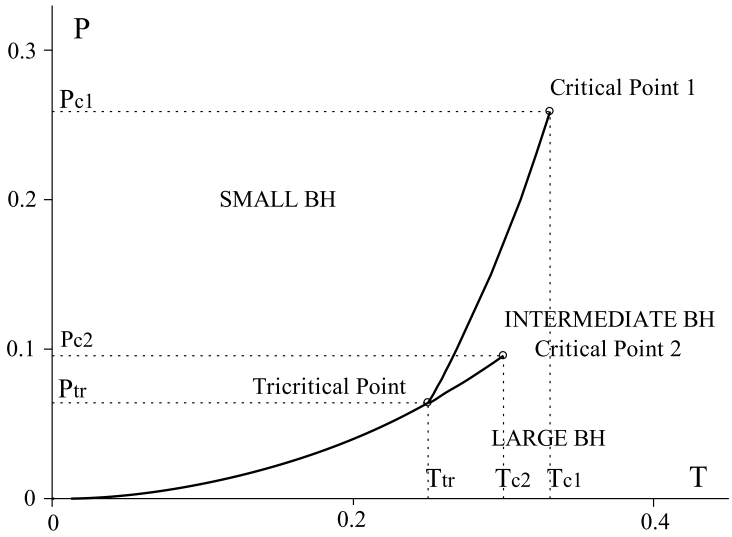

Figure 21. Critical pressures and variable q. Depending on the value of q, we observe one critical point or two critical points and one triple point. This figure displays the corresponding P_{c_1}, P_{c_2}, and P_{tr}. For $q < q_1$ only one critical point occurs: as $q \to 0$, P_{c_1} rapidly diverges to infinity and the coexistence line becomes infinitely long—this is an analogue of a solid/liquid phase transition. Between q_1 and q_2 we observe two critical points at P_{c_1} and P_{c_2}, displayed by solid thick black line and thin dashed line respectively, and a triple point displayed by the red solid curve. As q increases, P_{c_1} rapidly decreases until it meets P_{tr} at $q = q_2$ where it terminates; in between there exists $q = q_{eq}$ where $P_{c_1} = P_{c_2}$. Above q_2 only the second critical point at P_{c_2} exists.

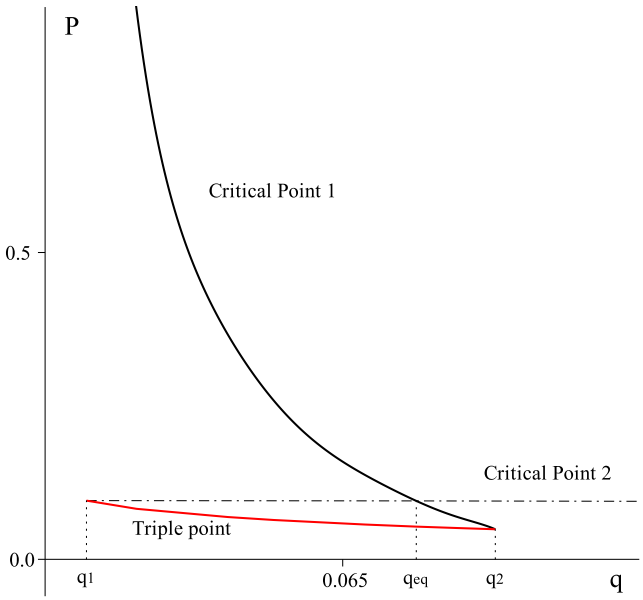

We remark that, similar to the reentrant phase transition, the analogue of a solid/liquid/gas phase transition as well as of the triple point occurs for any fixed P in the allowed range. Once again, the possibility for an AdS/CFT interpretation emerges: a corresponding phase transition may occur in the dual CFT within the allowed range of N. To stress this point we plot in Figure 22 a $q-T$ phase diagram, showing the existence of small/intermediate/large black hole phase transition and the corresponding triple point for a fixed pressure.

Figure 22. Kerr-AdS analogue of solid/liquid/gas phase transition in $q - T$ plane. The diagram is displayed for fixed pressure $l \approx 2.491$.

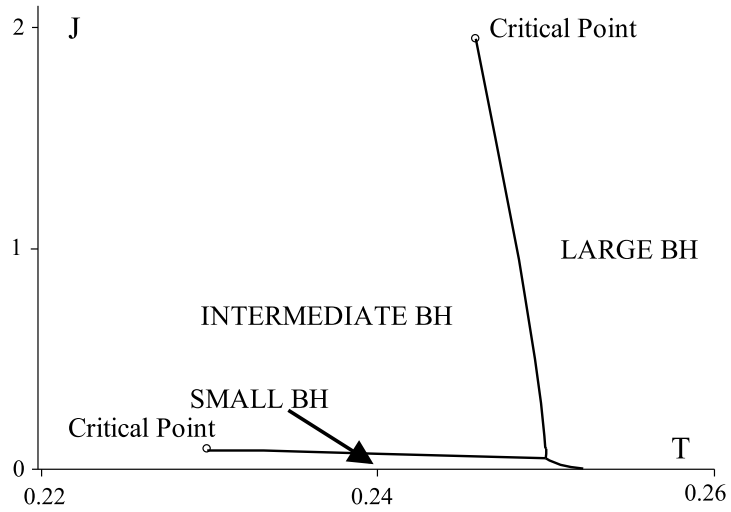

3.5.3. Van Der Waals Behavior

For $q > q_2$ only one small/large black hole coexistence line exists and terminates at a corresponding critical point. We observe an analogue of a van der Waals "liquid/gas" phase transition.

In fact, the situation is a little more subtle. For $q_2 < q < q_3 \approx 0.1274$, similar to the 'solid/liquid analogue', the second critical point still exists, but occurs for the locally unstable branch of black holes with negative heat capacity that does not globally minimize the Gibbs free energy. Hence, only one phase transition is physical. For $q > q_3$ this second critical point completely disappears. In both cases we observe a "standard liquid/gas" van der Waals phase transition, qualitatively similar to $d = 4, 5$ case and the case of equal spinning Kerr-AdS black holes in any dimension $d \geq 5$.

4. Myers–Perry Solutions

We now turn to consider the d-dimensional multi-rotating black holes with spherical horizon topology for which the cosmological constant and hence the pressure vanishes, described by the Myers–Perry solution [51]. The most interesting observation is that even in this asymptotically flat case we find that reentrant phase transitions can take place.

The Myers-Perry (MP) solutions are the most general rotating black hole solutions (with zero NUT charge) to the vacuum Einstein equations ($R_{ab} = 0$) of spherical horizon topology in d-dimensions [51]. The metric as well as its associated thermodynamic quantities, particularly thermodynamic volume, can

be obtained as the $\Lambda \to 0$ (or $l \to \infty$) limit of the general Kerr-AdS case discussed in previous section. In Boyer–Lindquist coordinates the metric reads:

$$\begin{aligned} ds^2 &= -d\tau^2 + \frac{2m}{U}\Big(d\tau - \sum_{i=1}^{N} a_i \mu_i^2 d\varphi_i\Big)^2 + \frac{U dr^2}{F - 2m} \\ &+ \sum_{i=1}^{N}(r^2 + a_i^2)\mu_i^2 d\varphi_i^2 + \sum_{i=1}^{N+\varepsilon}(r^2 + a_i^2)d\mu_i^2 \end{aligned} \tag{104}$$

where as before $\varepsilon = (1, 0)$ refers to (even, odd) spacetime dimensionality:

$$F = r^{\varepsilon-2}\prod_{i=1}^{N}(r^2 + a_i^2)\,, \quad U = F\Big(1 - \sum_{i=1}^{N}\frac{a_i^2\mu_i^2}{r^2 + a_i^2}\Big) \tag{105}$$

and the thermodynamic quantities are given by [51]:

$$\begin{aligned} M &= \frac{m\omega_{d-2}(d-2)}{8\pi}\,, \quad J_i = \frac{a_i m\omega_{d-2}}{4\pi}\,, \quad \Omega_i = \frac{a_i}{r_+^2 + a_i^2} \\ A &= \frac{\omega_{d-2}}{r_+^{1-\varepsilon}}\prod_{i=1}^{N}(a_i^2 + r_+^2)\,, \quad V = \frac{r_+ A}{d-1}\Big(1 + \frac{1}{d-2}\sum_{i=1}^{N}\frac{a_i^2}{r_+^2}\Big) \\ T &= \frac{1}{2\pi}\Big(\sum_{i=1}^{N}\frac{r_+}{a_i^2 + r_+^2} - \frac{1}{2^\varepsilon r_+}\Big)\,, \quad S = \frac{A}{4} \end{aligned} \tag{106}$$

The thermodynamic volume is the $l \to \infty$ limit of Equation (55). It inherits the property of obeying the reverse isoperimetric inequality Equation (11), provided in Equation (9) we identify $\mathcal{A} = A$ and $\mathcal{V} = V$.

4.1. Five-Dimensional Case

Let us first consider the $d = 5$ MP black hole solution, which in general admits two angular momenta J_1 and J_2. As with the Kerr-AdS case, we consider the ratio:

$$q = J_2/J_1 \tag{107}$$

and set $J_1 = 1$. As shown in Figure 23, we find that the Gibbs free energy shares qualitatively the same behaviour with the $d = 4$ Kerr metric for any value of $0 \leq q \leq 1$. Namely, two branches of black holes exist below the critical temperature at the cusp in G and no black holes are possible above this temperature. The lower, "fast spinning" branch of small black holes corresponds to the global minimum of the Gibbs free energy and possess positive C_P. The upper, "Schwarzschild-like", branch of slowly spinning large black holes is thermodynamically unstable.

Figure 23. Gibbs free energy: $d = 5$ MP black holes. The lower curve corresponds to the singly-spinning ($q = 0$) MP black hole whereas the upper curve is for equal spinning ($q = 1$) one. The qualitative behavior remains the same irrespective of the value of q and is similar to $d = 4$ Kerr case, cf. Figure 2.

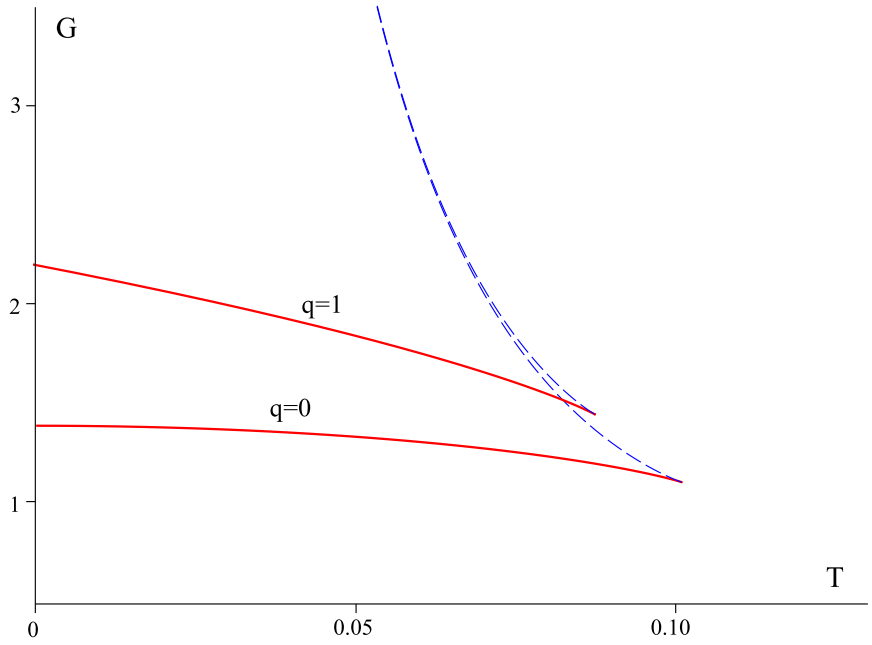

4.2. Reentrant Phase Transition

Next we consider the $d = 6$ MP solution with two angular momenta J_1 and J_2. As before, we consider the ratio Equation (107) and without loss of generality set $J_1 = 1$. We now observe various phenomena reflected in the behavior of the Gibbs free energy for various values of q, as shown in Figure 24. For $q = 0$ we observe a singly branch of thermodynamically unstable black holes with negative C_P; qualitatively same behavior occurs for singly spinning MP black holes in all $d \geq 6$. For larger values of q more interesting phase behavior occurs.

For $0 < q < q_t \approx 0.1082$ a new branch of small thermodynamically stable black holes appears, similar to the Kerr case in $d = 4$, except there is a swallowtail in the upper unstable branch of large black holes. In this range of q's the global minimum of G corresponds to small fast spinning black holes that exist up to some maximum temperature T_{max}. Above this temperature no black holes are possible; this "no black hole region" is shown in Figure 25. At $q = q_t \approx 0.1082$, Figure 24c, the swallowtail in the upper unstable branch reaches the lower stable branch and we observe the entrance of reentrant phase transition.

Figure 24. Reentrant phase transition: $d = 6$ doubly spinning MP black hole. The Gibbs free energy is displayed for various ratios of angular momenta $q = J_2/J_1 = \{0, 0.05, 0.1082, 0.112, 0.11715, 0.122, 0.1278, 0.5, 1\}$ (from top to bottom). Solid-red/dashed-blue lines correspond to C_P positive/negative respectively. (**a**) Shows the thermodynamically unstable branch of $q = 0$ black holes with negative C_P; qualitatively similar behaviour occurs for singly spinning MP black holes in all $d \geq 6$. When a second angular momentum is switched on; (**b**) a new branch of small thermodynamically stable black holes appears, similar to the $d = 4$ Kerr case. At $q = q_t \approx 0.1082$; (**c**) the swallowtail in the upper unstable branch touches the lower stable branch, and we observe the appearance of a reentrant phase transition; (**d**) displays typical behavior of G when the reentrant phase transition is present, $q \in (q_t, q_z)$, $q_z \approx 0.11715$. Black arrows indicate increasing r_+; (**e**) shows $q = q_z$ at which the reentrant phase transition terminates, while the first order phase transition at $T = T_1$ is still present. The first order phase transition continues to occur; (**f**) and (**g**) until at $q = q_c \approx 0.1278$ we observe a critical point at $T_c \approx 0.18577$. Above q_c the system displays "Kerr-like" behavior with no phase transitions.

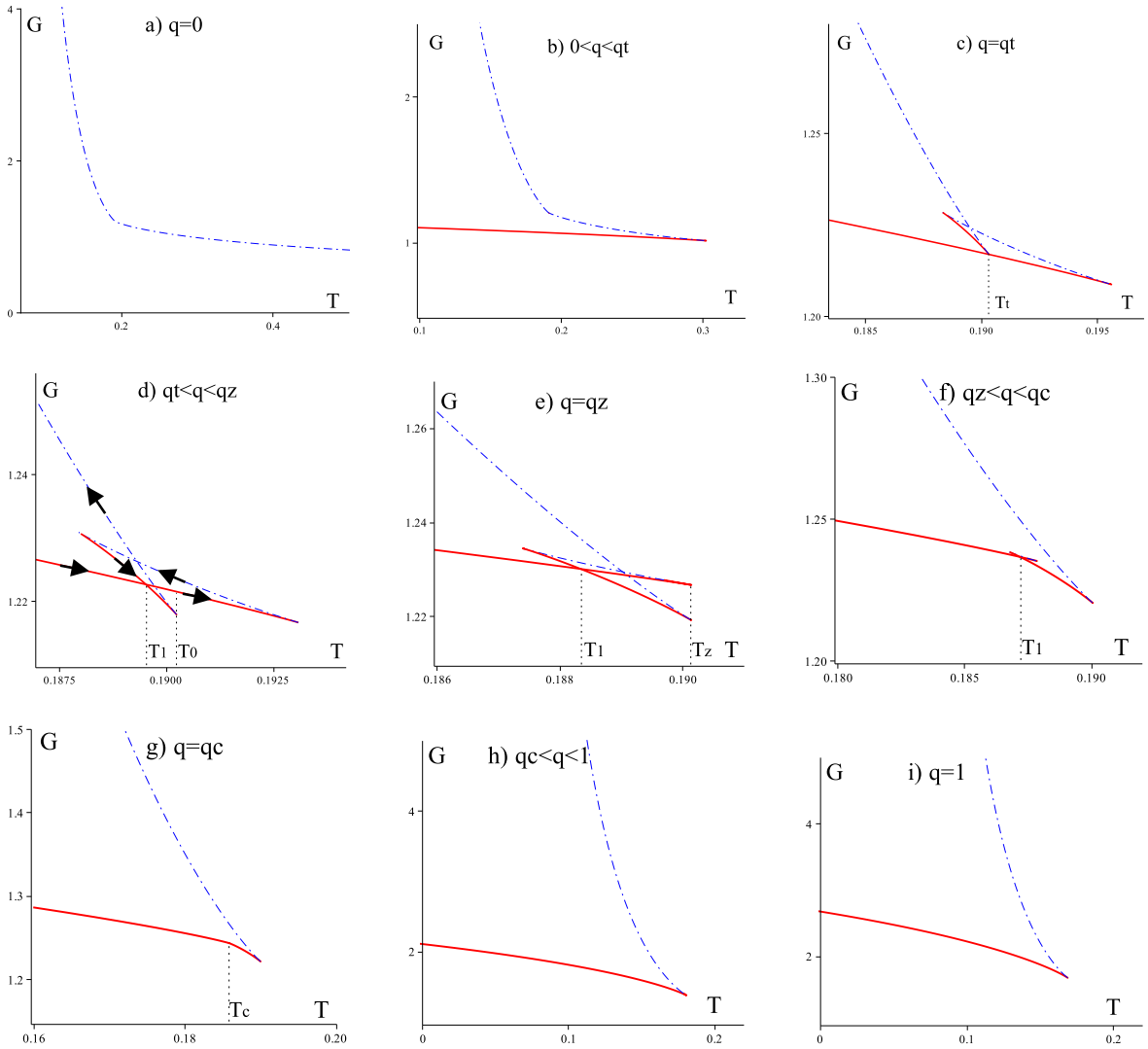

Figure 25. $q - T$ phase diagram: $d = 6$ MP black holes. The first order phase transition between small and large black holes is displayed by solid black curve; it terminates at a critical point characterized by (T_c, q_c). The solid red curve corresponds to the 0th-order phase transition between large and intermediate (small) black holes; it occurs for $q \in (q_t, q_z)$ and $T \in (T_t, T_z)$. In this range of q's reentrant phase transition is possible. The "no BH region" is outlined by thin dashed black curve.

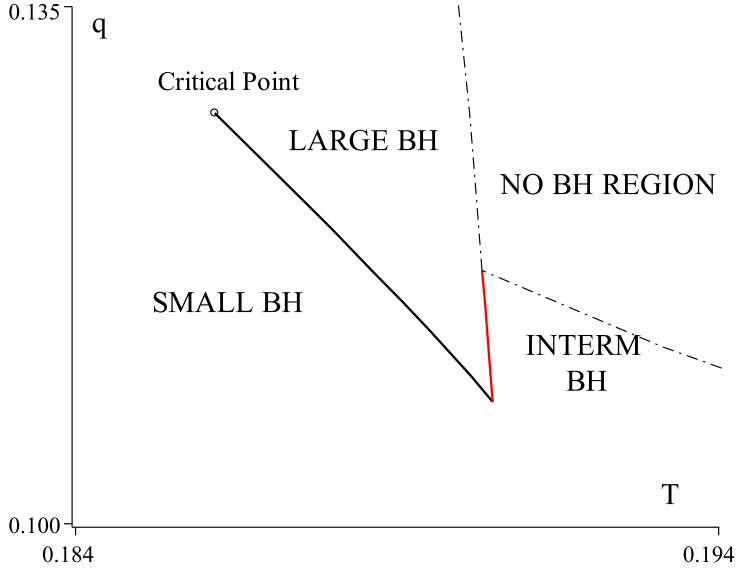

The typical behavior of G for $q \in (q_t, q_z)$ is displayed in Figure 24d (enlarged in Figure 26) and indicates the presence of the reentrant phase transition. If we start increasing the temperature from, say $T = 0.186$, the system follows the lower left horizontal solid red curve, describing small black holes. At $T = T_1$ it undergoes a first order phase transition and follows the lowest stable branch of large black holes until, at $T = T_0$, there is a cusp in G and this branch terminates. Beyond the cusp, as the temperature increases even further, there is a discontinuity in the global minimum of G, yielding a zeroth-order phase transition to the upper red branch of small black holes. In other words, we observe a SBH/LBH/SBH reentrant phase transition. This reentrant phase transition, however, stands in contrast to the situation in the Kerr-AdS case discussed in the previous section, cf. Figures 12, 13, 15. In the Kerr-AdS case the black holes undergoing the reentrant phase transition were singly spinning, the phase transition was of the LBH/SBH/LBH type with $T_0 < T_1$ and the 'no black hole region' occurred for small temperatures, whereas in the MP case the black holes must be doubly spinning, the phase transition is of the SBH/LBH/SBH type with $T_1 < T_0$, and the "no black hole region" occurs for high temperatures.

The reentrant phase transition terminates at $q = q_z \approx 0.11715$ as shown in Figure 24e. In between q_z and $q_c \approx 0.1278$ there is a first order SBH/LBH phase transition illustrated in Figure 24f. This transition terminates at a critical point at $T_c \approx 0.18577$, Figure 24g. Above q_c the system displays "Kerr-like" behavior with no phase transitions, as seen in Figures 24h,i. The overall situation is summarized in the $q - T$ phase diagram in Figure 25.

The important lesson of this section is that we showed that the reentrant phase transition can take place in black hole spacetimes without the cosmological constant, that is, when the system has zero

pressure. A gauge/gravity interpretation of this phenomenon, similar to the asymptotically AdS case, remains to be explored.

Figure 26. Enlargement of Figure 23d to better illustrate the typical behavior of G when the reentrant phase transition is present.

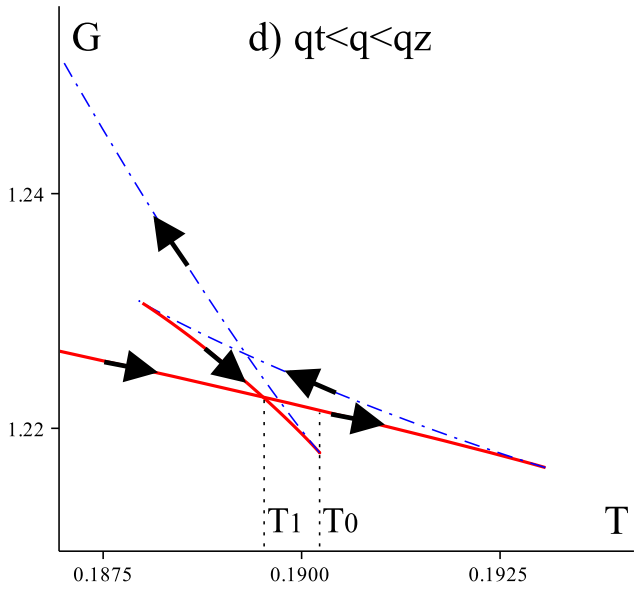

5. Five-Dimensional Black Rings and Black Saturns

In this section we look at the thermodynamics of other analytically known $d = 5$ black hole objects with horizon topologies more complicated than spherical, specifically singly spinning black rings and black saturns. Unfortunately, due to the lack of a generating technique for $\Lambda \neq 0$, only vacuum solutions are known. For this reason, there is no effective thermodynamic way to calculate the thermodynamic volume and the fluid equation of state is trivial; we limit ourselves to studying the Gibbs free energy for these objects and comparing it to the Gibbs free energy of the $d = 5$ MP solution. In the next section we shall try to circumvent the lack of knowledge of exact asymptotically AdS black ring solutions by considering the approximate thin AdS black rings constructed via the blackfold approach. In the given (fast spinning approximation) this will allow us to calculate the thermodynamic volume, verify the reverse isoperimetric inequality, and construct the corresponding equation of state.

5.1. Singly Spinning Black Ring

The exact solution for a singly spinning black ring in five dimensions was constructed by Emparan and Reall [110] and reads:

$$\begin{aligned} ds^2 &= -\frac{F(y)}{F(x)}\Big(dt - R\sqrt{\lambda(\lambda-\nu)}\frac{1+\lambda}{1-\lambda}\frac{1+y}{F(y)}d\phi_2\Big)^2 \\ &+ \frac{R^2F(x)}{(x-y)^2}\Big(\frac{dx^2}{G(x)} + \frac{G(x)}{F(x)}d\phi_1^2 - \frac{G(y)}{F(y)}d\phi_2^2 - \frac{dy^2}{G(y)}\Big) \end{aligned} \tag{108}$$

where:

$$F(\xi) = 1 + \lambda\xi\,, \quad G(\xi) = (1-\xi^2)(1+\nu\xi) \tag{109}$$

The dimensionful constant R sets a scale for the solution. The absence of conical singularities fixes λ and the periodicity of ϕ_1 and ϕ_2:

$$\lambda = \frac{2\nu}{1+\nu^2}\,, \quad 0 \leq \phi_1, \phi_2 \leq 2\pi\frac{\sqrt{1-\lambda}}{1-\nu} \tag{110}$$

while the remaining dimensionless parameter ν lies in the range $\nu \in (0,1)$. The coordinates x and y are restricted to the ranges $-1 \leq x \leq 1$ and $-1/\nu \leq y < -1$; the event horizon is located at $y = -1/\nu$.

The thermodynamic quantities are given by:

$$\begin{aligned} M &= \frac{3\pi R^2\nu}{2(1-\nu)(1+\nu^2)}\,, \quad J = \frac{\pi\nu R^3}{\sqrt{2}}\left(\frac{1+\nu}{(1-\nu)(1+\nu^2)}\right)^{3/2}, \quad \Omega = \frac{1}{R}\sqrt{\frac{\lambda-\nu}{\lambda(1+\lambda)}} \\ T &= \frac{(1-\nu)\sqrt{1+\nu^2}}{4\sqrt{2}\pi\nu R}\,, \quad S = \frac{2\sqrt{2}\pi^2R^3\nu^2}{(1-\nu)(1+\nu^2)^{3/2}} = \frac{A}{4} \\ C_P &= \frac{12\sqrt{2}\pi^2(\nu-1/2)\nu^2\sqrt{1+\nu^2}}{(1-\nu)(2+\nu^2)(1+\nu^2)^2}R^3 \end{aligned} \tag{111}$$

and using Equation (110) it is straightforward to show that the Smarr relation (5) holds. From the behavior of the heat capacity we see there is a clear distinction between *"fat" black rings* with $\nu > 1/2$ and $C_P > 0$, and *"thin" black rings* with $\nu < 1/2$ and $C_P < 0$.

It is not by any means obvious that the two kinds of black objects, the spherical MP black hole and the toroidal black ring, may be treated as "two phases" of the same system. Notwithstanding this concern, we plot the Gibbs free energy for the black ring:

$$G = M - TS = \frac{\pi R^2\nu(2+\nu)}{2(1+\nu^2)(1-\nu)} \tag{112}$$

parametrically in Figure 27, for $J = 1$, comparing it to the Gibbs free energy of the $d = 5$ singly spinning asymptotically flat MP black hole. We observe the following interesting behavior. There exists a special temperature T_r at which the branch of fat ($\nu > 1/2$) black rings terminates and is smoothly joined by the branch of thin black rings. At exactly the same temperature, G of MP black holes has a cusp. For temperatures below T_r we observe three branches of black holes: *small MP* black holes with positive C_P and the lowest Gibbs free energy, *fat black rings* with slightly higher Gibbs free energy and positive specific heat, and *large MP* black holes with the highest G and negative C_P, cf. $q = 0$ curves in Figure 23. Above T_r black holes are no longer possible and only a branch of thin black rings with negative C_P exists. We remark that very thin black rings are expected to be classically unstable due to the Gregory–Laflamme instability.

Figure 27. Gibbs free energy: black ring *vs.* black hole. The Gibbs free energy of black rings is compared to the Gibbs free energy of an MP black hole for $J = 1$. For temperatures below T_r we observe three branches of black holes: *small MP* black holes displayed by thick solid red curve have positive C_P and the lowest Gibbs free energy, *fat black rings* (depicted by the thick black solid curve slightly above the red curve) have positive C_P and are locally thermodynamically stable, and *large MP* black holes (upper branch depicted by the thin blue dashed curve) with negative C_P. Above T_r black holes are no longer possible (G has a cusp there) and only a branch of thin black rings (displayed by a thick solid blue curve) with $C_P < 0$ exists. The approximate thin black ring solution, constructed using the blackfold approach in the next section, is displayed by the thin dashed black curve. We observe that the approximation works well for high temperatures, whereas it is completely off for low temperatures. We also note that the exact Gibbs free energy is actually lower than the one given by the blackfold approximation.

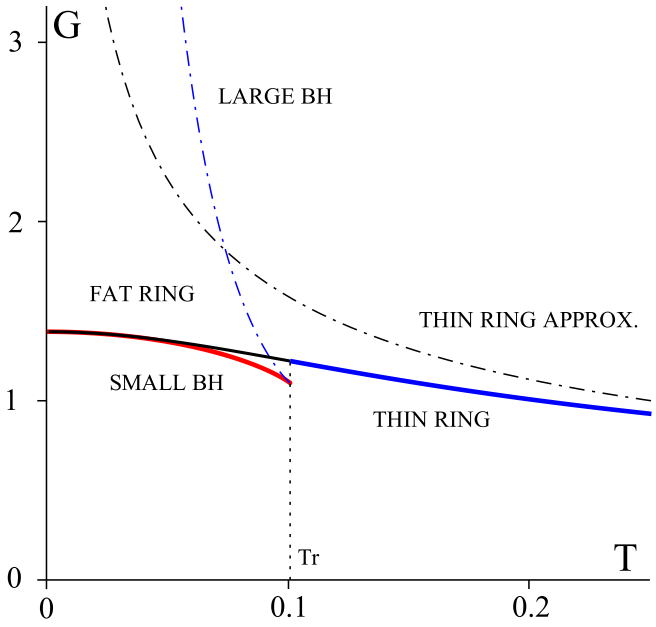

Our considerations imply that spherical black holes are thermodynamically preferable to fat black rings. This is supported by the study of the horizon areas, e.g., [110–115]. It is an open question as to whether there actually might be a phase transition from fat black rings to small MP black holes. Likewise one can ask if all thin rings, besides being thermodynamically unstable, are also classically unstable, see [116]. If so then are the small MP solutions the only stable vacuum black holes in five dimensions?

5.2. Black Saturn

This exact multi-black hole solution was constructed by Elvang and Figueras [117] and its "phases" and the first law were studied in [113]. The solution consists of a central rotating spherical black hole surrounded by a black ring. The solution depends on one dimensionful parameter L, and the

dimensionless parameters $0 \le \kappa_3 \le \kappa_2 < \kappa_1 \le 1$. The thermodynamic quantities associated with the two horizons are (using an abbreviation $\hat{\kappa}_i = 1 - \kappa_i$):

$$\begin{aligned}
\Omega_{BH} &= \frac{1+\kappa_2 c}{L}\sqrt{\frac{\kappa_2\kappa_3}{2\kappa_1}}\frac{\kappa_3\hat{\kappa}_1 - \kappa_1\hat{\kappa}_2\hat{\kappa}_3 c}{\kappa_3\hat{\kappa}_1 + \kappa_1\kappa_2\hat{\kappa}_2\hat{\kappa}_3 c^2}\\
\Omega_{BR} &= \frac{1+\kappa_2 c}{L}\sqrt{\frac{\kappa_1\kappa_3}{2\kappa_2}}\frac{\kappa_3 - \kappa_2\hat{\kappa}_3 c}{\kappa_3 - \kappa_3(\kappa_1-\kappa_2)c + \kappa_1\kappa_2\hat{\kappa}_3 c^2}\\
S_{BH} &= \frac{\pi^2 L^3}{(1+\kappa_2 c)^2}\sqrt{\frac{2\hat{\kappa}_1^3}{\hat{\kappa}_2\hat{\kappa}_3}}\Big(1 + \frac{\kappa_1\kappa_2\hat{\kappa}_2\hat{\kappa}_3 c^2}{\kappa_3\hat{\kappa}_1}\Big)\\
S_{BR} &= \frac{\pi^2 L^3}{(1+\kappa_2 c)^2}\sqrt{\frac{2\kappa_2(\kappa_2-\kappa_3)^3}{\kappa_1(\kappa_1-\kappa_3)\hat{\kappa}_3}}\Big(1 - (\kappa_1-\kappa_2)c + \frac{\kappa_1\kappa_2\hat{\kappa}_3 c^2}{\kappa_3}\Big)\\
T_{BH} &= \frac{1}{2\pi L}\sqrt{\frac{\hat{\kappa}_2\hat{\kappa}_3}{2\hat{\kappa}_1}}\frac{(1+\kappa_2 c)^2}{1 + \frac{\kappa_1\kappa_2\hat{\kappa}_2\hat{\kappa}_3}{\kappa_3\hat{\kappa}_1}c^2}\\
T_{BR} &= \frac{1}{2\pi L}\sqrt{\frac{\kappa_1\hat{\kappa}_3(\kappa_1-\kappa_3)}{2\kappa_2(\kappa_2-\kappa_3)}}\frac{(1+\kappa_2 c)^2}{1 - (\kappa_1-\kappa_2)c + \frac{\kappa_1\kappa_2\hat{\kappa}_3}{\kappa_3}c^2}
\end{aligned} \tag{113}$$

whereas the ADM mass M and angular momentum J are:

$$\begin{aligned}
M &= \frac{3\pi L^2}{4\kappa_3(1+\kappa_2 c)^2}\Big(\kappa_3(\hat{\kappa}_1+\kappa_2) - 2\kappa_2\kappa_3(\kappa_1-\kappa_2)c + \kappa_2\big[\kappa_1 - \kappa_2\kappa_3(\hat{\kappa}_2+\kappa_1)\big]c^2\Big)\\
J_{BH} &= -\frac{\pi L^3 c}{\kappa_3(1+\kappa_2 c)^2}\sqrt{\frac{\kappa_1\kappa_2}{2\kappa_3}}\left(\kappa_3\hat{\kappa}_1 + \kappa_1\kappa_2\hat{\kappa}_2\hat{\kappa}_3 c^2\right)\\
J_{BR} &= \frac{\pi L^3}{\kappa_3(1+\kappa_2 c)^3}\sqrt{\frac{\kappa_2}{2\kappa_1\kappa_3}}\big[\kappa_3 - \kappa_3(\kappa_1-\kappa_2)c + \kappa_1\kappa_2\hat{\kappa}_3 c^2\big]\big[\kappa_3 - \kappa_2(\kappa_1-\kappa_3)c + \kappa_1\kappa_2\hat{\kappa}_2 c^2\big]\\
J &= J_{BR} + J_{BH} = \frac{\pi L^3}{\kappa_3(1+\kappa_2 c)^2}\sqrt{\frac{\kappa_2}{2\kappa_1\kappa_3}}\Big(\kappa_3^2 - c\kappa_3\big[(\kappa_1-\kappa_2)(\hat{\kappa}_1+\kappa_3) + \kappa_2\hat{\kappa}_3\big]\\
&+ c^2\kappa_2\kappa_3\big[(\kappa_1-\kappa_2)(\kappa_1-\kappa_3) + \kappa_1(\hat{\kappa}_2+\kappa_1-\kappa_3)\big] - c^3\kappa_1\kappa_2\big[\kappa_1 - \kappa_2\kappa_3(\kappa_1-\hat{\kappa}_2-\hat{\kappa}_3)\big]\Big)
\end{aligned} \tag{114}$$

and a generalization of the Smarr formula (5):

$$\frac{3}{2}M = T_{BR}S_{BR} + T_{BH}S_{BH} + \Omega_{BR}J_{BR} + \Omega_{BH}J_{BH} \tag{115}$$

is again satisfied [117]. The absence of conical singularities requires:

$$c = \frac{1}{\kappa_2}\Big(\varepsilon\frac{\kappa_1-\kappa_2}{\sqrt{\kappa_1\hat{\kappa}_2\hat{\kappa}_3(\kappa_1-\kappa_3)}} - 1\Big) \tag{116}$$

with $\varepsilon = +1$ when $c > -1/\kappa_2$ and $\varepsilon = -1$ when $c < -1/\kappa_2$; $c = -1/\kappa_2$ is nakedly singular.

To ensure thermodynamic and mechanical equilibrium, we require:

$$T \equiv T_{BH} = T_{BR}\,, \quad \Omega \equiv \Omega_{BH} = \Omega_{BR} \tag{117}$$

This eliminates two of the dimensionless parameters, leaving one; let us say κ_2. In this case the system can be assigned a "total" Gibbs free energy:

$$G(T,J) = M - T(S_{BH} + S_{BR}) \tag{118}$$

As with the black ring, this can be plotted parametrically. We display the result in Figure 28, where it is compared to the Gibbs free energy of an MP black hole and black ring. Similar to the discussion in the previous subsection, when treated as different phases of one thermodynamic system, the spherical black hole phase is preferable in the range of temperatures $T \in (0, T_r)$ whereas the stability of the other black objects at higher temperatures is not known.

Figure 28. Gibbs free energy: $5d$ vacuum black holes. The Gibbs free energy of black saturn in thermodynamic and mechanical equilibrium (red curve) is compared to the Gibbs free energy of black ring (blue curve) and the MP spherical black hole (black curve). For temperatures below T_r, all three branches are possible, however, the spherical black hole branch globally minimizes the Gibbs free energy. We have set $J = 1$.

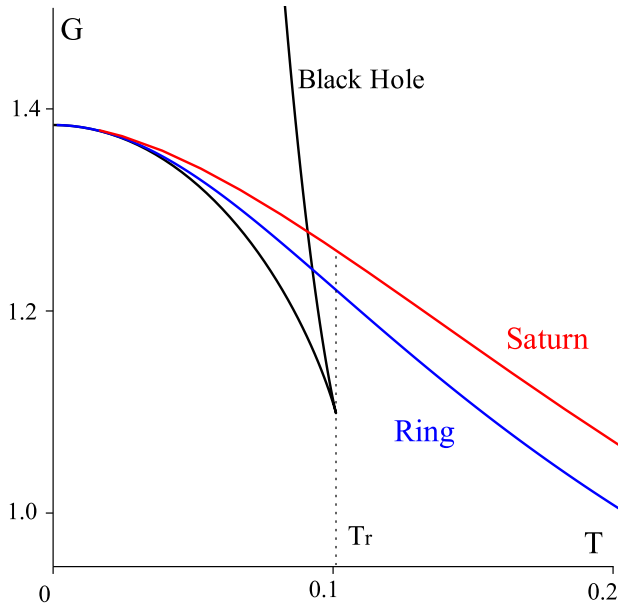

6. Thin Black Rings in AdS

6.1. Review of the Construction

Following [109] we briefly recapitulate the perturbative construction of an asymptotically AdS $d \geq 5$ singly spinning thin black ring with horizon topology $S^1 \times S^{d-3}$ using the blackfold approach [78,114]. Such a ring is characterized by the two radii R, corresponding to S^1, and r_0, associated with S^{d-3}. The idea of the construction is to "bend" a straight thin boosted black string of width r_0 into a circular shape of radius R. In the far region the ring is described by a distributional source of energy-momentum of a boosted string in the given (global) AdS$_d$ background:

$$\begin{aligned} ds^2 &= -f d\tau^2 + \frac{d\rho^2}{f} + \rho^2 (d\theta^2 + \sin^2\theta d\Omega_{d-4}^2 + \cos^2\theta d\psi^2) \\ f &= 1 + \frac{\rho^2}{l^2} \end{aligned} \tag{119}$$

placed at $\rho = R$ on the $\theta = 0$ plane. The magnitude of the boost of the string is determined from the equilibrium condition [118] and provides the correct centrifugal force to balance the ring tension and

the AdS gravitational potential. Once the correct magnitude of the boost is known, one can calculate the asymptotic charges using the energy momentum distribution. This gives the mass M and the angular momentum J of the ring. Due to the presence of the cosmological constant the boost increases with the radius R of the ring and approaches the speed of light in the limit $R \to \infty$. On the other hand the properties of the horizon, such as its area, angular velocity, or temperature, are determined from the characteristics of the boosted black string, as we shall point out below. Once constructed, the solution is valid provided the following approximation holds:

$$r_0 << \min(R, l) \tag{120}$$

This condition will play an important role in our discussion of the equation of state for these rings. Note that there is no restriction on the relation between R and l and so both large and small (with respect to the AdS radius) black rings are possible.

6.2. Thermodynamics

In terms of the dimensionless parameter:

$$\mathsf{R} = \frac{R}{l} \tag{121}$$

the thermodynamic quantities associated with the perturbative solution for a thin black ring in AdS are [109]:

$$\begin{aligned}
M &= \frac{r_0^{d-4} l}{8} \omega_{d-3} (d-2) \mathsf{R} \left(1+\mathsf{R}^2\right)^{\frac{3}{2}} \\
J &= \frac{\omega_{d-3} r_0^{d-4} l^2 \mathsf{R}^2}{8} \sqrt{\left(1+(d-2)\mathsf{R}^2\right)\left(d-3+(d-2)\mathsf{R}^2\right)} \\
S &= \frac{1}{2}\pi l r_0^{d-3} \omega_{d-3} \mathsf{R} \sqrt{\frac{d-3+(d-2)\mathsf{R}^2}{d-4}} = \frac{A}{4} \\
\Omega &= \frac{1}{l}\sqrt{\frac{(1+\mathsf{R}^2)(1+(d-2)\mathsf{R}^2)}{\mathsf{R}^2(d-3+(d-2)\mathsf{R}^2)}} \\
T &= \frac{(d-4)^{\frac{3}{2}}\sqrt{1+\mathsf{R}^2}}{4\pi r_0 \sqrt{d-3+(d-2)\mathsf{R}^2}}
\end{aligned} \tag{122}$$

The thermodynamic quantities of asymptotically flat thin black rings in higher dimensions [114] are obtained from these expressions by setting $l \to \infty$.

To plot the Gibbs free energy:

$$G = \frac{r_0^{d-4} l \mathsf{R}}{8} \omega_{d-3} \sqrt{1+\mathsf{R}^2} \left[2+(d-2)\mathsf{R}^2\right] \tag{123}$$

for fixed J and P we eliminate r_0 from the J equation:

$$r_0 = \left[\frac{128\pi}{(d-1)(d-2)\omega_{d-3}} \frac{P}{\mathsf{R}^2} \frac{J}{\sqrt{1+(d-2)\mathsf{R}^2}} \frac{1}{\sqrt{d-3+(d-2)\mathsf{R}^2}}\right]^{\frac{1}{d-4}} \tag{124}$$

to obtain G and T as functions of R, and plot parametrically. The behavior of G for a thin AdS black ring in $d = 6$ is illustrated in Figure 29 where it is compared to the corresponding Gibbs free energy of a singly spinning Kerr-AdS black hole. We observe that in the region of high temperature, where the blackfold approximation is valid, large Kerr-AdS black holes are thermodynamically preferred to thin AdS black rings. In the regime of small temperatures we cannot trust the blackfold approximation and the corresponding curve is unphysical. The Gibbs free energy of asymptotically flat thin rings is discussed in the next section, where it is compared to the Gibbs free energy of an MP black hole, leading to a more interesting behavior and a possible phase transition between black holes and black rings as shown in Figure 30.

The specific heat of AdS black rings can be analyzed in the same way as for black holes. We find that in a given approximation C_P is always negative. Hence higher-dimensional AdS thin black rings in this (fast spinning) approximation are thermodynamically unstable. We expect that this may not be longer true for the full, not necessarily thin, exact black ring solution, and perhaps "fat AdS ring analogues" with positive C_P exist in higher dimensions, cf. discussion of $d = 5$ exact asymptotically flat black rings in the previous section.

Figure 29. Gibbs free energy: thin AdS black rings vs. Kerr-AdS black holes in $d = 6$. The Gibbs free energy of thin black rings in the blackfold approximation is displayed for $P = \{0.2, 0.073, 0.0564, 0.04\}$ (the upper blue, red, black, and green curves that emerge from the left top corner) and is compared to the corresponding exact Gibbs free energy of Kerr-AdS black holes for the same pressures, cf. Figure 11. For large temperatures the branch of large Kerr-AdS black holes is thermodynamically preferred, whereas in the regime of small temperatures we cannot trust our blackfold approximation.

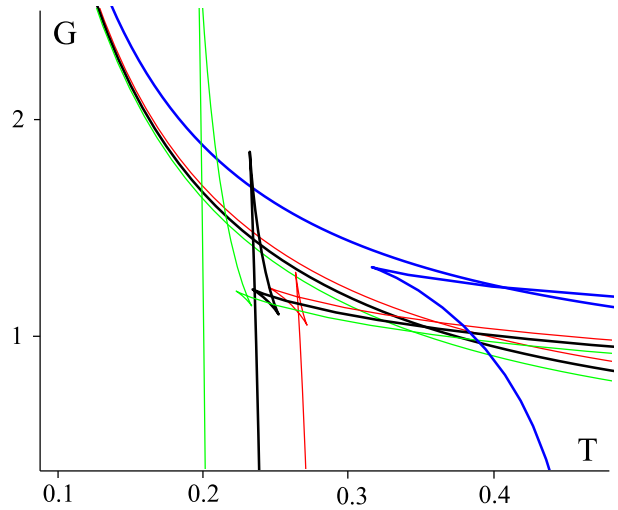

6.3. Thermodynamic Volume

Using the thermodynamic quantities Equation (122) and the Smarr relation Equation (5), the thermodynamic volume of thin AdS black rings reads:

$$V_{\text{AdS}} = \frac{\pi\omega_{d-3}l^3}{d-1}\mathsf{R}^3 r_0^{d-4}\sqrt{1+\mathsf{R}^2} = \frac{\pi\omega_{d-3}}{d-1}R^3 r_0^{d-4}\sqrt{1+R^2/l^2} \tag{125}$$

One can then readily verify that the first law Equation (4) is satisfied. It is obvious that the last formula has a smooth limit for $l \to \infty$. That is, a thermodynamic volume of an asymptotically flat black ring is:

$$V_{\text{flat}} = \frac{\pi \omega_{d-3}}{d-1} R^3 r_0^{d-4} \tag{126}$$

while its horizon area reads:

$$A = 2\pi r_0^{d-3} \omega_{d-3} R \sqrt{\frac{d-3}{d-4}} \tag{127}$$

Figure 30. Onsets of ultraspinning instabilities: $d = 6$ MP black holes. The Gibbs free energy of a singly spinning MP black hole with $J = 1$ (displayed by solid colored curves) is compared to the Gibbs free energy of a thin black ring constructed in the blackfold approximation (displayed by a black thin dashed curve); r_+ decreases from left to right. The onsets of ultraspinning instabilities Equation (147) are displayed by various colors as follows. The black solid line corresponds to MP black holes outside of the ultraspinning region (with only the $k = 0$ mode present). The $k = 1$ zero mode appears for $r_+ = r_1 \approx 0.605$ indicated by a point where solid red and black curves join together; the appearance of this zero mode can be predicted from thermodynamic considerations. The actual onsets of ultraspinning instabilities occur for $k = 2, 3, 4, \ldots$, and are displayed by onsets of green, blue, brown,. . . , curves; these indicate possible bifurcations to new families of stationary black holes. It is reasonable to conjecture that the actual G of an exact black ring is slightly smaller than that of the displayed approximation and would cross the G of an MP black hole close to $r_+ = r_2$, indicating a possible first order phase transition between the two kinds of black holes.

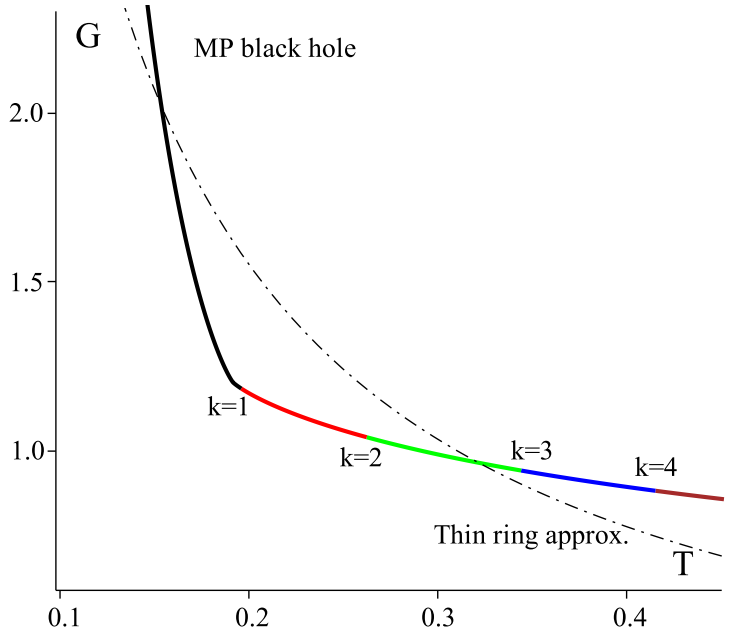

Let us briefly comment on the structure of formula for V_{flat}, Equation (126). We first note that a naive geometric volume of a string "bent to" a radius R goes as:

$$V' \propto 2\pi R r_0^{d-2} \tag{128}$$

This is fundamentally different from the computed thermodynamic volume Equation (126). However, we have seen in Section 3 that even for spherical black holes in the presence of rotation the two volumes, the geometric one and the thermodynamic one, are not the same and differ by a term proportional to J^2/M, see Equation (58) (we are grateful to Jennie Traschen and David Kastor for reminding us of this fact). For the black ring we find:

$$\frac{J^2}{M} = \frac{d-3}{8(d-2)}\omega_{d-3} r_0^{d-4} R^3 \tag{129}$$

Obviously, in the validity of our approximation, Equation (120), $R >> r_0$ and this term is much bigger than the contribution of the geometric volume V', Equation (128). This indicates that we are in fact in the ultraspinning regime. We find:

$$V_{\text{flat}} = \frac{8\pi}{d-1}\frac{d-2}{d-3}\frac{J^2}{M} \tag{130}$$

which replaces Equation (59) valid for ultraspinning spherical black holes. To summarize, the structure of the formula (126) is governed by the ultraspinning contribution rather than the geometric part of the volume, which explains otherwise puzzling dependence $V \propto R^3 r_0^{d-4}$. We expect that more generally, outside of the ultraspinning regime, one would have:

$$V_{\text{flat}} = V' + \frac{8\pi}{d-1}\frac{d-2}{d-3}\frac{J^2}{M} \tag{131}$$

in parallel with formula (58) for spherical black holes.

6.4. Isoperimetric Inequality

It was conjectured in [10] that a *reverse isoperimetric inequality* holds for a thermodynamic volume of any asymptotically AdS black holes, the statement being verified for a variety of (charged rotating) black holes with the horizon of spherical topology. Here we show that this conjecture remains true for asymptotically AdS black rings, at least in the thin ring (fast spinning) approximation.

Let us calculate the ratio $\mathcal{R}$ in Equation (9), identifying $\mathcal{A} = A$ and $\mathcal{V} = V$ as given by Equations (122) and (125) Then we have:

$$\begin{aligned}\mathcal{R}^{(d-1)(d-2)} &= \frac{\omega_{d-2}}{2^{d-1}\pi\omega_{d-3}}\left(\frac{R}{r_0}\right)^{2d-5}\frac{\left(1+\mathsf{R}^2\right)^{\frac{d-2}{2}}}{\left(\frac{d-3}{d-4}+\frac{d-2}{d-4}\mathsf{R}^2\right)^{\frac{d-1}{2}}} \\ &\geq \frac{\omega_{d-2}}{2^{d-1}\pi\omega_{d-3}}\left(\frac{R}{r_0}\right)^{2d-5}\left(\frac{d-4}{d-2}\right)^{\frac{d-1}{2}}\frac{1}{\sqrt{1+\mathsf{R}^2}}\end{aligned} \tag{132}$$

Now for $R \leq l$ we have $\sqrt{1+\mathsf{R}^2} \leq \sqrt{2}$ and hence the ratio Equation (9) is governed by:

$$\mathcal{R}^{(d-1)(d-2)} \geq \text{const} \times \left(\frac{R}{r_0}\right)^{2d-5} \gg 1 \tag{133}$$

by the assumption of the approximation, Equation (120). For $R > l$, $\sqrt{1+\mathsf{R}^2} \leq \sqrt{2}\mathsf{R} \ll \sqrt{2}R/r_0$. In this case, we have:

$$\mathcal{R}^{(d-1)(d-2)} \gg \text{const} \times \left(\frac{R}{r_0}\right)^{2d-6} \gg 1 \tag{134}$$

so in both cases the reverse isoperimetric inequality is comfortably satisfied in the given approximation Equation (120). Note that, similar to the Kerr-AdS case in the ultraspinning regimes, see Section 3, the ratio is much bigger than one; in fact in the full ultraspinning limit in both instances it diverges.

6.5. Equation of State

In order to find the equation of state for our black rings, we start from the expressions for J, T, and V in Equation (122). Expressing r_0 from the J equation as in (124), the V equation becomes a quadratic equation for R, and gives:

$$\mathsf{R}^2 = \frac{-1 \pm \sqrt{1-4k}}{2}\,, \quad k = \frac{\alpha(d-3)}{\alpha(d-2)^2-1}\,, \quad \alpha = \frac{1}{4\pi}\frac{d-1}{d-2}\frac{PV^2}{J^2} \geq 0 \tag{135}$$

In order R^2 be non-negative, we must have $k \leq 0$, *i.e.*, $\alpha \leq 1/(d-2)^2$, or, in terms of the physical quantities:

$$P \leq P_{\text{ultra}} \equiv \frac{4\pi}{(d-1)(d-2)}\frac{J^2}{V^2} \quad . \tag{136}$$

This bound is attained for ultraspinning black rings of radius R. Such black rings have in fact an infinite temperature (see next subsection).

The T Equation (122):

$$T = \frac{(d-4)^{\frac{3}{2}}\sqrt{1+\mathsf{R}^2}}{4\pi r_0\sqrt{d-3+(d-2)\mathsf{R}^2}} \tag{137}$$

with r_0 and R expressed by Equations (124) and (135), becomes an implicit equation of state, $P = P(V, T, J)$.

Note that, in the region of validity of our approximation we must have:

$$\frac{R}{r_0} = \frac{\sqrt{(d-1)(d-2)}}{4\sqrt{\pi P}}\frac{\mathsf{R}}{r_0} \gg 1\,, \quad \frac{l}{r_0} \gg 1 \tag{138}$$

while at the same time the condition (136) must be satisfied. For fixed J these conditions pick up a very narrow region in $P-v$ space of possible black ring configurations where we can trust our equation of state.

The resulting $P-v$ diagram is "trivial", as depicted in Figure 31 for $d=5$. In higher dimensions the situation is similar. The critical point, if it exists for AdS black rings, is outside of the domain of validity of our approximation. To see this we will have to wait until the exact AdS black ring solution is known.

Similar to the spherical black hole case we shall now study the ultraspinning regime. (The regime of slow rotation is excluded by the blackfold approximation).

6.6. Ultraspinning Expansion

By inspection, the ultraspinning limit, for which $\Omega l \to 1$, corresponds to the limit where we keep the mass of the black ring M fixed and let:

$$\mathsf{R} \to \infty \tag{139}$$

that is, the limit of the ultra-large black rings. In this limit, $r_0 \sim 1/\mathsf{R}^{\frac{4}{d-4}} \to 0$, $T \sim \mathsf{R}^{\frac{4}{d-4}} \to \infty$, whereas the quantities V and J remain finite.

Figure 31. Equation of state: thin AdS black ring. The "exact" equation of state, given implicitly by Equation (137), for $T \approx 0.133$ is displayed by the thick solid black curve, and compared to the ultraspinning equation of state (136), displayed by the thick dashed blue curve, and the first correction equation of state (142), displayed by the thick dashed green curve. The two conditions (138) are respectively displayed by thin dashed red and black curves. They almost coincide: setting $R/r_0 = N = l/r_0$, the approximation is valid when $N \gg 1$. As in the AdS/CFT correspondence, we set $N = 3 \gg 1$, which gives the curves; the approximation is valid above these curves. This means that we can trust our "exact" equation of state in the top left corner of the figure. In this region all three equations of state basically coincide.

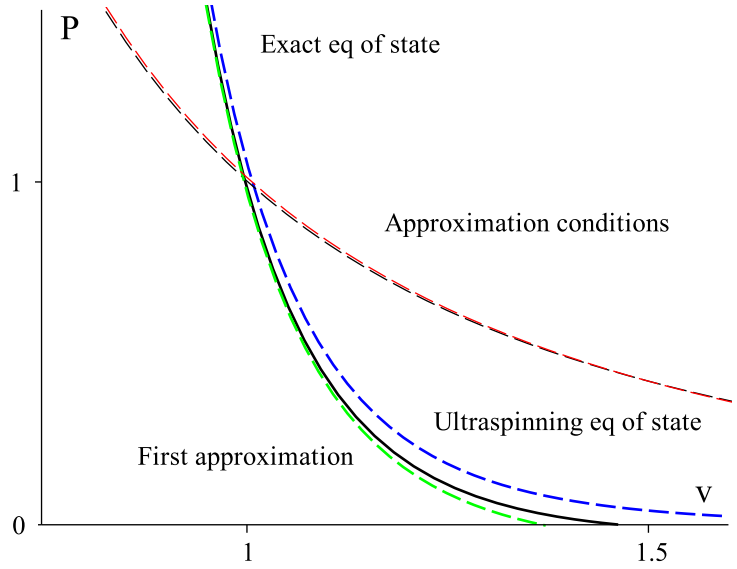

To write down the equation of state in this limit we proceed similar to the black hole case. Namely, we express r_0 from the M Equation (122) :

$$r_0 = \Big[\frac{8M}{l\omega_{d-3}(d-2)}\frac{1}{\mathsf{R}(1+\mathsf{R}^2)^{3/2}}\Big]^{\frac{1}{d-4}} \tag{140}$$

This is inserted into the equations for J, T, and V in Equation (122), and the result is expanded in large R, while we keep the quantities M and l fixed. The first few terms are:

$$\begin{aligned} J &= Ml\Big(1-\frac{1}{\mathsf{R}^2}+\frac{(d-1)(2d-5)}{2(d-2)^2\mathsf{R}^4}+\dots\Big) \\ T &= \frac{(d-4)^{3/2}}{4\pi\sqrt{d-2}}\Big(\frac{l\omega_{d-3}(d-2)}{8M}\Big)^{\frac{1}{d-4}}\mathsf{R}^{\frac{4}{d-4}} \\ &\quad\times\Big(1+\frac{2d-5}{(d-4)(d-2)}\frac{1}{\mathsf{R}^2}-\frac{5d^3-53d^2+172d-178}{4(d-4)^2(d-2)^2}\frac{1}{\mathsf{R}^4}+\dots\Big) \\ V &= \frac{8\pi l^2 M}{(d-1)(d-2)}\big(1-\frac{1}{\mathsf{R}^2}+\frac{1}{\mathsf{R}^4}+\dots\big) \end{aligned} \tag{141}$$

Consequently, we find the following approximate black ring equation of state:

$$P = P_{\text{ultra}} - \frac{2\omega_{d-3}(d-1)(d-3)(d-4)^{\frac{3d-12}{2}}}{4^d\pi^{d-3}(d-2)^{\frac{d-4}{2}}JT^{d-4}} + O\Big(\frac{1}{\mathsf{R}^4}\Big) \tag{142}$$

with P_{ultra} defined in Equation (136). This is displayed and compared to the "exact" equation of state Equation (137) in Figure 31.

Note the interesting coincidence that the first term, P_{ultra}, in the expansion coincides with the ultraspinning limit of the Kerr-AdS black hole equation of state. Therefore both the ultraspinning Kerr-AdS black holes and AdS black rings have infinite temperature and share the "same equation of state".

7. Beyond Thermodynamic Instabilities

Thus far we have considered only the thermodynamic behavior of black holes, using the global minimum of the Gibbs free energy (and the positivity of the specific heat) as a criterion for thermodynamic stability. However rotating black holes are subject to other kinds of (classical) instabilities. *Ultraspinning instabilities* can lead to bifurcations to new stationary black hole families [107,119–123]. *Superradiant instabilities* [124–126] amplify waves that scatter off of the AdS black hole, extracting its rotational energy and driving it to a new state.

A third instability is the so called (non-axisymmetric) *bar-mode instability* [107,127–129], which possibly occurs for both MP and Kerr-AdS black holes. However, nothing is known about the latter case, and even in the former case the mechanism as well as the endpoint of such instability (apart from the slowly spinning case which results in a slowly spinning MP black hole) is far from being well understood. It may result in the irradiation of the excessive angular momenta or even a fragmentation into a multiple black hole configuration [129]. We shall not consider this instability in further discussion.

7.1. Ultraspinning Instability

Ultraspinning (axisymmetric) instabilities occur for both asymptotically flat MP and Kerr-AdS black holes in all dimensions $d \geq 6$. It is related to the fact that in $d \geq 6$ the angular momentum of the black hole is not limited from above and in principle can grow all the way to infinity. In fact, even when the angular momenta are limited (for instance in the equal spinning MP case) the black hole can enter the ultraspining regime. Consequently as the angular momentum grows larger, the black hole horizon flattens, becomes pancake like, and the black hole enters the region of black membrane like behavior (see also Section 3). The resulting object is subject to the Gregory–Laflamme instability and the axisymmetric perturbations can lead to bifurcations to new stationary black hole families. In the absence of a decoupled master equation for gravitational perturbations in higher dimensions, the final endpoint as well as the exact onset of ultraspinning instabilities have to be investigated numerically [119–123]. However, for our purposes we just need to know when such an instability approximately "kicks in" and may have some effect on the thermodynamic considerations studied in previous sections.

The method for investigating ultraspinning instabilities consists of finding *zero modes* for stationary perturbations that preserve rotational symmetries. The onset of such instabilities can be assigned a "harmonic number" k. The $k = 0, 1$ modes respectively correspond to metric perturbations with $(0, 1)$ nodes. These are the so called *thermodynamic zero modes* and can be determined from the thermodynamic Hessian, as we shall discuss below. However, these modes do not correspond to

bifurcations to new families of stationary black holes; they can only change the black hole into another black hole of the same family, for example an MP black hole into another MP black hole.

The actual bifurcations occur for $k = 2$ and higher; the case of $k = 2$ corresponds to a new branch of black holes with a central pinch. For higher k further axisymmetric pinches appear. These cannot be obtained from thermodynamic considerations. However it has been conjectured [119] that the zero modes with $k \geq 2$ can only occur for rotations higher than that of the $k = 1$ modes. The $k = 1$ surface, calculable from thermodynamic considerations, is called the *ultra-spinning surface*: it encloses the region where the thermodynamic Hessian has less than two negative eigenvalues. For higher rotations the black holes are subject to ultraspinning instabilities leading to bifurcations to new black hole families [122].

Let us first illustrate this for a singly spinning $d = 6$ MP black hole.

7.1.1. Bifurcations of Singly Spinning MP Black Holes

A simple criterion [107] for the onset of ultraspinning instabilities of singly spinning MP black holes involves a consideration of the behaviour of the temperature T for a fixed mass M. For slowly spinning black holes this decreases, as is familiar for the Kerr solution, and in $d < 6$ reaches zero. However, for $d \geq 6$ the temperature instead reaches its minimum and diverges in the ultraspinning limit. This temperature growth is typical for black membranes.

Let us define a dimensionless parameter $x = \frac{a}{r_+}$, in terms of which we have, cf. J Equation (106):

$$r_+ = \left[\frac{8\pi}{\omega_{d-2}} \frac{J}{x(x^2+1)}\right]^{\frac{1}{d-2}} \tag{143}$$

The temperature of a singly spinning MP black hole is given by:

$$T = \frac{1}{4\pi}\left(\frac{r_+^{d-4}}{m} + \frac{d-5}{r_+}\right) \tag{144}$$

and reaches its minimum at $r_+ = r_1$, where:

$$m = \frac{d-4}{d-5} r_1^{d-3} \quad \Leftrightarrow \quad x_1 = \frac{a}{r_1} = \sqrt{\frac{d-3}{d-5}} \tag{145}$$

provided $d \geq 6$. For a fixed angular momentum, using Equation (143), this gives the following black hole radius:

$$r_1 = \left[\frac{4\pi}{\omega_{d-2}} \frac{d-5}{d-4} \sqrt{\frac{d-5}{d-3}} J\right]^{\frac{1}{d-2}} \tag{146}$$

The thermodynamic argument below leads to the same value of r_1—it gives the $k = 1$ zero mode. The $k = 0$ zero mode for singly spinning MP black holes is present for arbitrary spin.

The actual onsets of instabilities for perturbations preserving the original Killing symmetries of singly spinning MP black holes in $d = 6$ have been studied [121] and, in terms of a new parameter $y = a/r_m$, where $r_m^{d-3} = 2m$, were found to be:

$$\begin{aligned} y_1 = y(k=1) &\approx 1.097\,, \quad y_2 = y(k=2) \approx 1.572 \\ y_3 = y(k=3) &\approx 1.849\,, \quad y_4 = y(k=4) \approx 2.036 \end{aligned} \tag{147}$$

Since $y^{d-3} = x^{d-3}/(x^2+1)$, this gives:

$$x_1 \approx 1.751\,, \quad x_2 \approx 4.114\,, \quad x_3 \approx 6.472\,, \quad x_4 \approx 8.555 \tag{148}$$

To each x_k in Equation (148), we use Equation (143) to find the black hole radius r_k corresponding to the onset of instabilities with the harmonic number k. In particular, for $J = 1$ this gives $r_1 \approx 0.605, r_2 \approx 0.337, r_3 \approx 0.242, r_4 \approx 0.197$. The onset of ultraspinning instabilities leading to bifurcations to new branches of black holes occurs for $r \leq r_2$. The situation is displayed in Figure 30, where the exact Gibbs free energy of MP black holes, with corresponding onsets, is compared to the Gibbs free energy of approximate highly spinning asymptotically flat black rings constructed in the blackfold approximation of the previous section. From the discussion in the previous section we may expect that the approximation is valid for high temperatures, whereas it is completely off for small temperatures. In the middle region, we expect that the free energy G of the actual black ring may be slightly lower than that of the approximation. If so, it may be reasonable to expect that the crossover between G of an MP black hole and that of its exact (so far analytically unknown, but see [130] for numerical work) black ring counterpart may occur close to (or perhaps exactly at) r_2, where a first order phase transition in between the two kinds of black holes might occur.

7.1.2. Thermodynamic Argument and Other Examples

For more complicated black hole spacetimes, such as $d = 6$ doubly spinning Kerr-AdS black holes, the numeric results are not available (see, however, [123] for the multiply spinning MP case). However, the ultraspinning surface can be obtained from the following thermodynamic argument, e.g., [60,120–122] (see also [131]).

Let I be the (grand-canonical ensemble) Euclidean action, dependent on parameters y^α that completely characterize the black hole in this ensemble: $y^\alpha = y^\alpha(M, J_i)$. Then we consider the Hessian of the action, given by [120] (keeping Ω_i and T fixed):

$$I_{\alpha\beta} \equiv \frac{\partial^2 I}{\partial y^\alpha \partial y^\beta} = \left(\frac{1}{T}\frac{\partial^2 M}{\partial y^\alpha \partial y^\beta} - \frac{\partial^2 S}{\partial y^\alpha \partial y^\beta} - \frac{\Omega_i}{T}\frac{\partial^2 J_i}{\partial y^\alpha \partial y^\beta} \right) \tag{149}$$

In particular, as per usual, if we choose the parameters to be $x^\alpha = \{M, J_i\}$, we recover the familiar:

$$\left.\frac{\partial^2 I}{\partial y^\alpha \partial y^\beta}\right|_{y=x} = -\frac{\partial^2 S}{\partial x^\alpha \partial x^\beta} = -S_{\alpha\beta}(M, J_i) \tag{150}$$

The black hole has a thermodynamic negative mode, corresponding to a thermodynamic instability, if $I_{\alpha\beta}$ given by Equation (149) has a negative eigenvalue; thermodynamic zero modes correspond to vanishing eigenvalues.

For every asymptotically flat vacuum black hole $I_{\alpha\beta}$ possesses at least one negative eigenvalue and so all such black holes are locally thermodynamically unstable [120]. For $d \geq 6$ singly spinning MP black holes, as their rotation increases, we obtain an additional thermodynamic instability at precisely $r_+ = r_1$, as given by Equation (146) above. This determines the ultraspinning surface $k = 1$.

For singly spinning Kerr-AdS black holes in $d = 4$ and $d = 5$, one of the eigenvalues of the 2×2 Hessian matrix $I_{\alpha\beta}$ is always positive and the second one changes sign. We therefore have the $k = 0$

thermodynamic zero mode at $r_+ = r_0$, given by Equation (151) below; the $k = 1$ zero mode does not exist and the black holes are ultraspinning stable.

For the $d \geq 6$ singly spinning Kerr-AdS case one can show that two eigenvalues of the Hessian matrix change sign, giving two thermodynamic zero modes, $k = 0$ and $k = 1$. Solving for the zero eigenvalues of $I_{\alpha\beta}$ in Equation (149), taking $y^\alpha = \{r_+, a\}$, we obtain [122]:

$$\begin{aligned} r_0^2 &= \frac{d-3}{2(d-1)}\left(a^2 + l^2 + \sqrt{a^4 - \gamma_d a^2 l^2 + l^4}\right) \\ r_1^2 &= \frac{d-3}{2(d-1)}\left(a^2 + l^2 - \sqrt{a^4 - \gamma_d a^2 l^2 + l^4}\right) \end{aligned} \tag{151}$$

where $\gamma_d \equiv \frac{2(d^2-6d+1)}{(d-3)^2}$. For very large r_+, corresponding to slowly spinning Kerr-AdS black holes, there are no negative thermodynamic modes and the black holes are thermodynamically stable. As we decrease r_+, the $k = 0$ zero mode appears at r_0. Decreasing r_+ even further, an additional thermodynamic zero mode $k = 1$ occurs at r_1. Black holes with $r_+ < r_1$ are in the ultraspinning regime—they are subject to $k \geq 2$ zero modes and suffer from ulraspinning instabilities. We show in Figure 32 that the singly spinning Kerr-AdS black holes that play the role in the RPT studied in Section 3 are ultraspinning stable, though some of them may be subject to the superradiant instability, as studied in the next subsection.

We demonstrated in Section 4 that an RPT also occurs for the $d = 6$ doubly spinning MP black holes. Such black holes always possess a $k = 0$ negative mode. The thermodynamic argument gives the following formula for the appearance of the $k = 1$ zero mode:

$$r_1^2 = \frac{1}{6}\left(a^2 + b^2 + \sqrt{a^4 + 14a^2b^2 + b^4}\right) \tag{152}$$

where a and b are the two rotation parameters. In this case we find, see Figure 33, that the doubly spinning MP black holes that play the role in the RPT studied in Section 4 are in the ultraspinning regime.

Turning finally to the doubly spinning Kerr-AdS black holes and the corresponding 'solid/liquid/gas' phase transition studied in Section 3, no simple analytic formula for the appearance of thermodynamic zero modes exists, and we proceed numerically as displayed in Figure 34. We find that the part of the Gibbs diagram important for the existence of multiple first order phase transitions and possibly a triple point occurs in the ultraspinning region and is subject to the superradiant instability. Hence the observed thermodynamic phenomena have to "compete" with both the ultraspinning and the superradiant classical instabilities.

We pause here to note another suggestion for characterizing ultraspinning instabilities [9], based on the relation $\kappa = -\frac{1}{V}\frac{\partial V}{\partial P}|_{S,J_i}$ for the adiabatic compressibility κ. For MP black holes κ can be entirely expressed in terms of quadratic and quartic Casimir invariants of $SO(d-1)$. For non-rotating black holes, κ vanishes and the system is incompressible. However if some of the J_i are kept small while others diverge, then κ diverges and the black hole equation of state becomes soft. The suggestion is that large compressibility signals the onset of ultraspinning instability.

Figure 32. RPT and classical instabilities: $d = 6$ singly spinning Kerr-AdS black holes. The Gibbs free energy for the $d = 6$ singly spinning Kerr-AdS black hole is displayed for $J = 1$ and $P = 0.0564 \in (P_t P_z)$ for which the RPT is present, cf. Figure 12c. Black holes displayed by the solid black curve are classically stable (potentially subject to the bar-mode instability). The red curve indicates the branch of black holes subject to the superradiant instability, $r_+ < 1.11$. The blue dotted curve displays black holes in the ultraspinning region ($k \geq 1$ zero modes) derived from the thermodynamic argument, $r_+ < 0.55$. Such black holes are also superradiant unstable. We observe that black holes that play a role in the RPT are ultraspinning stable but some of them are subject to the superradiant instability.

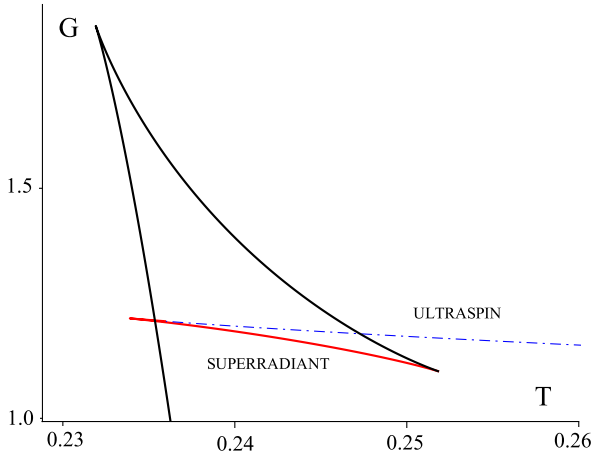

Figure 33. RPT and ultraspinning instability: $d = 6$ doubly spinning MP black holes. The Gibbs free energy for the $d = 6$ doubly spinning MP black hole is displayed for $q = 0.112 \in (q_t, q_z)$ for which the RPT is present, cf. Figure 24d. The black curve is classically stable (potentially subject to the bar-mode instability). The blue dotted curve indicates the branch of black holes subject to the ultraspinning instability, $r_+ < 0.613$. Hence, contrary to the Kerr-AdS case the MP black holes that play the role in the RPT are ultraspinning unstable.

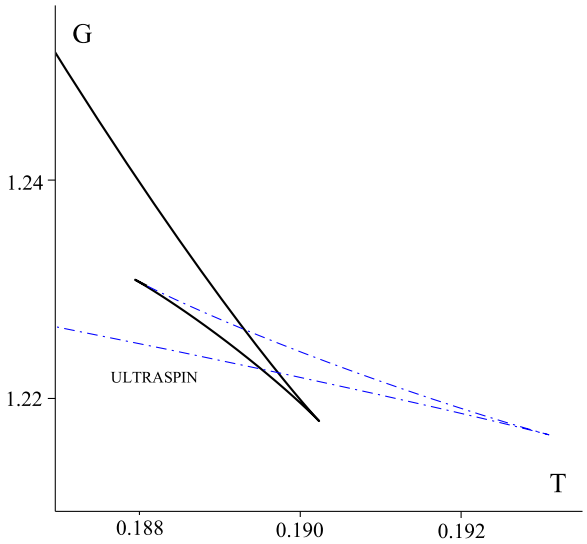

Figure 34. Classical instabilities: doubly spinning $d = 6$ Kerr-AdS black hole. The Gibbs free energy for the $d = 6$ doubly spinning Kerr-AdS black holes is displayed for $q = 0.05$ and various pressures (from top to bottom) $P = 0.260, 0.170, 0.087, 0.0642, 0.015$, for which we observe the SBH/IBH/LBH phase transition, cf. Figure 19. The black solid curves denote classically stable black holes (potentially subject to the bar-mode instability). The blue color indicates branches of black holes subject to both the ultraspinning and superradiant instabilities. The red curves correspond to black holes that are superradiant unstable and ultraspinning stable. We conclude that the Kerr-AdS black holes that play the role in the SBH/IBH/LBH phase transitions are potentially subject to both classical instabilities.

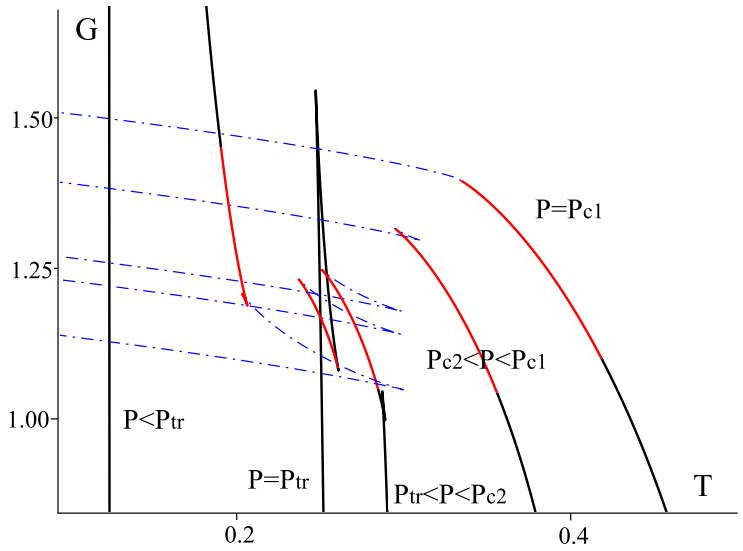

7.2. Superradiant Instabilities

Superradiant instabilities are potentially present for rapidly spinning Kerr-AdS black holes in all $d \geq 4$ dimensions. Interestingly, they also occur for the massive scalar field in the asymptotically flat $d = 4$ Kerr black hole spacetime [132,133]. The superradiant instability also occurs for [98]:

$$\Omega_i l > 1 \tag{153}$$

and is associated with perturbations that break the spacetime axisymmetry. For example a gravitational wave of frequency ω co-rotating with the background black hole can extract rotational energy from the black hole if $\omega < m\Omega_i$, where m is the wave angular momentum. The effect is called superradiance and represents a "field analogue" of the Penrose process. Superradiance occurs also in the asymptotically flat case. However, in the presence of the "AdS confining box", the amplified field reflects back on black hole and is amplified again and again, driving the system unstable whenever the condition (153) is satisfied.

Superradiant regions play an important role for the thermodynamic phase transitions we have studied. These instabilities are indicated in the $G - T$ diagrams for $d = 6$ singly and doubly spinning Kerr-AdS black hole in Figures 32 and 34. We find that the corresponding thermodynamic effects we have discovered so far must compete with the superradiant instability. Interestingly, this is even true for the van der Waals like phase transition that occur in $d = 4$ Kerr-AdS black hole spacetimes, see

Figure 35. However the time scale of these latter instabilities can vary widely, and so it may happen that the thermodynamic effects we have discovered can actually take place.

Figure 35. Superradiant instability: $d = 4$ Kerr-AdS black hole. The Gibbs free energy for the Kerr-AdS black hole in $d = 4$ is displayed for various pressures, $P/P_c = \{1.6, 1, 0.6, 0.2\}$, $P_c \approx 0.002856$, and fixed $J = 1$. The red curves display black holes that are subject to the superradiant instability, the black ones are superradiant stable. The figure clearly demonstrates that even the van der Waals like phase transition occurring for $d = 4$ Kerr-AdS black holes, discussed in Section 2, is subject to the superradiant instability.

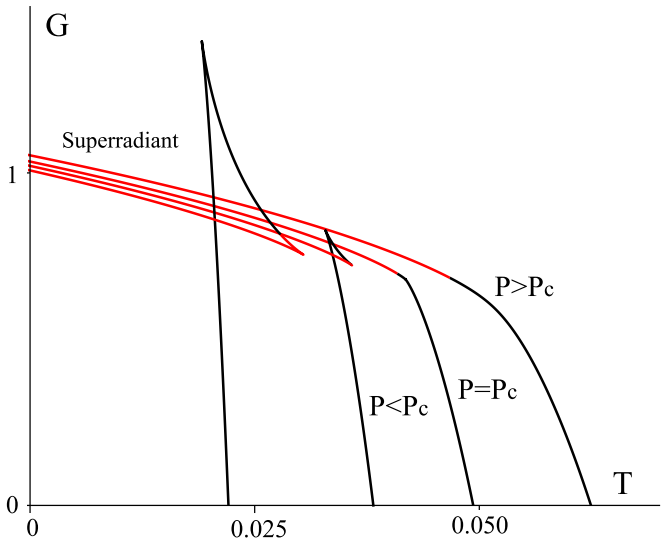

8. Conclusions

We have carried out a thorough study of the thermodynamics of higher-dimensional asymptotically flat and AdS rotating black holes with various horizon topologies in the *canonical* (fixed J) ensemble, interpreting the cosmological constant as thermodynamic pressure. By studying the corresponding thermodynamic potential—the Gibbs free energy—we uncovered a number of novel thermodynamic phase transitions in these black hole spacetimes.

We have shown that multiply-rotating Kerr-AdS black holes exhibit a rich set of interesting thermodynamic phenomena known from the every day thermodynamics of simple substances. Specifying to six dimensions, we have demonstrated that reentrant phase transitions, triple points (tricritical points), multiple first-order transitions, solid/liquid/gas phase transitions, and van der Walls liquid/gas phase transitions can all occur depending on the ratio of the two angular momenta. We have evidence that such phenomena will take place in dimensions $d > 6$, though the details remain to be worked out. Intriguingly, we have shown that reentrant phase transitions occur even for asymptotically flat Myers–Perry black holes. The cosmological constant is not necessary to observe this phenomenon.

We have also studied the thermodynamic volume, the corresponding equation of state, $P = P(V, T)$, as well as the associated reverse isoperimetric inequality. For the first time, we verified the validity of this inequality for the black hole spacetimes with non-spherical horizon topology, providing one more piece

of evidence for the conjecture [10] that a reverse isoperimetric inequality holds for any asymptotically AdS black hole.

In this paper we concentrated on a canonical ensemble where the angular momentum is fixed and the horizon angular velocity is allowed to vary. We showed that in this ensemble all possible kinds of interesting phase transitions happen. Alternatively, one could consider the thermodynamic behaviour of above black holes in the *grand-canonical ensemble*, where the angular velocity of the horizon is fixed and the angular momentum is free to vary, e.g., [4,62,104,134]. The corresponding thermodynamic potential G_Ω is related to the Gibbs free energy Equation (2) by the Legendre transformation:

$$G_\Omega \equiv G - \sum_i \Omega_i J_i - \Phi Q = G_\Omega(T, P, \Omega_i, \Phi) \tag{154}$$

However, for charged-AdS black holes it has previously been demonstrated [62] that the grand-canonical ensemble does not admit first-order phase transitions ala van der Waals. Indeed, the behaviour of G_Ω is rather "boring", reminiscent of the Schwarzschild-AdS behaviour. We have checked for singly-spinning Kerr-AdS black holes in $d = 6$ that a similar conclusion remains valid in the (higher-dimensional) rotating case (see also [104]). Specifically, the Gibbs free energy G_Ω exhibits Schwarzschild-like behaviour without any van der Waals like first-order phase transitions, as shown in Figure 36. A similar conclusion remains valid for multiply-spinning Kerr-AdS black holes in $d = 6$. For these reasons we expect that the phase structure of the grand-canonical ensemble is not "as interesting" as that of the canonical ensemble. (See, however, recent work [71].)

Figure 36. Grand-canonical thermodynamic potential. The grand-canonical thermodynamic potential G_Ω is displayed for $d = 6$ singly spinning Kerr-AdS black hole for fixed $\Omega = 1$ and various pressures (from left to right) $P = 0.5, 0.8, 1$. Its behaviour is qualitatively similar to the behavior of G for the Schwarzschild-AdS black hole. Namely, although we may observe an analogue of the Hawking–Page transition, there is no swallow tail present and hence no first order phase transition of the van der Waals type.

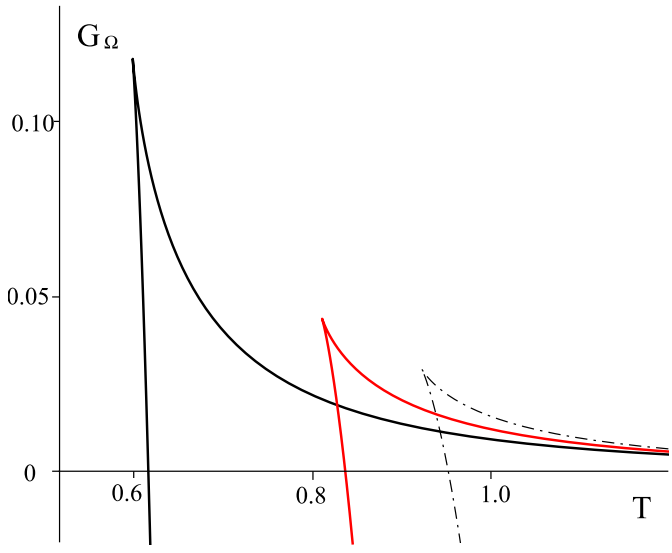

Another interesting open possibility left for future is to use an ensemble where the thermodynamic volume V rather than the cosmological constant Λ is fixed, with a corresponding thermodynamic

potential G_V related to G by $G_V \equiv G - PV = G_V(T, V, J_i, Q)$; and similarly for the grand-canonical ensemble. The question whether such an ensemble can be "prepared" for black hole spacetimes remains open.

Finally, we stress that all the results of this paper are entirely based on thermodynamic considerations. The phase transitions uncovered are thermodynamic phase transitions—determined entirely from the behavior of the black hole Gibbs free energy. In "non-ideal" black hole geometries perturbations will be present that may lead to classical instabilities and additional/alternative phase transitions. One may, for example, anticipate for small temperatures the formation of hairy black holes, or appearance of ultraspinning unstable modes for rapidly spinning black holes. Similarly, in the presence of radiation/matter, one might expect radiation/black hole phase transitions of the Hawking–Page type. The question as to which transition would actually 'win' and take place depends on the timescales of the corresponding phenomena. This, however, goes beyond the scope of the present paper.

Acknowledgments

We would like to thank Brian P. Dolan, Pau Figueras, David Kastor, Don N. Page, and Jennie H. Traschen for discussions and helpful comments on this work and Jorge E. Santos for useful comments and reading the manuscript. This research was supported in part by Perimeter Institute for Theoretical Physics and by the Natural Sciences and Engineering Research Council of Canada. Research at Perimeter Institute is supported by the Government of Canada through Industry Canada and by the Province of Ontario through the Ministry of Research and Innovation.

Conflicts of Interest

The authors declare no conflict of interest.

References

1. Hawking, S.; Page, D.N. Thermodynamics of black holes in anti-de sitter space. *Commun. Math. Phys.* **1983**, *87*, 577–588.
2. Kastor, D.; Ray, S.; Traschen, J. Enthalpy and the mechanics of AdS black holes. *Class. Quant. Gravity* **2009**, *26*, 195011, doi:10.1088/0264-9381/26/19/195011.
3. Creighton, J.; Mann, R.B. Quasilocal thermodynamics of dilaton gravity coupled to gauge fields. *Phys. Rev. D* **1995**, *52*, 4569–4587.
4. Caldarelli, M.M.; Cognola, G.; Klemm, D. Thermodynamics of Kerr-Newman-AdS black holes and conformal field theories. *Class. Quant. Gravity* **2000**, *17*, 399–420.
5. Dolan, B.P. The cosmological constant and black-hole thermodynamic potentials. *Class. Quant. Gravity* **2011**, *28*, 125020, doi:10.1088/0264-9381/28/12/125020.
6. Dolan, B.P. Pressure and volume in the first law of black hole thermodynamics. *Class. Quant. Gravity* **2011**, *28*, 235017, doi:10.1088/0264-9381/28/23/235017.
7. Dolan, B.P. Compressibility of rotating black holes. *Phys. Rev. D* **2011**, *84*, 127503, doi:10.1103/PhysRevD.84.127503.

8. Dolan, B.P. Where is the PdV Term in the Fist Law of Black Hole Thermodynamics? In *Open Questions in Cosmology*; Olmo, G.J., Ed.; InTech: Rijeka, Croatia, 2012.
9. Dolan, B.P. The compressibility of rotating black holes in D-dimensions. *Class. Quant. Gravity* **2014**, *31*, 035022, doi:10.1088/0264-9381/31/3/035022.
10. Cvetic, M.; Gibbons, G.; Kubiznak, D.; Pope, C. Black hole enthalpy and an entropy inequality for the thermodynamic volume. *Phys. Rev. D* **2011**, *84*, 024037, doi:10.1103/PhysRevD.84.024037.
11. Kastor, D.; Ray, S.; Traschen, J. Smarr formula and an extended first law for lovelock gravity. *Class. Quant. Gravity* **2010**, *27*, 235014, doi:10.1088/0264-9381/27/23/235014.
12. Larranaga, A.; Cardenas, A. Geometric thermodynamics of schwarzschild-AdS black hole with a cosmological constant as state variable. *J. Korean Phys. Soc.* **2012**, *60*, 987–992.
13. Larranaga, A.; Mojica, S. Geometric thermodynamics of Kerr-AdS black hole with a cosmological constant as state variable. *Abraham Zelmanov J.* **2012**, *5*, 68–77.
14. Gibbons, G. What is the shape of a black hole? *AIP Conf. Proc.* **2012**, *1460*, 90–100.
15. Kubiznak, D.; Mann, R.B. *P-V* criticality of charged AdS black holes. *J. High Energy Phys.* **2012**, *1207*, 033, doi:10.1007/JHEP07(2012)033.
16. Gunasekaran, S.; Kubiznak, D.; Mann, R. Extended phase space thermodynamics for charged and rotating black holes and Born-Infeld vacuum polarization. *J. High Energy Phys.* **2012**, *1211*, 110, doi:10.1007/JHEP11(2012)110.
17. Belhaj, A.; Chabab, M.; El Moumni, H.; Sedra, M.B. On thermodynamics of AdS black holes in arbitrary dimensions. *Chin. Phys. Lett.* **2012**, *29*, 100401, doi:10.1088/0256-307X/29/10/100401.
18. Lu, H.; Pang, Y.; Pope, C.N.; Vazquez-Poritz, J.F. AdS and lifshitz black holes in conformal and Einstein-Weyl gravities. *Phys. Rev. D* **2012**, *86*, 044011, doi:10.1103/PhysRevD.86.044011.
19. Smailagic, A.; Spallucci, E. Thermodynamical phases of a regular SAdS BH. *Int. J. Mod. Phys. D* **2013**, *22*, 1350010, doi:10.1142/S0218271813500107.
20. Spallucci, E.; Smailagic, A. Maxwell's equal area law for charged Anti-de Sitter black holes. *Phys. Lett. B* **2013**, *723*, 436–441.
21. Hendi, S.; Vahidinia, M. P-V criticality of higher dimensional black holes with nonlinear source. *Phys. Rev. D* **2013**, *88*, 084045, doi:10.1103/PhysRevD.88.084045.
22. Chen, S.; Liu, X.; Liu, C.; Jing, J. $P-V$ criticality of AdS black hole in $f(R)$ gravity. *Chin. Phys. Lett.* **2013**, *30*, 060401, doi:10.1088/0256-307X/30/6/060401.
23. Zhao, R.; Zhao, H.-H.; Ma, M.-S.; Zhang, L.-C. On the critical phenomena and thermodynamics of charged topological dilaton AdS black holes. *Eur. Phys. J. C* **2013**, *73*, 2645, doi:10.1140/epjc/s10052-013-2645-x.
24. Belhaj, A.; Chabab, M.; El Moumni, H.; Sedra, M. Critical behaviors of 3D black holes with a scalar hair. *ArXiv E-Prints*, **2013**, arXiv:1306.2518.
25. Altamirano, N.; Kubiznak, D.; Mann, R. Reentrant phase transitions in rotating antide Sitter black holes. *Phys. Rev. D* **2013**, *88*, 101502, doi:10.1103/PhysRevD.88.101502.
26. Altamirano, N.; Kubiznak, D.; Mann, R.B.; Sherkatghanad, Z. Kerr-AdS analogue of tricritical point and solid/liquid/gas phase transition. *ArXiv E-Prints*, **2014**, arXiv:1308.2672.

27. Cai, R.-G.; Cao, L.-M.; Li, L.; Yang, R.-Q. *P-V* criticality in the extended phase space of Gauss-Bonnet black holes in AdS space. *J. High Energy Phys.* **2013**, *2013*, doi:10.1007/JHEP09(2013)005.
28. Belhaj, A.; Chabab, M.; Moumni, H.E.; Medari, L.; Sedra, M. The thermodynamical behaviors of kerr–newman AdS black holes. *Chin. Phys. Lett.* **2013**, *30*, 090402, doi:10.1088/0256-307X/30/9/090402.
29. Spallucci, E.; Smailagic, A. Maxwell's equal area law and the Hawking-Page phase transition. *J. Gravity* **2013**, *2013*, 525696, doi:10.1155/2013/525696.
30. Mo, J.-X.; Zeng, X.-X.; Li, G.-Q.; Jiang, X.; Liu, W.-B. A unified phase transition picture of the charged topological black hole in Horava-Lifshitz gravity. *J. High Energy Phys.* **2013**, *2013*, 056, doi:10.1007/JHEP10(2013)056.
31. Xu, W.; Xu, H.; Zhao, L. Gauss-Bonnet coupling constant as a free thermodynamical variable and the associated criticality. *ArXiv E-Prints*, **2013**, arXiv:1311.3053.
32. Mo, J.-X.; Liu, W.-B. Ehrenfest scheme for P-V criticality in the extended phase space of black holes. *Phys. Lett. B* **2013**, *727*, 336–339.
33. Zou, D.-C.; Zhang, S.-J.; Wang, B. Critical behavior of Born-Infeld AdS black holes in the extended phase space thermodynamics. *ArXiv E-Prints*, **2013**, arXiv:1311.7299.
34. Ma, M.-S.; Zhao, H.-H.; Zhang, L.-C.; Zhao, R. Existence condition and phase transition of Reissner-Nordström-de Sitter black hole. *ArXiv E-Prints*, **2013**, arXiv:1312.0731.
35. Ulhoa, S.C.; Spaniol, E.P. On gravitational entropy of de Sitter universe. *ArXiv E-Prints*, **2013**, arXiv:1312.1367.
36. Castro, A.; Dehmami, N.; Giribet, G.; Kastor, D. On the universality of inner black hole mechanics and higher curvature gravity. *J. High Energy Phys.* **2013**, *1307*, 164, doi:10.1007/JHEP07(2013)164.
37. El-Menoufi, B.M.; Ett, B.; Kastor, D.; Traschen, J. Gravitational tension and thermodynamics of planar AdS spacetimes. *Class. Quantum Gravity* **2013**, *30*, 155003, doi:10.1088/0264-9381/30/15/155003.
38. Lu, H.; Pang, Y.; Pope, C. AdS dyonic black hole and its thermodynamics. *J. High Energy Phys.* **2013**, *2013*, 33, doi:10.1007/JHEP11(2013)033.
39. Mo, J.-X.; Liu, W.-B. $P-V$ Criticality of topological black holes in Lovelock-Born-Infeld gravity. *ArXiv E-Prints*, **2013**, arXiv:1401.0785.
40. Dolan, B.; Kastor, D.; Kubiznak, D.; Mann, R.; Traschen, J. Thermodynamic volumes and isoperimetric inequalities for de sitter black holes. *Phys. Rev. D* **2013**, *87*, 104017, doi:10.1103/PhysRevD.87.104017.
41. Gibbons, G.W.; Hawking, S.W. Cosmological event horizons, thermodynamics, and particle creation. *Phys. Rev. D* **1977**, *15*, 2738–2751.
42. Hayward, S. Unified first law of black hole dynamics and relativistic thermodynamics. *Class. Quantum Gravity* **1998**, *15*, 3147–3162,
43. Padmanabhan, T. Classical and quantum thermodynamics of horizons in spherically symmetric space-times. *Class. Quantum Gravity* **2002**, *19*, 5387–5408.

44. Cai, R.-G. Cardy-verlinde formula and asymptotically de Sitter spaces. *Phys. Lett. B* **2002**, *525*, 331–336.
45. Cai, R.-G. Cardy-Verlinde formula and thermodynamics of black holes in de Sitter spaces. *Nucl. Phys. B* **2002**, *628*, 375–386.
46. Sekiwa, Y. Thermodynamics of de Sitter black holes: Thermal cosmological constant. *Phys. Rev. D* **2006**, *73*, 084009, doi:10.1103/PhysRevD.73.084009.
47. Urano, M.; Tomimatsu, A.; Saida, H. The mechanical first law of black hole spacetimes with a cosmological constant and its application to Schwarzschild-de Sitter spacetime. *Class. Quantum Gravity* **2009**, *26*, 105010, doi:10.1088/0264-9381/26/10/105010.
48. Gibbons, G.; Perry, M.; Pope, C. Bulk/boundary thermodynamic equivalence, and the Bekenstein and cosmic-censorship bounds for rotating charged AdS black holes. *Phys. Rev. D* **2005**, *72*, 084028, doi:10.1103/PhysRevD.72.084028.
49. Bhattacharya, S.; Lahiri, A. Mass function and particle creation in Schwarzschild-de Sitter spacetime. *ArXiv E-Prints*, **2013**, arXiv:1301.4532.
50. Emparan, R.; Reall, H.S. Black holes in higher dimensions. *Living Rev. Relativ.* **2008**, *11*, 1–87.
51. Myers, R.C.; Perry, M.J. Black holes in higher dimensional space-times. *Ann. Phys.* **1986**, *172*, 304–347.
52. Weinberg, S. Does gravitation resolve the ambiguity among supersymmetry vacua? *Phys. Rev. Lett.* **1982**, *48*, 1776–1779.
53. Weinhold, F. Metric geometry of equilibrium thermodynamics. *J. Chem. Phys.* **1975**, *63*, 2479, doi:10.1063/1.431689.
54. Weinhold, F. Metric geometry of equilibrium thermodynamics. II. Scaling, homogeneity, and generalized Gibbs-Duhem relations. *J. Chem. Phys.* **1975**, *63*, 2484, doi:10.1063/1.431635.
55. Ruppeiner, G. Thermodynamics: A Riemannian geometric model. *Phys. Rev. A* **1979**, *20*, 1608–1613.
56. Ruppeiner, G. Riemannian geometry in thermodynamic fluctuation theory. *Rev. Mod. Phys.* **1995**, *67*, 605–659.
57. Quevedo, H. Geometrothermodynamics. *J. Math. Phys.* **2007**, *48*, 013506, doi:10.1063/1.2409524.
58. Liu, H.; Lu, H.; Luo, M.; Shao, K.-N. Thermodynamical metrics and black hole phase transitions. *J. High Energy Phys.* **2010**, *1012*, 54, doi:10.1007/JHEP12(2010)054.
59. Monteiro, R.; Santos, J. Negative modes and the thermodynamics of Reissner-Nordstrom black holes. *Phys. Rev. D* **2009**, *79*, 064006, doi:10.1103/PhysRevD.79.064006.
60. Monteiro, R.; Perry, M.J.; Santos, J.E. Thermodynamic instability of rotating black holes. *Phys. Rev. D* **2009**, *80*, 024041, doi:10.1103/PhysRevD.80.024041.
61. Witten, E. Anti-de Sitter space, thermal phase transition, and confinement in gauge theories. *Adv. Theor. Math. Phys.* **1998**, *2*, 505–532.
62. Chamblin, A.; Emparan, R.; Johnson, C.; Myers, R. Charged AdS black holes and catastrophic holography. *Phys. Rev. D* **1999**, *60*, 064018, doi:10.1103/PhysRevD.60.064018.

63. Chamblin, A.; Emparan, R.; Johnson, C.; Myers, R. Holography, thermodynamics and fluctuations of charged AdS black holes. *Phys. Rev. D* **1999**, *60*, 104026, doi:10.1103/PhysRevD.60.104026.
64. Cvetic, M.; Gubser, S. Phases of R charged black holes, spinning branes and strongly coupled gauge theories. *J. High Energy Phys.* **1999**, *9904*, 024, doi:10.1088/1126-6708/1999/04/024.
65. Tsai, Y.-D.; Wu, X.; Yang, Y. Phase structure of kerr-AdS black hole. *Phys. Rev. D* **2012**, *85*, 044005, doi:10.1103/PhysRevD.85.044005.
66. Hristov, K.; Toldo, C.; Vandoren, S. Phase transitions of magnetic AdS_4 black holes with scalar hair. *Phys. Rev. D* **2013**, *88*, 026019, doi:10.1103/PhysRevD.88.026019.
67. Johnson, C.V. Large N phase transitions, finite volume, and entanglement entropy. *ArXiv E-Prints*, **2013**, arXiv:1306.4955.
68. Niu, C.; Tian, Y.; Wu, X.-N. Critical phenomena and thermodynamic geometry of RN-AdS black holes. *Phys. Rev. D* **2012**, *85*, 024017, doi:10.1103/PhysRevD.85.024017.
69. Poshteh, M.B.J.; Mirza, B.; Sherkatghanad, Z. Phase transition, critical behavior, and critical exponents of Myers-Perry black holes. *Phys. Rev. D* **2013**, *88*, 024005, doi:10.1103/PhysRevD.88.024005.
70. Wei, S.-W.; Liu, Y.-X. Critical phenomena and thermodynamic geometry of charged Gauss-Bonnet AdS black holes. *Phys. Rev. D* **2013**, *87*, 044014, doi:10.1103/PhysRevD.87.044014.
71. Dutta, S.; Jain, A.; Soni, R. Dyonic black hole and holography. *J. High Energy Phys.* **2013**, *2013*, 60, doi:10.1007/JHEP12(2013)060.
72. Narayanan, T.; Kumar, A. Reentrant phase transitions in multicomponent liquid mixtures. *Phys. Rep.* **1994**, *249*, 135–218.
73. Maslov, V.P. Zeroth-order phase transitions. *Math. Notes* **2004**, *76*, 697–710.
74. Kubizňák, D.; Frolov, V.P. Hidden symmetry of higher dimensional Kerr-NUT-AdS spacetimes. *Class. Quantum Gravity* **2007**, *24*, 1–6.
75. Parikh, M. The Volume of black holes. *Phys. Rev. D* **2006**, *73*, 124021, doi:10.1103/PhysRevD.73.124021.
76. Ballik, W.; Lake, K. The volume of stationary black holes and the meaning of the surface gravity. *ArXiv E-Prints*, **2010**, arXiv:1005.1116.
77. Ballik, W.; Lake, K. The vector volume and black holes. *Phys. Rev. D* **2013**, *88*, 104038, doi:10.1103/PhysRevD.88.104038.
78. Emparan, R.; Harmark, T.; Niarchos, V.; Obers, N. Essentials of blackfold dynamics. *J. High Energy Phys.* **2010**, *2010*, 63, doi:10.1007/JHEP03(2010)063.
79. Gregory, R.; Laflamme, R. Black strings and p-branes are unstable. *Phys. Rev. Lett.* **1993**, *70*, 2837–2840.
80. Gubser, S.S.; Mitra, I. Instability of charged black holes in anti-de Sitter space. *ArXiv E-Prints*, **2000**, arXiv:hep-th/0009126.
81. Gubser, S.; Mitra, I. The Evolution of unstable black holes in anti-de Sitter space. *J. High Energy Phys.* **2001**, *2001*, 018, doi:10.1088/1126-6708/2001/08/018.
82. Reall, H.S. Classical and thermodynamic stability of black branes. *Phys. Rev. D* **2001**, *64*, 044005, doi:10.1103/PhysRevD.64.044005.

83. Figueras, P.; Murata, K.; Reall, H.S. Black hole instabilities and local Penrose inequalities. *Class. Quantum Gravity* **2011**, *28*, 225030, doi:10.1088/0264-9381/28/22/225030.
84. Hollands, S.; Wald, R.M. Stability of black holes and black branes. *Commun. Math. Phys.* **2013**, *321*, 629–680.
85. Goldenfeld, N. *Lectures on Phase Transitions and the Renormalization Group*; Westview Press: New York, NY, USA, 1992.
86. Bertoldi, G.; Burrington, B.A.; Peet, A.W. Thermal behavior of charged dilatonic black branes in AdS and UV completions of Lifshitz-like geometries. *Phys. Rev. D* **2010**, *82*, 106013, doi:10.1103/PhysRevD.82.106013.
87. Berglund, P.; Bhattacharyya, J.; Mattingly, D. Charged dilatonic AdS black branes in arbitrary dimensions. *J. High Energy Phys.* **2012**, *1208*, 42, doi:10.1007/JHEP08(2012)042.
88. Banerjee, R.; Modak, S.K.; Samanta, S. Second order phase transition and thermodynamic geometry in Kerr-AdS black hole. *Phys. Rev. D* **2011**, *84*, 064024, doi:10.1103/PhysRevD.84.064024.
89. Carlip, S.; Vaidya, S. Phase transitions and critical behavior for charged black holes. *Class. Quantum Gravity* **2003**, *20*, 3827–3838.
90. Gubser, S. Breaking an Abelian gauge symmetry near a black hole horizon. *Phys. Rev. D* **2008**, *78*, 065034, doi:10.1103/PhysRevD.78.065034.
91. Hartnoll, S.; Herzog, C.; Horowitz, G. Building a holographic superconductor. *Phys. Rev. Lett.* **2008**, *101*, 031601, doi:10.1103/PhysRevLett.101.031601.
92. Hartnoll, S.A.; Herzog, C.; Horowitz, G. Holographic superconductors. *J. High Energy Phys.* **2008**, *2008*, 015, doi:10.1088/1126-6708/2008/12/015.
93. Maeda, K.; Koga, J.-I.; Fujii, S. The final fate of instability of Reissner-Nordström-anti-de Sitter black holes by charged complex scalar fields. *ArXiv E-Prints*, **2010**, arXiv:1003.2689.
94. Basu, P.; Bhattacharya, J.; Bhattacharyya, S.; Loganayagam, R.; Minwalla, S.; Umesh, A. Small hairy black holes in global AdS spacetime. *J. High Energy Phys.* **2010**, *1010*, 45, doi:10.1007/JHEP10(2010)045.
95. Dias, O.; Figueras, P.; Minwalla, S.; Mitra, P.; Monteiro, R.; Santos, J. Hairy black holes and solitons in global AdS_5. *J. High Energy Phys.* **2012**, *1208*, 117, doi:10.1007/JHEP08(2012)117.
96. Horowitz, G. Introduction to holographic superconductors. *Lect. Notes Phys.* **2011**, *828*, 313–347.
97. Hartmann, B. Stability of black holes and solitons in Anti-de Sitter space-time. *ArXiv E-Prints*, **2013**, arXiv:1310.0300.
98. Hawking, S.; Reall, H. Charged and rotating AdS black holes and their CFT duals. *Phys. Rev. D* **2000**, *61*, 024014, doi:10.1103/PhysRevD.61.024014.
99. Sonner, J. A rotating holographic superconductor. *Phys. Rev. D* **2009**, *80*, 084031, doi:10.1103/PhysRevD.80.084031.
100. Dias, O.J.; Monteiro, R.; Reall, H.S.; Santos, J.E. A Scalar field condensation instability of rotating anti-de Sitter black holes. *J. High Energy Phys.* **2010**, *2010*, 36, doi:10.1007/JHEP11(2010)036.
101. Cardoso, V.; Dias, O.C.; Hartnett, G.S.; Lehner, L.; Santos, J. Holographic thermalization, quasinormal modes and superradiance in Kerr-AdS. *ArXiv E-Prints*, **2013**, arXiv:1312.5323.

102. Gibbons, G.W.; Lü, H.; Page, D.N.; Pope, C.N. Rotating black holes in higher dimensions with a cosmological constant. *Phys. Rev. Lett.* **2004**, *93*, 171102, doi:10.1103/PhysRevLett.93.171102.
103. Gibbons, G.W.; Lü, H.; Page, D.N.; Pope, C.N. The general Kerr-de Sitter metrics in all dimensions. *J. Geom. Phys.* **2005**, *53*, 49–73.
104. Hawking, S.W.; Hunter, C.J.; Taylor-Robinson, M.M. Rotation and the AdS/CFT correspondence. *Phys. Rev. D* **1999**, *59*, 064005, doi:10.1103/PhysRevD.59.064005.
105. Frolov, V.P.; Kubizňák, D. Higher-dimensional black holes: Hidden symmetries and separation of variables. *Class. Quantum Gravity* **2008**, *25*, 154005, doi:10.1088/0264-9381/25/15/154005.
106. Gibbons, G.; Perry, M.; Pope, C. The First law of thermodynamics for Kerr-anti-de Sitter black holes. *Class. Quantum Gravity* **2005**, *22*, 1503–1526.
107. Emparan, R.; Myers, R.C. Instability of ultra-spinning black holes. *J. High Energy Phys.* **2003**, *2003*, 025, doi:10.1088/1126-6708/2003/09/025.
108. Armas, J.; Obers, N.A. Blackfolds in (Anti)-de Sitter Backgrounds. *Phys. Rev. D* **2011**, *83*, 084039, doi:10.1103/PhysRevD.83.084039.
109. Caldarelli, M.; Emparan, R.; Rodriguez, M.J. Black rings in (Anti)-deSitter space. *J. High Energy Phys.* **2008**, *2008*, 011, doi:10.1088/1126-6708/2008/11/011.
110. Emparan, R.; Reall, H.S. A rotating black ring in five dimensions. *Phys. Rev. Lett.* **2002**, *88*, 101101, doi:10.1103/PhysRevLett.88.101101.
111. Emparan, R. Rotating circular strings, and infinite nonuniqueness of black rings. *J. High Energy Phys.* **2004**, *2004*, 064, doi:10.1088/1126-6708/2004/03/064.
112. Emparan, R.; Reall, H.S. Black rings. *Class. Quantum Gravity* **2006**, *23*, R169, doi:10.1088/0264-9381/23/20/R01.
113. Elvang, H.; Emparan, R.; Figueras, P. Phases of five-dimensional black holes. *J. High Energy Phys.* **2007**, *2007*, 056, doi:10.1088/1126-6708/2007/05/056.
114. Emparan, R.; Harmark, T.; Niarchos, V.; Obers, N.A.; Rodriguez, M. The phase structure of higher-dimensional black rings and black holes. *J. High Energy Phys.* **2007**, *2007*, 110, doi:10.1088/1126-6708/2007/10/110.
115. Emparan, R.; Figueras, P. Multi-black rings and the phase diagram of higher-dimensional black holes. *J. High Energy Phys.* **2010**, *2010*, 022, doi:10.1007/JHEP11(2010)022.
116. Elvang, H.; Emparan, R.; Virmani, A. Dynamics and stability of black rings. *J. High Energy Phys.* **2006**, *2006*, 074, doi:10.1088/1126-6708/2006/12/074.
117. Elvang, H.; Figueras, P. Black saturn. *J. High Energy Phys.* **2007**, *2007*, 050, doi:10.1088/1126-6708/2007/05/050.
118. Carter, B. Essentials of classical brane dynamics. *Int. J. Theor. Phys.* **2001**, *40*, 2099–2130.
119. Dias, O.; Figueras, P.; Monteiro, R.; Santos, J.E.; Emparan, R. Instability and new phases of higher-dimensional rotating black holes. *Phys. Rev. D* **2009**, *80*, 111701, doi:10.1103/PhysRevD.80.111701.
120. Dias, O.; Figueras, P.; Monteiro, R.; Reall, H.; Santos, J. An instability of higher-dimensional rotating black holes. *J. High Energy Phys.* **2010**, *2010*, 076, doi:10.1007/JHEP05(2010)076.
121. Dias, O.; Figueras, P.; Monteiro, R.; Santos, J. Ultraspinning instability of rotating black holes. *Phys. Rev. D* **2010**, *82*, 104025, doi:10.1103/PhysRevD.82.104025.

122. Dias, O.; Figueras, P.; Monteiro, R.; Santos, J. Ultraspinning instability of anti-de Sitter black holes. *J. High Energy Phys.* **2010**, *2010*, 067, doi:10.1007/JHEP12(2010)067.
123. Dias, O.; Monteiro, R.; Santos, J. Ultraspinning instability: The missing link. *J. High Energy Phys.* **2011**, *2011*, 139, doi:10.1007/JHEP08(2011)139.
124. Cardoso, V.; Dias, O.; Lemos, J.P.S.; Yoshida, S. The black hole bomb and superradiant instabilities. *Phys. Rev. D* **2004**, *70*, 044039, doi:10.1103/PhysRevD.70.049903.
125. Cardoso, V.; Dias, O.J.C. Small Kerr-anti-de Sitter black holes are unstable. *Phys. Rev. D* **2004**, *70*, 084011, doi:10.1103/PhysRevD.70.084011.
126. Cardoso, V.; Dias, O.C.; Yoshida, S. Classical instability of Kerr-AdS black holes and the issue of final state. *Phys. Rev. D* **2006**, *74*, 044008, doi:10.1103/PhysRevD.74.044008.
127. Shibata, M.; Yoshino, H. Nonaxisymmetric instability of rapidly rotating black hole in five dimensions. *Phys. Rev. D* **2010**, *81*, 021501, doi:10.1103/PhysRevD.81.021501.
128. Shibata, M.; Yoshino, H. Bar-mode instability of rapidly spinning black hole in higher dimensions: Numerical simulation in general relativity. *Phys. Rev. D* **2010**, *81*, 104035, doi:10.1103/PhysRevD.81.104035.
129. Hartnett, G.S.; Santos, J.E. Non-axisymmetric instability of rotating black holes in higher dimensions. *Phys. Rev. D* **2013**, *88*, 041505, doi:10.1103/PhysRevD.88.041505.
130. Kleihaus, B.; Kunz, J.; Radu, E. Black rings in six dimensions. *Phys. Lett. B* **2013**, *718*, 1073–1077.
131. Dolan, B.P. On the thermodynamic stability of rotating black holes in higher dimensions—A comparison of thermodynamic ensembles. *ArXiv E-Prints*, **2013**, arXiv:1312.6810.
132. Detweiler, S. Klein–Gordon equation and rotating black holes. *Phys. Rev. D* **1980**, *22*, 2323–2326.
133. Dolan, S. Instability of the massive Klein-Gordon field on the Kerr spacetime. *Phys. Rev. D* **2007**, *76*, 084001, doi:10.1103/PhysRevD.76.084001.
134. Peca, C.; Lemos, J. Thermodynamics of Reissner-Nordstrom Anti-de Sitter black holes in the grand canonical ensemble. *Phys. Rev. D* **1999**, *59*, 124007, doi:10.1103/PhysRevD.59.124007.